Quantification of the Impact of Uncertainty in Power Systems using Convex Optimization

A THESIS
SUBMITTED TO THE FACULTY OF THE GRADUATE SCHOOL
OF THE UNIVERSITY OF MINNESOTA
BY

Hyungjin Choi

IN PARTIAL FULFILLMENT OF THE REQUIREMENTS
FOR THE DEGREE OF
Doctor of Philosophy

Sairaj V. Dhople

June, 2017

Acknowledgements

I want to express my sincere gratitude to Professor Sairaj Dhople, my adviser, for giving me opportunity to begin my research career by taking me as his PhD student, guiding me through the years with great patience, and supporting me generously in both academic and personal circumstances.

I also thank Professor Peter Seiler for his advice and his toolboxes, which were very essential for my research.

I am thankful to Professor Bruce Wollenberg and Professor Ned Mohan for their guidance in subjects of power systems and power electronics. Professor Wollenberg's expertise and experience in power systems engineering helped me learn not only textbook knowledges but also real-world perspectives. I want to thank Professor Mohan for advising me to take control and optimization courses in the early stage of my graduate study. The training and knowledge from those courses helped my research later when I started my PhD.

I also would like to thank my lab mates, Mohit Sinha, Swaroop Guggilam, Victor Purba, and Sukumar Santhanam who were willing to help me in every aspect of laboratory life and made the long journey of the PhD more enjoyable.

Dedication

This dissertation is dedicated to my wife, *Yun*, and my parents. I would have not been able to finish my PhD without their support, devotion, and love.

Abstract

Rampant integration of renewable resources (e.g., photovoltaic and wind-energy conversion systems) and uncontrollable and elastic loads (e.g., plug-in hybrid electric vehicles) are rapidly transforming power systems. In this environment, an analytic method to quantify the impact of parametric and input uncertainty will be critical to ensure the reliable operation of next-generation power systems. This task is analytically and computationally challenging since power-system dynamics are nonlinear in nature.

In this thesis, we present analytic methods to quantify the impact of parametric and input uncertainties for two important applications in power systems: i) uncertainty propagation in power-system differential-algebraic equation model and power flow, and ii) robust stability assessment of power-system dynamics. For the first topic, an optimization-based method is presented to estimate maximum and minimum bounds on state variables while acknowleding worst-case parametric and input uncertainties in the model. The approach leverages a second-order Taylor-series expansion of the states around a nominal (known) solution. Maximum and minimum bounds are then estimated from either Semidefinite relaxation of Quadratically-Constrained Quadratic-Programming or Alternating Direction Method of Multipliers. For the second topic, an analytical method to quantify power systems stability margins while acknowleding uncertainty is presented within the framework of Lyapunov's direct method. It focuses on the algorithmic construction of Lyapunov functions and the estimation of the robust Region-Of-Attraction with Sum-of-Squares optimization problems which can be translated into semidefinite problems. For both topics, numerical case studies are presented for different test systems to demonstrate and validate the proposed methods.

Contents

List of Tables

List of Figures

Chapter 1

Introduction

1.1 Motivation

Increased integration of renewable resources (e.g., photovoltaic and wind energy conversion systems) and elastic loads (e.g., plug-in hybrid electric vehicles), coupled with the rampant modernization of metering, computing, and communication infrastructure are rapidly transforming power systems. To enable these transformations while maintaining reliability, there is a pressing need to quantify the impact of parametric and input uncertainty in power-system dynamic models on all aspects of power-systems operations including planning, scheduling, dispatch, and control [1, 2]. This task is analytically and computationally challenging since power-system dynamics are described by nonlinear differential algebraic equations (DAEs)—systems for which there are limited uncertainty analysis methods for reliability and stability of power systems. With regard to parametric uncertainty, precise values of generator settings, transmission-line impedances, and control set points are seldom perfectly known; similarly, with regard to input uncertainty, loads, mechanical power inputs, wind speeds, and solar irradiation are often times uncertain. Patently, repeated simulations are not only computationally burdensome, they also do not afford the option of examining the impact of all possible values of parametric and/or input uncertainty [3]. Therefore, analytical methods that quantify the impact of uncertainty will be important in ensuring the reliable operation of next-generation power systems. In this thesis, we present analytical methods for two main topics: i) estimating reachable sets that capture all possible solutions

of power-system dynamical models with parametric and input uncertainties based on formulating quadratic programming problems with sensitivity variables and implementing optimization methods including quadratically-constrained quadratic-programming (QCQP) with semi-definite programming (SDP) Relaxation and Alternating Direction Method of Multipliers (ADMM), and ii) estimating a region-of-attraction (ROA) for power-system dynamic models with parametric and input uncertainty based on formulating Lyapunov's stability criteria as sum-of-squares (SOS) optimization problems and subsequent SDP relaxation.

1.2 Prior Work and Contribution

1.2.1 Uncertainy Propagation In Power System DAE Model

Propagating uncertainty in power-system DAE models is a challenging task because of the nonlinear nature of power system models. In this part of the thesis, we present a method to propagate the impact of parametric and input uncertainty to the dynamic and algebraic states in power-system DAE models. We adopt a worst-case unknown-but-bounded model for the uncertainties, i.e., we only assume that maximum and minimum values are known, and given this information, we outline an approach based on SDP relaxation to estimate maximum and minimum bounds on the dynamic and algebraic states. The approach leverages a second-order Taylor-series approximation of the system's state variables along the solution trajectories as a function of the uncertain elements. This requires one to obtain the nominal solution of the DAE (corresponding to nominal values of the uncertain parameters and inputs) as well as pertinent sensitivities of the state trajectories to the uncertain elements. With the Taylor-series approximation serving as a surrogate to the actual value of the states, computing maximum and minimum values of these states amounts to solving QCQPs. These problems are generally non convex, and we leverage Lagrangian relaxations to derive SDPs, the solutions of which return provable bounds to the optimal solutions of the QCQPs. The bounds that our approach returns are indeed approximate since they stem from a Taylor-series approximation of the state trajectories. However, the proposed method is grounded in system theory, and can be applied to quantify the impact of both parametric *and* input

uncertainty on dynamic *and* algebraic states in nonlinear DAE models in a computationally efficient manner.

Closely related to our approach are so-called reachability methods, where convex sets (such as ellipsoids and zonotopes) are computed to bound system state variables at each time step. This is typically accomplished with a set-theoretic examination of an affine approximation to the system dynamics [4–7]. Applications of these set-theoretic methods to the problems of: i) uncertainty quantification in power-system dynamic models can be found in [8–14], and ii) design verification of power-system components such as dc-dc converters and wind generators can be found in [13, 15]. Compared to [8–14] that are only applicable to ordinary-differential equations (ODEs), our approach applies to the (more complicated) DAE models that accurately describe power-system dynamics. While DAE models are addressed in [14], our algorithm is structurally different since we compute bounds on state variables at each instant of time (as opposed to propagating uncertainty forward in time) with a second-order approximation of the solution. Also, our approach does not require dedicated software packages; our algorithms are grounded in solving convex optimization problems, a task which can be easily accomplished with widely available software. (We use the MATLAB-based mincx solver; other widely used software include CVX, SeDuMi, etc.) We close the literature review with a comment about probabilistic uncertainty propagation efforts. Here, uncertain inputs and model parameters are modeled as stochastic processes or random variables, and of interest is the probability distribution of the power-system dynamic and algebraic states. This is a mature research direction in itself, and some pertinent illustrative references include [16–22].

A key ingredient in our methodology is the dynamic model that governs the evolution of first- and second-order trajectory sensitivities of the dynamic and algebraic states in the power system DAE model. We demonstrate that these sensitivities are themselves governed by DAEs. In this context, it is worth pointing out the efforts [23–30], which leveraged (first-order) trajectory sensitivities in a variety of applications. The method we propose is (particularly) closely related to [27], where an affine approximation of state trajectories is proposed leveraging first-order sensitivities. Obtaining bounds on the states then amounts to just checking the vertices of the uncertainty set. Our approach recovers this as a special case (by neglecting second-order sensitivities), but we show

through simulations that the second-order Taylor-series approximation yields increased accuracy.

1.2.2 Uncertainty Propagation In Power Flow

Numerous approaches have been proposed to propagate uncertainty in power-flow models, and they can be broadly classified into probabilistic methods, robust optimization methods, and interval/set analysis. A detailed review of several recent methods can be found in [31, 32]. Probabilistic methods model uncertain elements as random variables with known probability density functions, and leverage Monte Carlo simulations or analytical approaches to propagate uncertainty [33–36]. Robust optimization methods model uncertainties as interval quantities, and involve optimization problems to solve for bounds on states [37,38]. In interval/set analysis, uncertainties are modeled as intervals or sets and the bounds on the outputs are estimated by using interval/set arithmetic [8, 9, 39–42].

Structurally, our method is closely aligned with the robust optimization approaches discussed above since a worst-case model is adopted for the uncertainties, and the task of estimating bounds is cast as an optimization problem. However, there are some key points of difference that also serve as indicators of contributions over prior art. First, we adopt quadratic (as opposed to linear) approximations for the states which increases accuracy. Furthermore, we apply pertinent decoupling assumptions to formally derive auxiliary algebraic equations that yield sensitivities up to second order. These sensitivities are instrumental to formulate the quadratic approximations, and the systematic application of the decoupling assumptions is critical to ensure that they can be computed with minimal burden in large systems. From an algorithmic perspective, we apply the ADMM to solve the formulated optimization problems and demonstrate convergence of our approach leveraging the seminal advances outlined in the recent work [43]. The algorithmic approach outlined here based on the ADMM promotes the scalability of the method as we will numerically demonstrate the validity of the approach for a 1354-bus test system with 2447 states and 76 sources of uncertainty. (We can apply SDP relaxation approach discussed in Section 3 for the DAE setting to solve power flow with uncertainty [44, 45]. However, the method using the ADMM is scalable to much larger system sizes and uncertainty sets compared to the SDP approach as we will discuss in

Section 4) Indeed, the application of the ADMM and the decoupling assumptions to solve for the sensitivities serve as key contributions over prior art.

1.2.3 Robust Region-of-Attraction Estimation

Within the realm of analytical approaches to quantify power-system stability, Lyapunov's direct method has received significant attention [46–48]. Lyapunov functions can provide estimates of the ROA of stable equilibrium points which is useful in multiple contexts, e.g., this allows one to determine the critical clearing times of synchronous generators [46, 48, 49]. However, let alone incorporating parametric/input uncertainty, synthesizing Lyapunov functions and finding the ROA even in general deterministic settings is a difficult task [47, 50]. In this regard, the key challenge this thesis addresses relates to formulating an optimization-based algorithmic method to synthesize Lyapunov functions for power system dynamic models when the model parameters and/or inputs are uncertain.

We formulate the Lyapunov-function synthesis and ROA-estimation task as a SOS optimization program. The essence of the approach pertains to translating statements from pertinent Lyapunov stability theorems into polynomial constraints and objective functions. SOS optimization problems are a type of polynomial optimization problems tailored to polynomials that can be written as finite linear combinations of squared polynomials. They can be translated into SDPs which can be solved with readily available software. Our approach provides a systematic solution to: i) constructing Lypapunov functions and obtaining the ROA without imposing any structural limitations on the system (some previous approaches, as discussed subsequently, predicate the existence of transfer conductances or require Lipschitz conditions on nonlinearities in the dynamic models); ii) incorporating uncertainties in model parameters and inputs to obtain robust estimates of the ROA. Relevant to our approach are recent efforts in the application of SOS-optimization based tools to determine Lyapunov functions in *deterministic* power system dynamic models [51]. Our work offers two contributions to [51]: i) we address the challenge of algorithmically computing the ROA in power-system dynamic models while incorporating the impact of unknown-but-bounded (worst-case) parametric and input uncertainty; ii) the strategy adopted in this work pertaining to the polynomial approximation of sinusoidal functions in the system dynamic model (that appear due to

the power flow equations) differs from [51], where the sinusoidal terms are replaced by auxiliary variables which requires the introduction of additional algebraic constraints.

With regard to the relevant concern of problem scalability, we are able to handle the same order of dynamical system as the previous effort in this domain [51], however, we demonstrate how multiple sources of uncertainty can be systematically accommodated to compute the robust ROA. Furthermore, our case studies include combinations of synchronous and doubly-fed induction generators; systems where analytically determining the ROA (let alone the robust ROA) is intractable.

To our best knowledge, there is no prior work related to the estimation of robust ROA for power system dynamics; this is indeed the main contribution of our approach. Central to the proposed method is the approximation of the nonlinear power system dynamic models with a polynomial differential equation model that is affine in uncertain parameters and/or inputs. This facilitates the application of robust versions of SOS methods [52]. In this regard, the polynomial approximations of the system dynamics (different from [51]) are crucial. In addition, we suggest a computationally tractable approach to contend with many uncertainties by sequentially updating the Lyapunov function based on an a-priori estimation of its sensitivity to uncertainties.

The main limitation of the proposed SOS-based approach is related to problem scalability as the dimension of the dynamical systems' state-space increases [53]. However, several ongoing research efforts are addressing problem scalability, and encouraging results are reported in, e.g., [54–56]. In spite of this limitation, the main advantage of the SOS approach is that it provides the ability to analyze systems without any a-priori assumptions on system structure. Therefore, SOS optimization techniques have been used in several recent investigations to estimate the ROA [51, 57–60].

Related research pertaining to estimating Lyapunov functions for deterministic power system dynamic models includes several classical approaches such as the first-integral, Krasovskii's, and variable-gradient methods [46, 61]. However, these approaches typically impose a strict structure on the system model. For example, the first integral method requires the system to be conservative (i.e., no damping terms or transfer conductances are allowed). Krasovskii's method is confined to Lyapunov functions that have a quadratic form. Similarly, the variable gradient method applies to settings where the

gradient vector of the Lyapunov function is identically zero. Other methods that have received attention in this domain are Zubov's and Popov's methods [62]. Zubov's method requires solving linear partial differential equations, and it gives the exact Lyapunov function for the system if a closed-form solution for the differential equations exists, which is generally intractable. Popov's method is based on frequency domain analysis and has recently been applied for stability analysis of AC microgrids [63]. However, it requires nonlinearities to lie within the first and third quadrants, which is not always true [46,64]. Classical methods such as Gorev's energy criteria, Magnusson's method of transitional energy, and Aylett's energy integral criterion do not yield systematic procedures because they ignore the existence of transfer conductances [61]. Recent approaches to find Unstable Equilibrium Points (UEP) algorithmically such as Closest Unstable Equilibrium Point, Boundary Controlling Unstable equilibrium point, and Potential Energy Boundary Surface methods are also based on the direct method [3, 61, 65–67], and have found applicability in practical systems [68,69]. However, these have not been extended to cover model uncertainty.

1.3 Detailed Description of Chapter Contents

- Chapter 1 - Introduction: introduces motivation regarding to quantifying the impact of uncertainty in power systems, reviews prior approaches related to uncertainty propagation and robust stability analysis in power systems, and describes our contribution over the prior works.

- Chapter 2 - Power Systems and Uncertainty Model: describes power system dynamical model and parametric and input uncertainty model which are the modeling basis of our analysis in this thesis.

- Chapter 3 - Uncertainty Propagation in Power-system DAE Model: presents an analytic method to propagate parametric and input uncertainty in power-system DAE model based on the formulation of sensitivity equations and QCQP/SDP relaxation. (Published in [44, 70].)

- Chapter 4 - Uncertainty Propagation in Power Flow: presents an analytic method to propagate parametric and input uncertainty in power flow equations based on

the formulation of sensitivity equations and ADMM. (Published in [45], and [71] in review.)

- Chapter 5 - Robust Stability Assessment of Power Systems: presents an analytic method to estimate robust ROA for power-system transient stability with parametric and input uncertainty based on the formulation of Lyapunov's stability conditions using SOS optimization method. (Published in [72].)
- Chapter 6 - Conclusion and Discussion

Chapter 2

Power Systems and Uncertainty Model

In this chapter, we present power systems and uncertainty models that we adopt in this thesis. First, we present DAEs that describe electro-mechanical dynamics as well as power-flow balance in power systems. Following this, we introduce unknown-but-bounded uncertainty models to describe a bounded set for parameters and inputs that are uncertain.

2.1 Power System Model

Power-system dynamics can be described by a set of differential-algebraic equations (DAEs) as follows:

$$\frac{dx}{dt} = g(x, y, u), \tag{2.1a}$$

$$0 = h(x, y, u), \tag{2.1b}$$

$$x(t_0) = x_0, \quad y(t_0) = y_0,$$

where $x = [x_1, \ldots, x_D]^{\mathrm{T}} \in \mathbb{R}^D$ is the dynamical-state vector, $y = [y_1, \ldots, y_A]^{\mathrm{T}} \in \mathbb{R}^A$ is the algebraic-state vector, $u = [u_1, \ldots, u_I]^{\mathrm{T}} \in \mathbb{R}^I$ collects all the parameters and inputs in the system that are uncertain. Initial conditions are specified at some time $t_0 \geq 0$ for the dynamic and algebraic states, and they are denoted by $x_0 \in \mathbb{R}^D$ and

$y_0 \in \mathbb{R}^A$, respectively. Dynamic states of interest typically include rotor electrical angular positions and frequencies, turbine powers, etc.; algebraic states typically include bus-voltage magnitudes and phases. For ease of exposition, we refer to u simply as the input; and for notational convenience, we will define the vector $z = [x^{\mathrm{T}}, y^{\mathrm{T}}]^{\mathrm{T}} \in \mathbb{R}^{D+A}$ that collects both the dynamic and algebraic states.

For example, a standard one-axis model for synchronous generators (SGs) in the power system [46] is described by the following differential equations:

$$\begin{aligned} \frac{\mathrm{d}\delta_i}{\mathrm{d}t} &= \omega_i - \omega_{\mathrm{s}}, \\ \frac{\mathrm{d}\omega_i}{\mathrm{d}t} &= \frac{1}{M_i}\left(P_i - P_i^{\mathrm{elec}} - D_i(\omega_i - \omega_{\mathrm{s}})\right), \end{aligned} \tag{2.2}$$

where δ_i and ω_i are the rotor angle and speed, M_i and D_i are the inertia constant and damping coefficient for the ith machine, and P_i and P_i^{elec} are the mechanical-input power and electrical-output power, respectively. Similarly, the electromechanical model adopted for doubly-fed induction generator (DFIG) wind turbines is given by [73]:

$$\begin{aligned} \frac{\mathrm{d}\delta_i}{\mathrm{d}t} &= (\omega_i - \omega_{\mathrm{s}}) - \frac{1}{|E_i|T_i}\left(\frac{X_i - X_i'}{X_i'}|V_j|\sin(\delta_i - \theta_j) + T_i\omega_{\mathrm{s}}|V_i^{\mathrm{rotor}}|\cos(\delta_i - \theta_i^{\mathrm{rotor}})\right), \\ \frac{\mathrm{d}\omega_i}{\mathrm{d}t} &= \frac{1}{M_i}\left(P_i\frac{\omega_{\mathrm{s}}}{\omega_i} - P_i^{\mathrm{elec}}\right), \end{aligned} \tag{2.3}$$

where, for the ith DFIG, $|E_i|$ is the generator-voltage magnitude, T_i is the transient open-circuit constant, X_i' is the transient reactance, X_i is the stator reactance, $|V_j|$ and θ_j are the terminal-voltage magnitude and angle, and $|V_i^{\mathrm{rotor}}|$ and $\theta_i^{\mathrm{rotor}}$ are the rotor-voltage magnitude and angle. In (2.2) and (2.3), the electrical output power of the generators can be expressed as:

$$P^{\mathrm{elec}} = \mathrm{Re}\Big\{|E_i|\angle\delta_i \sum_{j\in\mathcal{G}_i} Y_{ij}^*|V_j|\angle - \theta_j\Big\}, \tag{2.4}$$

where $|E_i|\angle\delta_i$ is the generator voltage phasor at bus i, Y_{ij} is the (i,j) entry in the (complex-valued) admittance matrix of the network; and $\mathcal{G}_i$ is the set that captures all nodes electrically connected to the generator at node i.

Combined with the differential equations in (2.2)– (2.4), we also have algebraic equations that describe real- and reactive-power-flow balance in the system given as

below:

$$0 = \mathrm{Re}\Big\{ |V_i| \angle \theta_i \sum_{j \in \mathcal{N}_i} Y_{ij}^* |V_j| \angle - \theta_j \Big\} + P_i^{\mathrm{L}} - P_i^{\mathrm{G}}, \tag{2.5a}$$

$$0 = \mathrm{Im}\Big\{ |V_i| \angle \theta_i \sum_{j \in \mathcal{N}_i} Y_{ij}^* |V_j| \angle - \theta_j \Big\} + Q_i^{\mathrm{L}} - Q_i^{\mathrm{G}}, \tag{2.5b}$$

where $\{P_i^{\mathrm{L}}, Q_i^{\mathrm{L}}\}$ ($\{P_i^{\mathrm{G}}, Q_i^{\mathrm{G}}\}$) are the real- and reactive-power consumed (generated) at bus i, and $\mathcal{N}_i$ is the set that captures all nodes electrically connected to node i. For the above DAE models, dynamic states, $x = [\delta_i, \omega_i]$, and algebraic states, $y = [|V_j|, \theta_j]$.

In sinusoidal steady state, the dynamics simplify to power-flow equations which are algebraic equations of the form:

$$0 = h(y, u). \tag{2.6}$$

In particular, for power flow studies, we assume that dynamic states such as generator frequency is already in steady-state, and we only consider the real- and reactive-power balance equations in the model (2.5).

2.2 Unknown-but-bounded Uncertainty Model

We assume a worst-case uncertainty model for the inputs and parameters that are not perfectly known. By this we mean that in addition to a nominal value, upper and lower bounds for entries in u are known. Let us define the nominal value, upper, and lower limits of the ith uncertainty variable, u_i, as $\overline{u}_i$, $u_i^{\max}$, and $u_i^{\min}$, respectively. Then the set of all possible values of uncertainty variables is denoted by $\mathcal{U}$, and defined as:

$$\mathcal{U} := \left\{ u_i \in \mathbb{R} | u_i^{\min} \leq u_i \leq u_i^{\max}, \forall i =, 1, \ldots, I \right\}. \tag{2.7}$$

For notational ease, it is convenient to assume that each uncertain parameter or input can vary based on a percentage uncertainty, ρ_i; in particular,

$$u_i \in \left[u_i^{\min}, u_i^{\max} \right] := \left[\overline{u}_i \left(1 - \frac{\rho_i}{100} \right), \overline{u}_i \left(1 + \frac{\rho_i}{100} \right) \right]. \tag{2.8}$$

The set $\mathcal{U}$ is described by an I-dimensional polytope. For example, Fig. 2.1 illustrates a setting with three uncertainties where the uncertainty set $\mathcal{U}$ is described by the 3-dimensional polytope that captures all possible values of uncertainty variables, u_1–u_3.

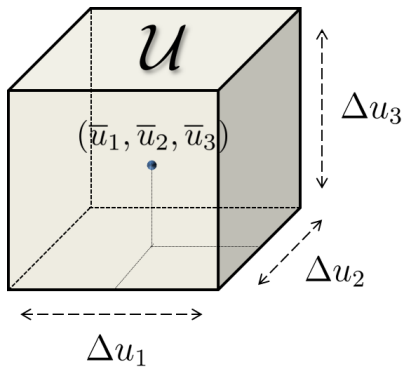

Figure 2.1: Unknown-but-bounded uncertainty set for three uncertainties.

In this case, Δu_i represents variations of each uncertainty variable u_i around the nominal values denoted by $\overline{u}_i$. We illustrate the notation introduced with an example next.

Example 1 *Figure 2.2 depicts a single-machine infinite-bus (SMIB) system. It is composed of a synchronous generator (at bus 1), a constant PQ load (at bus 3), and the infinite bus (bus 2). Let $|V_i|$ and θ_i denote the voltage magnitudes and angles at bus i, respectively. Let δ and ω denote the synchronous-generator rotor angular position and velocity, respectively. With reference to* (2.1)*, differential and algebraic equations in* (2.9a) *and* (2.9b) *correspond to* (2.1a) *and* (2.1b)*, respectively; the dynamic and algebraic states are collected in $x = [\delta, \omega]^{\mathrm{T}}$ and $y = [|V_3|, \theta_3]^{\mathrm{T}}$, respectively; and $z = [\delta, \omega, |V_3|, \theta_3]^{\mathrm{T}}$. The DAE model is then*

$$g_1(x,y,u) := \frac{d\delta}{dt} = \omega - \omega_{\mathrm{s}}, \tag{2.9a}$$

$$g_2(x,y,u) := \frac{d\omega}{dt} = \frac{P}{M} - \frac{|E||V_3|}{MX_M}\sin(\delta - \theta_3) - \frac{D}{M}(\omega - \omega_{\mathrm{s}}),$$

$$h_1(x,y,u) := \frac{|E||V_3|}{X_M}\sin(\theta_3 - \delta) + \frac{|V_2||V_3|}{X_L}\sin(\theta_3 - \theta_2) + P^{\mathrm{L}} = 0, \tag{2.9b}$$

$$h_2(x,y,u) := \frac{|V_3|^2}{X_M} + \frac{|V_3|^2}{X_L} - \frac{|E||V_3|}{X_M}\cos(\theta_3 - \delta) - \frac{|V_3||V_2|}{X_L}\cos(\theta_3 - \theta_2) + Q^{\mathrm{L}} = 0,$$

where ω_{s} is the synchronous speed, P is the mechanical input power, M is the inertia constant, D is the damping coefficient, $|E|$ is the internal voltage, X_M is the synchronous reactance, and X_L is the reactance of line $(2, 3)$.

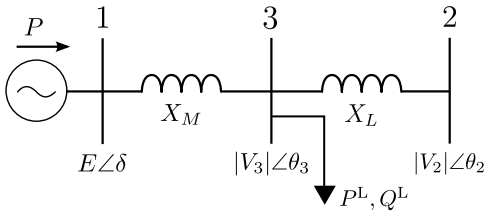

Figure 2.2: One-line diagram of the SMIB model studied in Example 1.

Possible sources of parametric and input uncertainty includes the infinite-bus voltage magnitude and angle, $|V_2|$ and θ_2; real power of the load bus, P^{L}; mechanical input power, P; inertia constant, M; damping coefficient, D; internal voltage, $|E|$; synchronous reactance, X_M; and reactance of line $(2,3)$, X_L. Assume that the infinite-bus voltage magnitude, $|V_2|$, and real power of the load bus, P^{L} are uncertain. In this case, the uncertainties, $u = [u_1, u_2]^{\mathrm{T}} = [|V_2|, P^{\mathrm{L}}]^{\mathrm{T}}$ and the uncertainty set that contains the possible values of uncertainty variables are described by a rectangle. We also suppose the nominal values, $\overline{u} = [\overline{u}_1, \overline{u}_2]^{\mathrm{T}} = [\overline{|V|}_2, \overline{P}^{\mathrm{L}}]^{\mathrm{T}} = [1,1]^{\mathrm{T}}$. When we solve the equations in (2.1), power-flow equations in (2.9) for $u = \overline{u}$, we get the nominal values, $\overline{x} = [\overline{\delta}, \overline{\omega}]^{\mathrm{T}} = [0.3154, 376.9911]^{\mathrm{T}}$, and $\overline{y} = [\overline{|V|}_3, \overline{\theta}_3]^{\mathrm{T}} = [1.0064, 0]^{\mathrm{T}}$. ■

Example 2 *In this example, we illustrate the power-flow equations discussed above for the two-bus power system sketched in Fig. 2.3, composed of a PQ load at bus 2 connected to the infinite bus at bus 1 through a transmission line with line reactance, X_L.. Nominal parameters and inputs are $|V_1| = 1$, $\theta_1 = 0$, $X_L = 0.15$, $P^{\mathrm{L}} = 0.2$, $Q^{\mathrm{L}} = 0.1$. (All values are in per-unit unless explicitly specified.) The power-flow equations for real- and reactive-power balance at bus 2 (the load bus) are*

$$\begin{aligned} 0 = h_1(x,u) :=& \frac{|V_1||V_2|}{X_L}\sin\theta_2 + P^{\mathrm{L}}, \\ 0 = h_2(x,u) :=& \frac{|V_2|^2}{X_L} - \frac{|V_1||V_2|}{X_L}\cos\theta_2 + Q^{\mathrm{L}}. \end{aligned} \tag{2.10}$$

Assume that the infinite-bus voltage magnitude, $|V_1|$, and real power of the load bus, P^{L}, are uncertain and can vary up to $\pm 10\,\%$ around their nominal values (i.e., $\rho_1 = \rho_2 = 10$). In this case, the state variables, $x = [x_1, x_2]^{\mathrm{T}} = [|V_2|, \theta_2]^{\mathrm{T}}$, and the uncertainties, $u = [u_1, u_2]^{\mathrm{T}} = [|V_1|, P^{\mathrm{L}}]^{\mathrm{T}}$. We will suppose the nominal values, $\overline{u} = [\overline{u}_1, \overline{u}_2]^{\mathrm{T}} = [1, 0.2]^{\mathrm{T}}$. When we solve the power-flow equations in (2.10) for $u = \overline{u}$,

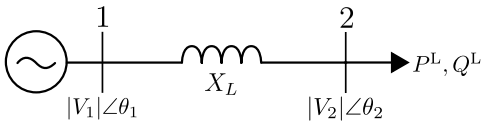

Figure 2.3: An illustrative power-system model for Example 2.

we get the nominal value of the voltage magnitude, $|V_2|$*,* $\overline{x}_1(\overline{u}) = 0.9843$*, and the nominal value of the phase,* θ_2*,* $\overline{x}_2(\overline{u}) = -0.0305\,[\mathrm{rad}]$*.* ■

Chapter 3

Uncertainty Propagation in Power-system DAE Models

In this chapter, we outline a convex-optimization-based method to estimate maximum and minimum bounds on states of DAEs that describe the electromechanical dynamics of power systems while acknowledging parametric and input uncertainty in the model. The method is based on a second-order Taylor-series approximation of the DAE-model state trajectories as a function of the uncertainties. A key contribution in this regard is the derivation of a DAE model that governs the second-order trajectory sensitivities of states to uncertainties in the model. Bounds on the states are then obtained by solving semidefinite programs, where the objective is to maximize / minimize the Taylor-series approximations subject to constraints that describe the uncertainty space. While the computed bounds are approximate (since they are derived from a Taylor-series approximation of the state trajectories) the method nevertheless is an efficient system-theoretic approach to uncertainty propagation for power-system DAE models.

The remainder of this chapter is organized as follows. In Section 3.1, we formulate the Taylor-series approximation of the system states. In Section 3.2, we derive the DAE model that governs the trajectory sensitivities. In Section 3.3, we derive the SDPs to estimate the upper and lower bounds on system states. In Section 3.4, numerical case studies are presented for a DAE model of the IEEE 39-bus New England system to

demonstrate scalability and validate the approach.

3.1 Quadratic Approximation of System States

Suppose we have power system model described by DAEs in (2.1). Also assume that the unknown-but-bounded uncertainty model in (2.7) is adopted for the analysis. Central to the proposed uncertainty-propagation algorithm is a second-order approximation of the solution to (2.1) as a function of $\Delta u := u - \overline{u}$. Utilizing a Taylor-series approximation, we write the ith state at time t as follows:

$$z_i(t,u) \approx \overline{z}_i(t,\overline{u}) + J_i \Delta u + \frac{1}{2}\Delta u^{\mathrm{T}} H_i \Delta u, \tag{3.1}$$

where $\overline{z}_i(t,\overline{u})$ is the solution for the nominal input $u = \overline{u}$, and $J_i \in \mathbb{R}^{1\times I}$ and $H_i \in \mathbb{R}^{I\times I}$ are given by

$$J_i = \left[\frac{\partial z_i}{\partial u_1}, \ldots, \frac{\partial z_i}{\partial u_I}\right]; H_i = \begin{bmatrix} \frac{\partial^2 z_i}{\partial u_1^2} & \cdots & \frac{\partial^2 z_i}{\partial u_1 \partial u_I} \\ \vdots & \ddots & \vdots \\ \frac{\partial^2 z_i}{\partial u_I \partial u_1} & \cdots & \frac{\partial^2 z_i}{\partial u_I^2} \end{bmatrix},$$

with their entries evaluated for $(t,\overline{u})$. To capture pertinent sensitivities for all the dynamical and algebraic states, $z_i, \forall i = 1,\ldots,D+A$, to the inputs $u_j, \forall j = 1,\ldots,I$ with approximations in (3.1), we have to track the evolution of entries of J_i and H_i. This requires describing the evolution of the following $(D+A)\times I$ first-order, $(D+A)\times I$ second-order, and $\frac{1}{2}(D+A)\times I(I-1)$ mixed sensitivity-related states:

$$\left\{\frac{\partial z_1}{\partial u_1}, \ldots, \frac{\partial z_1}{\partial u_I}, \ldots, \frac{\partial z_{D+A}}{\partial u_1}, \ldots, \frac{\partial z_{D+A}}{\partial u_I}\right\}, \tag{3.2}$$

$$\left\{\frac{\partial^2 z_1}{\partial u_1^2}, \ldots, \frac{\partial^2 z_1}{\partial u_I^2}, \ldots, \frac{\partial^2 z_{D+A}}{\partial u_1^2}, \ldots, \frac{\partial^2 z_{D+A}}{\partial u_I^2}\right\}, \tag{3.3}$$

$$\left\{\frac{\partial^2 z_1}{\partial u_1 \partial u_2}, .., \frac{\partial^2 z_1}{\partial u_{I-1} \partial u_I}, .., \frac{\partial^2 z_{D+A}}{\partial u_1 \partial u_2}, .., \frac{\partial^2 z_{D+A}}{\partial u_{I-1} \partial u_I}\right\}. \tag{3.4}$$

For the approximation (3.1), we are interested in:

$$z_i^{\min}(t) := \min_{u\in\mathcal{U}} \; z_i(t,u), \quad z_i^{\max}(t) := \max_{u\in\mathcal{U}} \; z_i(t,u). \tag{3.5}$$

Note that it is analytically intractable to compute the above bounds for the exact solution of (2.1). However, given the quadratic approximation for the states in (3.1), and the uncertainty model for the inputs in (2.8), we show in Section 3.3 that the problems in (3.5) are QCQPs, and describe an approach to solve them. But first, we derive the DAEs that have to be simulated to obtain entries of (3.2)-(3.4), so that the Taylor-series expansion for each state variable can be obtained.

3.2 Dynamics of Sensitivity Variables

Suppose the differential and algebraic equations in (2.1) are continuous in (x, y, u), have continuous first- and second-order partial derivatives with respect to (x, y, u), and the system (2.1) admits a unique solution for the nominal uncertain input $\overline{u}$. Express the solution of the kth differential equation in (2.1), $g_k(x, y, u)$, for $u = \overline{u}$ and at time t as:

$$x_k(t, u) = x_k(t_0, \overline{u}) + \int_{\tau=t_0}^{t} g_k(x, y, \overline{u}) d\tau. \tag{3.6}$$

First-order Sensitivities

Consider entries in the set (3.2). Define the following D- and A-dimensional first-order-sensitivity state vectors $\forall i = 1, \ldots, I$

$$f_{x,u_i} := \left[\frac{\partial x_1}{\partial u_i}, \ldots, \frac{\partial x_D}{\partial u_i}\right]^{\mathrm{T}}, \; f_{y,u_i} := \left[\frac{\partial y_1}{\partial u_i}, \ldots, \frac{\partial y_A}{\partial u_i}\right]^{\mathrm{T}}. \tag{3.7}$$

Denote the kth (ℓth, respectively) entry of the vector f_{x,u_i} (f_{y,u_i}, respectively) by f_{x_k,u_i} (f_{y_ℓ,u_i}, respectively). Taking the partial derivative of $x_k(t, u)$ given in (3.6) with respect to u_i:

$$\frac{\partial x_k}{\partial u_i} = \int_{\tau=t_0}^{t} \sum_{m=1}^{D} \frac{\partial g_k}{\partial x_m} \frac{\partial x_m}{\partial u_i} + \sum_{n=1}^{A} \frac{\partial g_k}{\partial y_n} \frac{\partial y_n}{\partial u_i} + \frac{\partial g_k}{\partial u_i} d\tau. \tag{3.8}$$

By taking the derivative of (3.8) with respect to t, and leveraging the notation established in (3.7), we get:

$$\frac{d}{dt} f_{x_k,u_i} = \sum_{m=1}^{D} \frac{\partial g_k}{\partial x_m} f_{x_m,u_i} + \sum_{n=1}^{A} \frac{\partial g_k}{\partial y_n} f_{y_n,u_i} + \frac{\partial g_k}{\partial u_i}. \tag{3.9}$$

The vector field that governs the evolution of f_{x_k,u_i} depends on entries of the vector f_{y,u_i}, i.e., the first-order sensitivities of the algebraic states. This suggests that we also need the following complementary algebraic equations $\forall \ell = 1, \ldots, A$ which are recovered from the algebraic equations in (2.1):

$$0 = \sum_{m=1}^{D} \frac{\partial h_\ell}{\partial x_m} f_{x_m,u_i} + \sum_{n=1}^{A} \frac{\partial h_\ell}{\partial y_n} f_{y_n,u_i} + \frac{\partial h_\ell}{\partial u_i}. \tag{3.10}$$

Collecting (3.9) and (3.10) in a matrix-vector form $\forall k = 1, ..., D$, and $\forall \ell = 1, ..., A$, we get the following DAE model that governs the dynamics of the first-order sensitivities:

$$\begin{aligned} \frac{d}{dt} f_{x,u_i} &= \nabla_x g \cdot f_{x,u_i} + \nabla_y g \cdot f_{y,u_i} + \frac{\partial g}{\partial u_i}, \\ 0 &= \nabla_x h \cdot f_{x,u_i} + \nabla_y h \cdot f_{y,u_i} + \frac{\partial h}{\partial u_i}, \end{aligned} \tag{3.11}$$

where $\frac{\partial g}{\partial u_i}$, $\nabla_x g$, and $\nabla_y g$ are given by

$$\frac{\partial g}{\partial u_i} = \left[\tfrac{\partial g_1}{\partial u_i}, \tfrac{\partial g_2}{\partial u_i}, \ldots, \tfrac{\partial g_D}{\partial u_i}\right]^{\mathrm{T}},$$

$$\nabla_x g = \begin{bmatrix} \frac{\partial g_1}{\partial x_1} & \cdots & \frac{\partial g_1}{\partial x_D} \\ \vdots & \ddots & \vdots \\ \frac{\partial g_D}{\partial x_1} & \cdots & \frac{\partial g_D}{\partial x_D} \end{bmatrix}, \nabla_y g = \begin{bmatrix} \frac{\partial g_1}{\partial y_1} & \cdots & \frac{\partial g_1}{\partial y_A} \\ \vdots & \ddots & \vdots \\ \frac{\partial g_D}{\partial y_1} & \cdots & \frac{\partial g_D}{\partial y_A} \end{bmatrix},$$

with all entries evaluated at $u = \overline{u}$. Entries of $\frac{\partial h}{\partial u_i}$, $\nabla_x h$, and $\nabla_y h$ are defined similarly, and not reported for conciseness. Simulating the DAE model composed of copies of (3.11) $\forall i = 1, \ldots, I$ yields all the first-order sensitivities in the set (3.2).

Second-order Sensitivities

Now consider entries in the set (3.3). Denote the following D- and A-dimensional second-order-sensitivity state vectors $\forall i = 1, \ldots, I$

$$s_{x,u_i} = \left[\frac{\partial^2 x_1}{\partial u_i^2}, \ldots, \frac{\partial^2 x_D}{\partial u_i^2}\right]^{\mathrm{T}}, s_{y,u_i} = \left[\frac{\partial^2 y_1}{\partial u_i^2}, \ldots, \frac{\partial^2 y_A}{\partial u_i^2}\right]^{\mathrm{T}}. \tag{3.12}$$

Following an approach analogous to the first-order sensitivities, we get the following DAE model that governs the evolution of the second-order sensitivities:[1]

$$\begin{aligned}\frac{d}{dt}s_{x,u_i} =&\nabla_x g \cdot s_{x,u_i} + \nabla_y g \cdot s_{y,u_i} + \frac{\partial \nabla_x g}{\partial u_i} \cdot f_{x,u_i} + \frac{\partial \nabla_y g}{\partial u_i} \cdot f_{y,u_i} + \frac{\partial^2 g}{\partial u_i^2} \\ &+ \left[(1_D \otimes f_{x,u_i})^{\mathrm{T}}\right]^{\dagger} \left[\nabla_x^2 g_1, \ldots, \nabla_x^2 g_p\right]^{\dagger} (1_D \otimes f_{x,u_i}) \\ &+ \left[(1_A \otimes f_{y,u_i})^{\mathrm{T}}\right]^{\dagger} \left[\nabla_y^2 g_1, \ldots, \nabla_y^2 g_p\right]^{\dagger} (1_A \otimes f_{y,u_i}), \\ 0 =&\nabla_x h \cdot s_{x,u_i} + \nabla_y h \cdot s_{y,u_i} + \frac{\partial \nabla_x h}{\partial u_i} \cdot f_{x,u_i} + \frac{\partial \nabla_y h}{\partial u_i} \cdot f_{y,u_i} + \frac{\partial^2 h}{\partial u_i^2} \\ &+ \left[(1_D \otimes f_{x,u_i})^{\mathrm{T}}\right]^{\dagger} \left[\nabla_x^2 h_1, \ldots, \nabla_x^2 h_q\right]^{\dagger} (1_D \otimes f_{x,u_i}) \\ &+ \left[(1_A \otimes f_{y,u_i})^{\mathrm{T}}\right]^{\dagger} \left[\nabla_y^2 h_1, \ldots, \nabla_y^2 h_q\right]^{\dagger} (1_A \otimes f_{y,u_i}),\end{aligned} \tag{3.13}$$

where $\frac{\partial^2 h}{\partial u_i^2}$, $\nabla_x^2 g_i$, and $\frac{\partial \nabla_x g}{\partial u_i}$, are given by

$$\frac{\partial^2 h}{\partial u_i^2} = \left[\frac{\partial^2 g_1}{\partial u_i^2}, \frac{\partial^2 g_2}{\partial u_i^2}, \ldots, \frac{\partial^2 g_D}{\partial u_i^2}\right]^{\mathrm{T}},$$

$$\nabla_x^2 g_i = \begin{bmatrix} \frac{\partial^2 g_i}{\partial x_1^2} & \frac{\partial^2 g_i}{\partial x_1 \partial x_2} & \cdots & \frac{\partial^2 g_i}{\partial x_1 \partial x_D} \\ \vdots & \vdots & \ddots & \vdots \\ \frac{\partial^2 g_i}{\partial x_D \partial x_1} & \frac{\partial^2 g_i}{\partial x_D \partial x_2} & \cdots & \frac{\partial^2 g_i}{\partial x_D^2} \end{bmatrix},$$

$$\frac{\partial \nabla_x g}{\partial u_i} = \begin{bmatrix} \frac{\partial^2 g_1}{\partial u_i \partial x_1} & \cdots & \frac{\partial^2 g_1}{\partial u_i \partial x_D} \\ \vdots & \ddots & \vdots \\ \frac{\partial^2 g_D}{\partial u_i \partial x_1} & \cdots & \frac{\partial^2 g_D}{\partial u_i \partial x_D} \end{bmatrix},$$

with all entries evaluated for $u = \overline{u}$. Entries of $\nabla_y^2 g_i$, $\frac{\partial \nabla_y g}{\partial u_i}$, $\frac{\partial^2 h}{\partial u_i^2}$, $\nabla_x^2 h_i$, $\nabla_y^2 h_i$, $\frac{\partial \nabla_x h}{\partial u_i}$, and $\frac{\partial \nabla_y h}{\partial u_i}$ follow similarly and are not reported for conciseness. As before, simulating the DAE model composed of copies of (3.13) $\forall i = 1, \ldots, I$ yields the dynamics of all entries in (3.3). More details on the derivation to obtain (3.13) are provided in Appendix A.

[1] 1_N and 0_N denote N-dimensional vectors with all entries equal to 1 and 0, respectively. $x \otimes y$ denotes the Kronecker product of x and y. Also, $[X_1, \ldots, X_N]^{\dagger}$ denotes a block diagonal matrix with square matrices $X_1, \ldots, X_N$ stacked along the diagonal, e.g., for vector $X = [X_1, X_2]^{\mathrm{T}}$, $X^{\dagger} := \mathrm{diag}\{X_1, X_2\}$.

Mixed Sensitivities

Finally, consider entries in the set (3.4). Define the following D- and A-dimensional mixed sensitivity state vectors $\forall i = 1, \ldots, I$

$$m_{x,u_{ij}} = \left[\frac{\partial^2 x_1}{\partial u_i \partial u_j}, \ldots, \frac{\partial^2 x_D}{\partial u_i \partial u_j}\right]^{\mathrm{T}}, \tag{3.14}$$
$$m_{y,u_{ij}} = \left[\frac{\partial^2 y_1}{\partial u_i \partial u_j}, \ldots, \frac{\partial^2 y_A}{\partial u_i \partial u_j}\right]^{\mathrm{T}}.$$

Again, following an approach analogous to the first-order sensitivities, we get the following DAE model that governs the evolution of the mixed sensitivities:

$$\begin{aligned}
\frac{d}{dt} m_{x,u_{ij}} =& \nabla_x g \cdot m_{x,u_{ij}} + \nabla_y g \cdot m_{y,u_{ij}} + \frac{\partial \nabla_x g}{\partial u_j} \cdot f_{x,u_i} + \frac{\partial \nabla_y g}{\partial u_j} \cdot f_{y,u_i} + \frac{\partial^2 g}{\partial u_i \partial u_j} \\
&+ \left[(1_D \otimes f_{x,u_i})^{\mathrm{T}}\right]^{\dagger} \left[\nabla_x^2 g_1, \ldots, \nabla_x^2 g_p\right]^{\dagger} (1_D \otimes f_{x,u_j}) \\
&+ \left[(1_A \otimes f_{y,u_i})^{\mathrm{T}}\right]^{\dagger} \left[\nabla_y^2 g_1, \ldots, \nabla_y^2 g_p\right]^{\dagger} (1_A \otimes f_{y,u_j}), \\
0 =& \nabla_x h \cdot m_{x,u_{ij}} + \nabla_y h \cdot m_{y,u_{ij}} + \frac{\partial \nabla_x h}{\partial u_j} \cdot f_{x,u_i} + \frac{\partial \nabla_y h}{\partial u_j} \cdot f_{y,u_i} + \frac{\partial^2 h}{\partial u_i \partial u_j} \\
&+ \left[(1_D \otimes f_{x,u_i})^{\mathrm{T}}\right]^{\dagger} \left[\nabla_x^2 h_1, \ldots, \nabla_x^2 h_q\right]^{\dagger} (1_D \otimes f_{x,u_j}) \\
&+ \left[(1_A \otimes f_{y,u_i})^{\mathrm{T}}\right]^{\dagger} \left[\nabla_y^2 h_1, \ldots, \nabla_y^2 h_q\right]^{\dagger} (1_A \otimes f_{y,u_j}),
\end{aligned} \tag{3.15}$$

where $\frac{\partial^2 g}{\partial u_i \partial u_j}$ is given by

$$\frac{\partial^2 g}{\partial u_i \partial u_j} = \left[\tfrac{\partial^2 g_1}{\partial u_i \partial u_j}, \tfrac{\partial^2 g_2}{\partial u_i \partial u_j}, \ldots, \tfrac{\partial^2 g_D}{\partial u_i \partial u_j}\right]^{\mathrm{T}}, \tag{3.16}$$

with all entries evaluated for $u = \overline{u}$. Entries of $\frac{\partial^2 h}{\partial u_i \partial u_j}$ follow similarly and are not reported for conciseness. Simulating the DAE model composed of copies of (3.15) $\forall i, j$ yields all entries in the set (3.4). More details on the derivation to obtain (3.15) are provided in Appendix A.

To summarize, in addition to simulating (2.1) for $u = \overline{u}$, we also simulate the DAEs given in (3.11), (3.13), and (3.15). These dynamics provide all entries in the sets (3.2), (3.3), and (3.4). With this information, we can approximate at any instant t the state variable z_i with the Taylor-series expansion in (3.1).

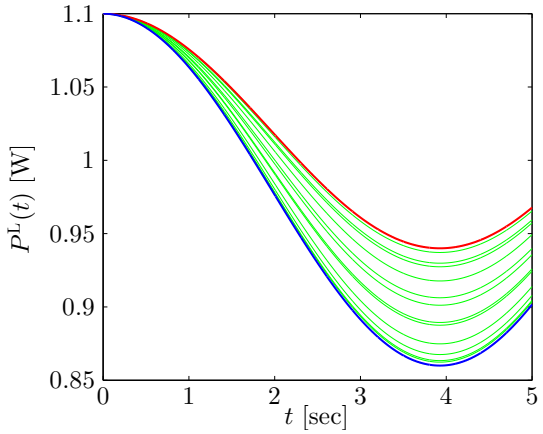

Figure 3.1: Profile of real-power load, P^{L}.

Example 3 *(Continued from Example 1) With reference to the power-system DAE model presented in* (2.9)*, we assume that the real-power component of the PQ load at bus* 2*,* P^{L}*, is time varying, and described by the following sinusoidal function:*

$$P^{\mathrm{L}} = p_0 + (1 - p_1) + (p_2 - (1 - p_1))\cos(0.8t), \tag{3.17}$$

where p_0 *and* p_2 *are constants. The value of* p_1 *is assumed to be unknown but bounded (i.e.,* $u = p_1$*), with nominal value* $\overline{u} = \overline{p}_1$ *and percentage uncertainty* ρ*. In Fig 3.1, we show 200 realizations of* P *in green lines corresponding to different values of* p_1 *in the range* $\left[\overline{p}_1\left(1 - \frac{\rho}{100}\right), \overline{p}_1\left(1 + \frac{\rho}{100}\right)\right]$ *sampled from a uniform distribution. (All model-parameter values are reported in Appendix B.1.) Red and blue lines denote the worst-case bounds on* P^{L}*. The model adopted for* P^{L} *is without loss of generality, and here, it is intended to represent the scenario of increasing uncertainty in accurately forecasting the load. Based on* (3.2)-(3.3)*, the first-, and second-order sensitivity variables for the DAE model in* (2.9) *are given below:*

$$f_{x,u} = [f_{x_1,u}, f_{x_2,u}]^{\mathrm{T}} := \left[\frac{\partial \delta}{\partial p_1}, \frac{\partial \omega}{\partial p_1}\right]^{\mathrm{T}}, \tag{3.18a}$$

$$f_{y,u} = [f_{y_1,u}, f_{y_2,u}]^{\mathrm{T}} := \left[\frac{\partial |V_3|}{\partial p_1}, \frac{\partial \theta_3}{\partial p_1}\right]^{\mathrm{T}}, \tag{3.18b}$$

$$s_{x,u} = [s_{x_1,u}, s_{x_2,u}]^{\mathrm{T}} := \left[\frac{\partial^2 \delta}{\partial p_1^2}, \frac{\partial^2 \omega}{\partial p_1^2}\right]^{\mathrm{T}}, \tag{3.18c}$$

$$s_{y,u} = [s_{y_1,u}, s_{y_2,u}]^{\mathrm{T}} := \left[\frac{\partial^2 |V_3|}{\partial p_1^2}, \frac{\partial^2 \theta_3}{\partial p_1^2}\right]^{\mathrm{T}}. \tag{3.18d}$$

Note that there are no mixed sensitivities in this case since we have a single uncertainty in the model. For the DAE in (2.9)*, we can express the dynamics for the first-order sensitivity variables in* (3.18a)–(3.18b) *in the general form* (3.11)*, where*

$$\nabla_x g = \begin{bmatrix} 0 & 1 \\ -\frac{|E||\overline{V}_3|\cos(\bar{\delta}-\bar{\theta}_3)}{MX_M} & -\frac{D}{M} \end{bmatrix},$$

$$\nabla_x h = \begin{bmatrix} -\frac{|E||\overline{V}_3|\cos(\bar{\delta}-\bar{\theta}_3)}{X_M} & 0 \\ \frac{|E||\overline{V}_3|\sin(\bar{\delta}-\bar{\theta}_3)}{X_M} & 0 \end{bmatrix},$$

$$\nabla_y g = \begin{bmatrix} 0 & 0 \\ -\frac{|E||\overline{V}_3|\sin(\bar{\delta}-\bar{\theta}_3)}{MX_M} & \frac{|E||\overline{V}_3|\cos(\bar{\delta}-\bar{\theta}_3)}{MX_M} \end{bmatrix},$$

$$\nabla_y h = \begin{bmatrix} -\frac{|E||\overline{V}_3|\sin(\bar{\delta}-\bar{\theta}_3)}{X_M} + \frac{\sin(\bar{\theta}_3)}{X_L} & \frac{|E||\overline{V}_3|\cos(\bar{\delta}-\bar{\theta}_3)}{X_M} + \frac{|\overline{V}_3|\cos(\bar{\theta}_3)}{X_L} \\ \frac{2|\overline{V}_3|}{X_M} + \frac{2|\overline{V}_3|}{X_L} + \frac{|E|\cos(\bar{\delta}-\bar{\theta}_3)}{X_M} - \frac{\cos(\bar{\theta}_3)}{X_L} & \frac{|E||\overline{V}_3|\sin(\bar{\delta}-\bar{\theta}_3)}{X_M} + \frac{|\overline{V}_3|\sin(\bar{\theta}_3)}{X_L} \end{bmatrix},$$

$$\frac{\partial h}{\partial u} = \begin{bmatrix} -1 + \cos(0.8t) & 0 \end{bmatrix}^{\mathrm{T}},$$

$$\frac{\partial g}{\partial u} = \begin{bmatrix} 0 & 0 \end{bmatrix}^{\mathrm{T}}.$$

We refrain from reporting the dynamics of the second-order sensitivities due to space constraints. ■

3.3 Computing Bounds on System States

In this section, we demonstrate that the problems in (3.5) are QCQPs. Then, we leverage SDP relaxations to solve them.

3.3.1 Formulation of QCQP Problems

Given the dynamical system (2.1), the DAE model that captures the dynamics of the sensitivity variables in (3.11), (3.13) and (3.15), and the second-order Taylor-series approximation (3.1), the problems in (3.5) can be written explicitly as the following QCQPs:

$$z_i^{\max}(t) \;=\; \max_{u} \quad \begin{bmatrix}1\\ u\end{bmatrix}^{\mathrm{T}} M_i(t) \begin{bmatrix}1\\ u\end{bmatrix} \tag{3.19a}$$

$$\text{s.t.} \quad \begin{bmatrix}1\\ u\end{bmatrix}^{\mathrm{T}} C_k \begin{bmatrix}1\\ u\end{bmatrix} \leq 0, k = 1, \ldots, I. \tag{3.19b}$$

$$z_i^{\min}(t) \;=\; \min_{u} \quad \begin{bmatrix}1\\ u\end{bmatrix}^{\mathrm{T}} M_i(t) \begin{bmatrix}1\\ u\end{bmatrix} \tag{3.20a}$$

$$\text{s.t.} \quad \begin{bmatrix}1\\ u\end{bmatrix}^{\mathrm{T}} C_k \begin{bmatrix}1\\ u\end{bmatrix} \leq 0, k = 1, \ldots, I. \tag{3.20b}$$

The objective functions in (3.19a) and (3.20a) boil down to the Taylor-series approximation in (3.1) with the choice

$$M_i(t) = \begin{bmatrix} \overline{z}_i(t, \overline{u}) - J_i\overline{u} + \frac{1}{2}\overline{u}^{\mathrm{T}} H_i \overline{u} & \frac{1}{2}\left(J_i - \overline{u}^{\mathrm{T}} H_i\right) \\ \frac{1}{2}\left(J_i - \overline{u}^{\mathrm{T}} H_i\right)^{\mathrm{T}} & \frac{1}{2} H_i \end{bmatrix}. \tag{3.21}$$

With reference to the constraints in (3.19b) and (3.20b), we define

$$C_k = \begin{bmatrix} -\overline{u}_k^2 \left(\left(\frac{\rho_k}{100}\right)^2 - 1\right) & B \\ B^{\mathrm{T}} & D \end{bmatrix}, \; k = 1, \ldots, I, \tag{3.22}$$

where $B \in \mathbb{R}^{1\times I}$ is a vector with the kth entry equal to $-\overline{u}_k$ and all other entries equal to 0, and $D \in \mathbb{R}^{I\times I}$ is a matrix with the kth diagonal entry equal to 1 and all other entries equal to 0. With this choice for C_k, the kth constraint is represented as $(u_k - \overline{u}_k)^2 \leq \left(\frac{\rho_k}{100}\overline{u}_k\right)^2$, which is a surrogate to (2.8).

Notice that we do not have any a priori guarantees on the positive/negative definiteness of $M_i(t)$. This motivates the development of SDP relaxations to bound the solutions of the QCQPs in (3.19)–(3.20). We discuss this next.

3.3.2 SDP Relaxation of QCQP Problems

We can obtain upper and lower bounds to the optimal solutions of (3.19) and (3.20)—quantities we denote by $\overline{z}_i^{\max}(t)$ and $\overline{z}_i^{\min}(t)$, respectively—by solving the following SDPs:

$$\begin{aligned} \overline{z}_i^{\max}(t) \;=\; & \min_{\gamma\in\mathbb{R},\,\{\lambda_k\}_{k=1}^{I}} \gamma \\ & \text{s.t. } \begin{bmatrix}\gamma & 0\\ 0 & 0_I\end{bmatrix} - M_i(t) - \sum_{k=1}^{I}\lambda_k C_k \succeq 0 \\ & \lambda_k \geq 0,\, k=1,\ldots,I. \end{aligned} \tag{3.23}$$

$$\begin{aligned} \overline{z}_i^{\min}(t) \;=\; & \max_{\gamma\in\mathbb{R},\,\{\lambda_k\}_{k=1}^{I}} \gamma \\ & \text{s.t. } -\begin{bmatrix}\gamma & 0\\ 0 & 0_I\end{bmatrix} + M_i(t) - \sum_{k=1}^{I}\lambda_k C_k \succeq 0 \\ & \lambda_k \geq 0,\, k=1,\ldots,I. \end{aligned} \tag{3.24}$$

In particular, we can guarantee that $\overline{z}_i^{\max}(t) \geq z_i^{\max}(t)$, and $\overline{z}_i^{\min}(t) \leq z_i^{\min}(t)$. The SDPs in (3.23)–(3.24) follow from (3.19)–(3.20) via a Lagrangian relaxation and weak duality [70, 74].

An alternate approach to tackle the QCQPs in (3.19)–(3.20) is to solve the following SDPs:

$$\begin{aligned} \widetilde{z}_i^{\min/\max}(t) \;=\; & \min/\max_{U\succeq 0, U_{11}=1} \operatorname{trace}\{M_i(t)U\} \\ & \text{s.t. } \operatorname{trace}\{C_k U\} \preceq 0,\; k=1,\ldots,I. \end{aligned} \tag{3.25}$$

To see this, begin by expressing the quadratic functions in (3.19)–(3.20) as $\operatorname{trace}\{M_i(t)U\}$ and $\operatorname{trace}\{C_k U\}$, with $U = \begin{bmatrix}1\\ u\end{bmatrix}\begin{bmatrix}1\\ u\end{bmatrix}^{\mathrm{T}}$. The formulation in (3.25) follows by recognizing that $U \succeq 0, U_{11} = 1$, and dropping the $\operatorname{rank}\{U\} = 1$ constraint. The SDPs in (3.23)-(3.24) and in (3.25) demonstrate strong duality, i.e., $\overline{z}_i(t)^{\min/\max} = \widetilde{z}_i(t)^{\min/\max}$ if there exist feasible solutions for both SDPs [74, 75].

The formulation in (3.23)–(3.24) suggests that the bounds have to be computed: i) for all dynamic/algebraic states, ii) at every time instant, and iii) over the entire

duration of the time-domain simulation. However, this might be overly cautious and the bounds could only be computed for pertinent states every few time steps of the numerical simulation, and only for a fraction of the total simulation horizon. (In all simulation results that follow, we compute the bounds for every time step of the simulation, but in Fig. 3.6(c) we demonstrate how the bounds can be computed only for a short time horizon.) For a given system, the total number of SDPs that need to be solved is twice the product of the number of states of interest and the number of time steps corresponding to the duration of interest (the factor of two comes from the fact that for each state we solve a problem for the minimum and one for the maximum).

Example 4 *(Continued from Examples 1 and 3)*

Recall the DAE model presented for the SMIB system in Example 1. The real-power load at bus 3 is uncertain (realizations are plotted in Fig. 3.1), and we are interested in estimating minimum and maximum bounds on the dynamic states δ, ω, and algebraic states $|V_3|$, θ_3. Leveraging the approach outlined in Section 3.2, we simulate the dynamics of the sensitivity variables in (3.18) *so that the Taylor-series approximation in* (3.1) *can be obtained for each state in $z = [\delta, \omega, |V_3|, \theta_3]^{\mathrm{T}}$. Next, we solve (at each instant)* 8 *optimization problems (*4 *states* $\times$ 2 *problems per state for the minimum and maximum values). The optimization problem for the maximum value of each state is given in* (3.23)*, and the problem to compute the minimum of each state is the one given in* (3.24)*. For z_i, the matrix M_i in* (3.21) *(which defines the objective function) and the matrix C in* (3.22) *(which defines the constraint equation) are given by*

$$M_i = \begin{bmatrix} \overline{z}_i - f_{z_i,u}\overline{p}_1 + \frac{1}{2}s_{z_i,u} & \frac{1}{2}\Big(f_{z_i,u} - \overline{p}_1 s_{z_i,u}\Big) \\ \frac{1}{2}\Big(f_{z_i,u} - \overline{p}_1 s_{z_i,u}\Big) & \frac{1}{2}s_{z_i,u} \end{bmatrix}, \tag{3.26}$$

$$C = \begin{bmatrix} -\overline{p}_1^2\left((\frac{\rho}{100})^2 - 1\right) & -\overline{p}_1 \\ -\overline{p}_1 & 1 \end{bmatrix}. \tag{3.27}$$

Figures 3.2(a) and 3.2(d) show the estimated minimum and maximum bounds on δ, ω (dynamic states) and θ_3, $|V_3|$ (algebraic states) in solid blue and solid red, respectively. The bounds are superimposed to results of repeated time-domain simulations of the original DAE model in (2.9) *for* 200 *different realizations of the load P^{L} shown in green traces in Fig. 3.1. These results establish the validity of the proposed method.*

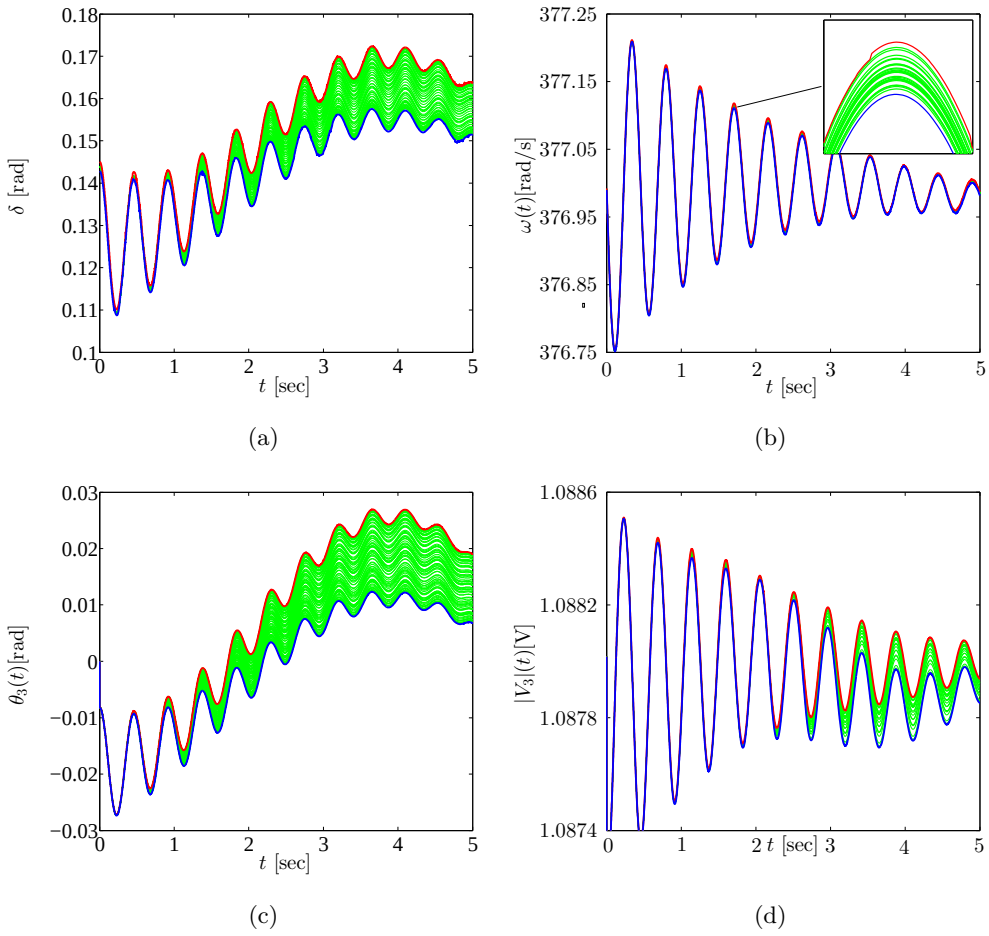

Figure 3.2: Result of bound estimation for SMIB DAE Model.

Next, we depart from the uncertainty model adopted for P^{L}*, and discuss how the approach performs as the number of uncertain elements is changed. Figures 3.3(a)-3.3(d) show the results for different number of uncertain elements (1, 3, 5, and 10 in (a), (b), (c), (d), respectively) for generator frequency,* ω*, in the SMIB system. In each plot, estimated upper/lower bounds (red and blue lines) are superimposed to repeated time-domain simulations (green lines with extrema in bold) for different uncertainty variables:* $u = P$ *in Fig. 3.3(a),* $u = [P, D, P^{\mathrm{L}}]^{\mathrm{T}}$ *in Fig. 3.3(b),* $u = [P, D, P^{\mathrm{L}}, Q^{\mathrm{L}}, |V_2|]^{\mathrm{T}}$ *in Fig. 3.3(c), and* $u = [P, D, P^{\mathrm{L}}, Q^{\mathrm{L}}, |E|, |V_2|, \theta_2, M, X_L, X_M]^{\mathrm{T}}$ *in Fig. 3.3(d). (See Appendix B for details.) As expected, we see that as the number of uncertain elements increase, the bounds become more conservative; this could conceivably be addressed with higher-order Taylor-series approximations. The computation time for our approach in the three cases is* $3.34, 8.48, 15.39, 144.91$ [sec] *and that for* 600 *repeated simulations is* $264.78, 271.12, 273.95, 266.66$ [sec]*. Again, as expected with increasing number of uncertain parameters, the computational burden is increased.* ■

The proposed method is summarized in the block diagram shown in Fig. 3.4. This figure depicts all the approximations and relaxations, including: i) the formulation of the 2nd-order Taylor series approximation, ii) formulation of the QCQP to estimate bounds on the state variables, and iii) SDP relaxation of the QCQP problem. We provide some remarks on the approximations and their impact in each step next. For the second-order Taylor approximation, the approximation error is bounded in Lagrangian form by the remainder term in Taylor's theorem [76]. To obtain the QCQP, constraints in uncertainty variables are transformed into quadratic functions. The solutions of the SDPs provide guaranteed bounds to those of the QCQPs [70, 74].

To demonstrate scalability of the approach to realistic power-system dynamic models, we next document results from simulations performed for the IEEE 39-bus New England test system. In so doing, we validate the accuracy of the approach and investigate possible errors and conservatism introduced due to the approximations and relaxations adopted in the approach. We also highlight some unique features of the method, such as the ability to compute the bounds on predefined time intervals.

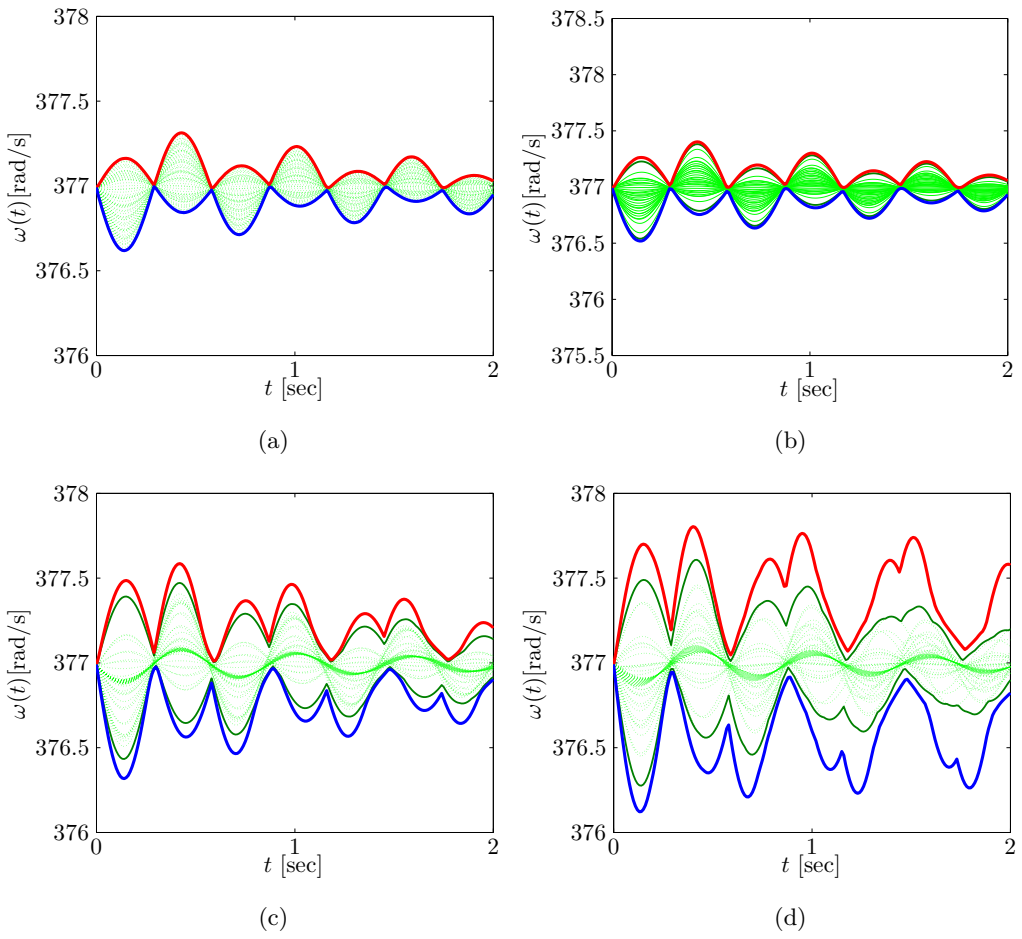

Figure 3.3: Estimated upper/lower bounds for different number of uncertainty variables.

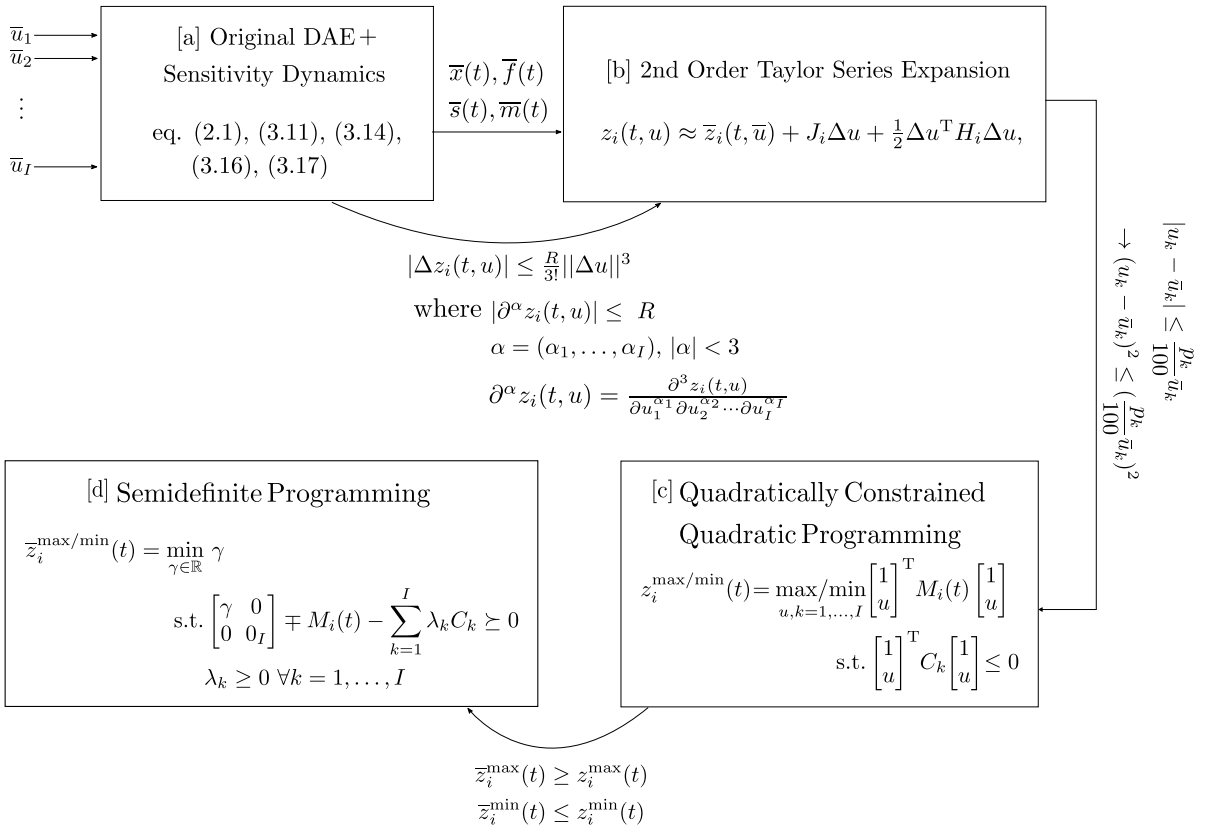

Figure 3.4: Overview of the steps of the proposed method described in this Chapter for estimating the upper/lower bounds on the system states.

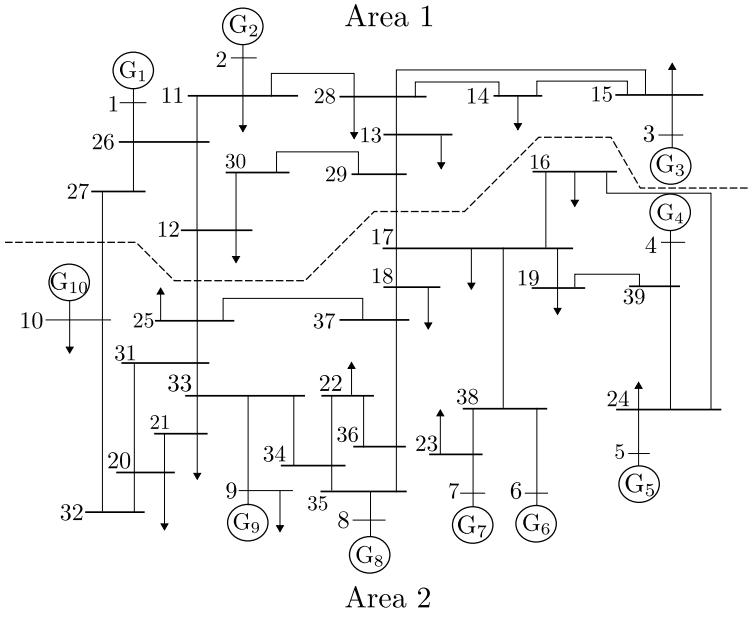

Figure 3.5: One-line diagram of the New England test system.

3.4 Numerical Case Study

We demonstrate the scalability and accuracy of our approach with simulations performed for the New England Power System. This system is composed of 10 generators and 39 buses, and the corresponding DAE model has 32 dynamic and 58 algebraic states. Figure 3.5 depicts a one-line diagram: generators are at buses $1, \ldots, 10$, and non-zero constant-power loads are at buses $9, \ldots, 25$. For the purposes of Automatic Generation Control (AGC), we divide the system into two balancing areas. Area 1 has generators $1, 2, 3$, while Area 2 has generators $4, \ldots, 10$. We acknowledge multiple sources of uncertainty in inputs and parameters; particularly, we model uncertainty in a generator damping constant, an economic-dispatch signal, and a real-power load.

We begin this section with a description of the DAE model for the system. Following this, we describe the uncertainty model, and then present some pertinent results from numerical simulations.

3.4.1 Power-system DAE Model

The DAE model includes a three-state model for the synchronous generators, controller dynamics to implement AGC, and the algebraic power-balance equations.

Synchronous-generator Electromechanical Dynamics

We adopt a three-state model for the electromechanical dynamics of the synchronous generators in the system. Following [77], for the ith generator, we model the evolution of the rotor electrical angle, δ_i (with respect to a rotating reference frame at $\omega_{\rm s}$), rotor electrical frequency, ω_i, and turbine power, P_i, with the following dynamics:

$$\frac{d\delta_i}{dt} = \omega_i - \omega_{\rm s}, \tag{3.28a}$$

$$M_i \frac{d\omega_i}{dt} = P_i - P_i^{\rm G} - D_i(\omega_i - \omega_{\rm s}), \tag{3.28b}$$

$$\tau_i \frac{dP_i}{dt} = -(P_i - P_i^{\rm ref}) - \frac{1}{\omega_{\rm s} r_i}(\omega_i - \omega_{\rm s}), \tag{3.28c}$$

where M_i is the inertia constant, D_i is the damping coefficient, τ_i is the governor time constant, and r_i is the slope of the speed-droop characteristic. In (3.28c), $P_i^{\rm ref}$ is the reference power for the ith generator (we discuss how this is computed in the next section), and in (3.28b), $P_i^{\rm G}$ is the output real power of the ith generator, and it is given by

$$P_i^{\rm G} = {\rm Re}\Big\{ |E_i| \angle \delta_i \sum_{j \in \mathcal{G}_i} Y_{ij}^* |V_j| \angle - \theta_j \Big\} + P_i^{\rm L},$$

where $|E_i|$ is the machine terminal voltage, Y_{ij} is the (i,j) entry of the network's admittance matrix, $P_i^{\rm L}$ is the active power of the load at bus i, $|V_j|\angle\theta_j$ is the voltage phasor at bus j, and $\mathcal{G}_i$ is the set of all buses connected to the generator at bus i. The three-state model in (3.28) has been utilized to study time frames of interest for AGC [77, 78]. Indeed, more detailed models incorporating dynamics of, e.g., voltage regulators, exciters, and damper windings, can be investigated depending on the time scales of interest.

Algebraic Power-balance Equations

Real- and reactive-power balance at load buses (i.e., buses $11, \ldots, 39$) is captured by the following algebraic power-flow equations:

$$0 = \mathrm{Re}\Big\{|V_i|\angle\theta_i \sum_{j\in\mathcal{N}_i} Y_{ij}^*|V_j|\angle-\theta_j\Big\} + P_i^{\mathrm{L}}, \tag{3.29a}$$

$$0 = \mathrm{Im}\Big\{|V_i|\angle\theta_i \sum_{j\in\mathcal{N}_i} Y_{ij}^*|V_j|\angle-\theta_j\Big\} + Q_i^{\mathrm{L}}, \tag{3.29b}$$

where P_i^{L} and Q_i^{L} are the active and reactive power of the load at bus i (they are set to zero if there is no PQ load at bus i), and $\mathcal{N}_i$ is the set of all buses connected to the load at bus i.

Automatic Generation Control

For AGC, notice from Fig. 3.5 that we divide the system into two balancing areas. Consider the following controller dynamics for area k

$$\frac{d\xi_k}{dt} = \mathrm{ACE}_k - \sum_{j\in\mathcal{G}_k}\Big(P_j^{\mathrm{ref}} - P_j^{\mathrm{G}}\Big), \tag{3.30}$$

where $\mathcal{G}_k$ is the set that collects all generators in area k (i.e., $\mathcal{G}_1 = \{1,2,3\}$, and $\mathcal{G}_2 = \{4,\ldots,10\}$). The Area Control Error (ACE) for area k is denoted by ACE_k, and given by:

$$\mathrm{ACE}_k = \sum_{j\in\mathcal{A}_k}\Big(P_{kj} - P_{kj}^{\mathrm{sch}}\Big) - b_k\Big(\frac{1}{|\mathcal{G}_k|}\sum_{j\in\mathcal{G}_k}\omega_j - \omega_{\mathrm{s}}\Big), \tag{3.31}$$

where $\mathcal{A}_k$ is the set representing all neighboring balancing areas connected to area k by tie lines, $|\mathcal{G}_k|$ is the cardinality of $\mathcal{G}_k$, P_{kj} is the sum of all active-power flows from area k to j, P_{kj}^{sch} is the scheduled power flow from area k to j, and b_k is the bias factor for area k. The reference power for the i generator, P_i^{ref} is then determined as:

$$P_i^{\mathrm{ref}} = P_i^{\mathrm{ed}} + a_i\Big(\xi_k - \sum_{j\in\mathcal{G}_k} P_j^{\mathrm{ed}}\Big),$$

where P_i^{ed} is the economically-dispatched power reference for the ith generator, and a_i is the ACE participation factor.

With reference to the DAE model in (2.1), the generator and AGC dynamics in (3.28) and (3.30), respectively, constitute the differential equations in the model, and the

power-balance expressions in (3.29) are the algebraic equations. In all, we have $D = 32$ dynamic states: $\{\delta_i\}_{i=1}^{10}$, $\{\omega_i\}_{i=1}^{10}$, $\{\xi_i\}_{i=1}^{2}$; and $A = 58$ algebraic states: $\{V_i\}_{i=1}^{29}$, $\{\theta_i\}_{i=1}^{29}$.

3.4.2 Uncertainty Model

We consider three sources of uncertainty in the DAE model described above. Particularly, we assume that the economic-dispatch signal for generator 4, P_4^{ed}, the damping constant of generator 8, D_8, and the real-power drawn at bus 25, P_{25}^{L}, are all unknown but bounded around known nominal values. The choice of uncertain variables demonstrates the ability of our approach in contending with both input uncertainty (P_4^{ed} and P_{25}^{L}), and parametric uncertainty (D_8). We assume $\pm 30\%$ uncertainty in P_4^{ed}, P_{25}^{L}, and D_8.

3.4.3 Uncertainty Propagation

To propagate the impact of the parametric and input uncertainty discussed above to dynamic and algebraic states of interest in the model, we: i) leverage the approach outlined in Section 3.2 to simulate the dynamics of sensitivity variables; ii) build the Taylor-series approximation in (3.1); and iii) solve optimization problems given in (3.23) and (3.24).

Some representative results from the method described above are plotted in Figs. 3.6 (a)-(f). In each case, minimum and maximum bounds on the states—as obtained from our approach—are plotted in solid blue and solid red, respectively. Results from repeated time-domain solutions of the DAE model discussed in Section 3.4.1 for different values of the uncertain elements ($P_4^{\text{ed}}, P_{25}^{\text{L}}, D_8$) are shown in green lines. (Particularly, we sample 50 realizations from a uniform distribution.) Without loss of generality, we plot results for four dynamic states: the AGC control state for area 1, ξ_1, the electrical angle, frequency, and turbine power of generator 10, ω_{10}, δ_{10}, and P_{10}, respectively; and two algebraic states: the voltage magnitude and angle at bus 12, $|V_{12}|$ and θ_{12}, respectively.

The simulations are obtained by perturbing the angle of generator 1 from its equilibrium value. The simulations therefore capture the dynamics in a post-fault state which may have been triggered due to a loss of load or line.

The result in Fig. 3.6 (a) illustrates the effectiveness of our method. In particular, note that: i) the second-order Taylor-series approximation is accurate even for uncertainties as large as ±30%, and ii) the SDP relaxations (3.23)–(3.24) of the original QCQP problems (3.19)–(3.20) do not result in overly conservative upper and lower bounds on the states. Furthermore, the computation time was 109.3 [sec] for the repeated time-domain simulations, while it was 102 [sec] for the proposed method. (The computation time for the repeated time-domain simulations increases with the number of samples—it is 215.3 [sec] for 100 samples, 444.5 [sec] for 200 samples.)

In Fig 3.6 (b), we depict the bounds on the AGC control state in area 1, ξ_1 computed with the second-order Taylor-series approximation (in solid red and blue), and with a first-order Taylor-series approximation (in dashed red and blue). Since the first-order approximation indicates that the state is affinely related to the uncertain inputs/parameters, the maximum and minimum bounds on the state can be obtained by just sampling the vertices of the set $\mathcal{U}$ [27]. Furthermore, for this approach, we have to only simulate the first-order sensitivity dynamics in (3.11). However, we see that the reduced computational and simulation burden comes with the cost of poor accuracy in estimating the maximum and minimum values.

Figure 3.6 (c) illustrates that the bounds on the states can be selectively estimated for a given time horizon by solving (3.23)–(3.24) only over that horizon. Here, we estimate bounds on the bus-voltage magnitude $|V_{12}|$ only over the period $[0.3, 3\,]$[sec]. In general, once the dynamics of the states and sensitivity variables are at hand, the optimization problems in (3.23)–(3.24) can be solved selectively to focus on particular time horizons of interest and only for the states of interest. This aspect can be leveraged to reduce computational burden.

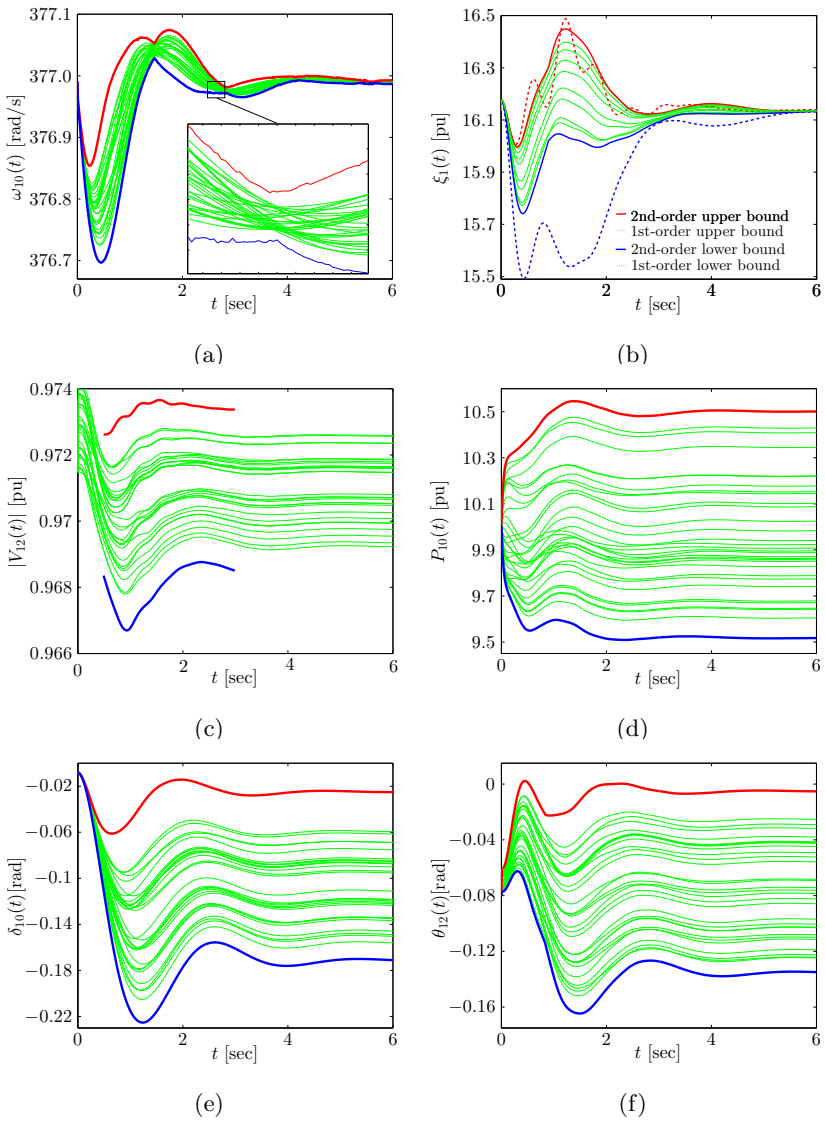

Figure 3.6: Simulation results for the New England system.

Chapter 4

Uncertainty Propagation in Power Flow

In this chapter, we develop an optimization-based method to propagate input and parametric uncertainty to the power flow solution. The approach is based on maximizing and minimizing quadratic approximations of the power-flow states as a function of the uncertainties subject to inequality constraints that capture all possible values the uncertain elements can take. A major computational bottleneck in such an approach is that the formulation of the quadratic approximations requires the solution of sensitivities (up to second order) from algebraic equations that are derived from the power flow equations. We demonstrate how decoupling assumptions based on the form and function of power networks can be applied to facilitate computations in this regard. The formulated quadratic programs are non-convex in general, and we adopt the ADMM to solve them. Conditions for convergence in this non-convex setting are established leveraging recent advances in optimization theory.

The remainder of this chapter is organized as follows. In Section 4.1, we formulate quadratic expressions for the algebraic variables of the power-flow equations. In Section 4.2, we derive the algebraic equations that yield the sensitivities to formulate the quadratic approximations for the states. In Section 4.3, we present the decoupling assumptions to improve computation for sensitivity equations. In Section 4.4, we formulate the task of estimating minimum and maximum bounds on the states as nonconvex

quadratic programs, and highlight the ADMM algorithm to solve the problems. In Section 4.5, numerical simulations for the MATPOWER 1354-bus test system are provided to validate the accuracy and demonstrate the scalability of the approach.

4.1 Quadratic Approximation of Algebraic Variables

We are interested in finding upper and lower bounds on the solutions of the power-flow balance equations in (2.6) given $u \in \mathcal{U}$. Particularly, for the ℓth algebraic state, x_ℓ, with $u \in \mathcal{U}$, we are interested in computing:

$$x_\ell^{\min} := \min_{u \in \mathcal{U}} \; x_\ell(u), \quad x_\ell^{\max} := \max_{u \in \mathcal{U}} \; x_\ell(u). \tag{4.1}$$

The above problems are challenging because there exist no analytical closed-form expressions for $x_\ell(u)$ due to the nonlinear nature of the power-flow equations. Furthermore, it is computationally infeasible to get the above bounds by extensively searching the space $\mathcal{U}$ especially if many uncertainties are to be acknowledged. As discussed in the introduction, we approach this problem based on a quadratic approximation of $x_\ell(u)$. In particular, we approximate the ℓ-th state with the following second-order Taylor-series approximation around $u = \overline{u}$:

$$x_\ell(u) \approx \overline{x}_\ell(\overline{u}) + J_\ell \Delta u + \frac{1}{2} \Delta u^{\mathrm{T}} H_\ell \Delta u, \tag{4.2}$$

where $\overline{x}_\ell(\overline{u})$ is the ℓth element of the solution to (2.6) for $u = \overline{u}$, $\Delta u := u - \overline{u}$, and $J_\ell \in \mathbb{R}^{1 \times I}$ and $H_\ell \in \mathbb{R}^{I \times I}$ are given by

$$J_\ell = \left[\frac{\partial x_\ell}{\partial u_1}, \ldots, \frac{\partial x_\ell}{\partial u_I} \right], H_\ell = \begin{bmatrix} \frac{\partial^2 x_\ell}{\partial u_1^2} & \cdots & \frac{\partial^2 x_\ell}{\partial u_1 \partial u_I} \\ \vdots & \ddots & \vdots \\ \frac{\partial^2 x_\ell}{\partial u_I \partial u_1} & \cdots & \frac{\partial^2 x_\ell}{\partial u_I^2} \end{bmatrix}, \tag{4.3}$$

where the values of the entries are evaluated at $u = \overline{u}$.

Example 5 (continued from Example 2) *In this example, we return to the system introduced in Example 2, and formulate the quadratic approximations of the algebraic*

states, $|V_2|$, θ_2, and indicate the corresponding entries of J_ℓ and H_ℓ. From the power-balance expressions in (2.10)*, we get:*

$$\begin{aligned} |V_2| = x_1 &\approx \overline{x}_1(\overline{u}) + J_1 \Delta u + \frac{1}{2}\Delta u^{\mathrm{T}} H_1 \Delta u, \\ \theta_2 = x_2 &\approx \overline{x}_2(\overline{u}) + J_2 \Delta u + \frac{1}{2}\Delta u^{\mathrm{T}} H_2 \Delta u, \end{aligned} \tag{4.4}$$

with $J_1 = \left[\frac{\partial |V_2|}{\partial |V_1|}, \quad \frac{\partial |V_2|}{\partial P^{\mathrm{L}}}\right]$, $J_2 = \left[\frac{\partial \theta_2}{\partial |V_1|}, \quad \frac{\partial \theta_2}{\partial P^{\mathrm{L}}}\right]$,

$$H_1 = \begin{bmatrix} \frac{\partial^2 |V_2|}{\partial |V_1|^2} & \frac{\partial^2 |V_2|}{\partial P^{\mathrm{L}} \partial |V_1|} \\ \frac{\partial^2 |V_2|}{\partial |V_1| \partial P^{\mathrm{L}}} & \frac{\partial^2 |V_2|}{\partial P^{\mathrm{L}^2}} \end{bmatrix}, \; H_2 = \begin{bmatrix} \frac{\partial^2 \theta_2}{\partial |V_1|^2} & \frac{\partial^2 \theta_2}{\partial P^{\mathrm{L}} \partial |V_1|} \\ \frac{\partial^2 \theta_2}{\partial |V_1| \partial P^{\mathrm{L}}} & \frac{\partial^2 \theta_2}{\partial P^{\mathrm{L}^2}} \end{bmatrix},$$

and $\overline{x}_1(\overline{u}), \overline{x}_2(\overline{u})$ denoting the values of $|V_2|$ and θ_2 for the nominal values of P^{L} and $|V_1|$. ■

4.2 Formulation of Sensitivity Equations

Consider the first-order, second-order, and mixed partial derivatives of the state variables in terms of the uncertain inputs in the quadratic expansion (4.2). These terms are denoted by f_{u_i}, s_{u_i}, and $m_{u_{ij}}$, and they are formally defined below:

$$\begin{aligned} f_{u_i} &= [f_{1,u_i}, \ldots, f_{A,u_i}]^{\mathrm{T}} := \left[\frac{\partial x_1}{\partial u_i}, \ldots, \frac{\partial x_A}{\partial u_i}\right]^{\mathrm{T}}, \\ s_{u_i} &= [s_{1,u_i}, \ldots, s_{A,u_i}]^{\mathrm{T}} := \left[\frac{\partial^2 x_1}{\partial u_i^2}, \ldots, \frac{\partial^2 x_A}{\partial u_i^2}\right]^{\mathrm{T}}, \\ m_{u_{ij}} &= \left[m_{1,u_{ij}}, ..., m_{A,u_{ij}}\right]^{\mathrm{T}} := \left[\frac{\partial^2 x_1}{\partial u_i \partial u_j}, ..., \frac{\partial^2 x_A}{\partial u_i \partial u_j}\right]^{\mathrm{T}}. \end{aligned} \tag{4.5}$$

To get the values of f_{u_i}, s_{u_i}, and $m_{u_{ij}}$, we first assume that for the algebraic equations in (2.6), there exist continuous first- and second-order partial derivatives with respect to (x, u). Then, we have to solve the following set of algebraic equations for each

$k = 1, \ldots, A$ (derived by appropriately taking partial derivatives of (2.6)):

$$0 = \frac{\partial h_k}{\partial u_i} = \sum_{n=1}^{A} \frac{\partial h_k}{\partial x_n} f_{n,u_i} + \frac{\partial h_k}{\partial u_i}, \tag{4.6a}$$

$$0 = \frac{\partial^2 h_k}{\partial u_i^2} = \sum_{r=1}^{A} \frac{\partial^2 h_k}{\partial u_i \partial x_r} f_{r,u_i} + \frac{\partial^2 h_k}{\partial u_i^2} + \sum_{q=1}^{A} \Big(\frac{\partial h_k}{\partial x_q} s_{q,u_i} + \sum_{n=1}^{A} \frac{\partial^2 h_k}{\partial x_q \partial x_n} f_{q,u_i} f_{n,u_i} \Big), \tag{4.6b}$$

$$0 = \frac{\partial^2 h_k}{\partial u_i \partial u_j} = \sum_{r=1}^{A} \frac{\partial^2 h_k}{\partial u_j \partial x_r} f_{r,u_i} + \frac{\partial^2 h_k}{\partial u_i \partial u_j} + \sum_{q=1}^{A} \Big(\frac{\partial h_k}{\partial x_q} m_{q,u_{ij}} + \sum_{n=1}^{A} \frac{\partial^2 h_k}{\partial x_q \partial x_n} f_{q,u_i} f_{n,u_j} \Big). \tag{4.6c}$$

By defining $h := [h_1, \ldots, h_A]^{\mathrm{T}}$, we can obtain the following compact expressions from (4.6a)-(4.6c) for all $k = 1, \ldots, A$:[1]

$$0 = \nabla_x h \cdot f_{u_i} + \frac{\partial h}{\partial u_i}, \tag{4.7a}$$

$$0 = \nabla_x h \cdot s_{u_i} + \frac{\partial \nabla_x h}{\partial u_i} \cdot f_{u_i} + \frac{\partial^2 h}{\partial u_i^2} + \left[(1_A \otimes f_{u_i})^{\mathrm{T}} \right]^{\dagger} [\nabla_x^2 h_1, \ldots, \nabla_x^2 h_A]^{\dagger} (1_A \otimes f_{u_i}), \tag{4.7b}$$

$$0 = \nabla_x h \cdot m_{u_{ij}} + \frac{\partial \nabla_x h}{\partial u_j} \cdot f_{u_i} + \frac{\partial^2 h}{\partial u_i \partial u_j} + \left[(1_A \otimes f_{u_i})^{\mathrm{T}} \right]^{\dagger} [\nabla_x^2 h_1, \ldots, \nabla_x^2 h_A]^{\dagger} (1_A \otimes f_{u_j}), \tag{4.7c}$$

where

$$\nabla_x h = \begin{bmatrix} \frac{\partial h_1}{\partial x_1} & \cdots & \frac{\partial h_1}{\partial x_A} \\ \vdots & \ddots & \vdots \\ \frac{\partial h_A}{\partial x_1} & \cdots & \frac{\partial h_A}{\partial x_A} \end{bmatrix}, \nabla_x^2 h_i = \begin{bmatrix} \frac{\partial^2 h_i}{\partial x_1^2} & \frac{\partial^2 h_i}{\partial x_1 \partial x_2} & \cdots & \frac{\partial^2 h_i}{\partial x_1 \partial x_A} \\ \vdots & \vdots & \ddots & \vdots \\ \frac{\partial^2 h_i}{\partial x_A \partial x_1} & \frac{\partial^2 h_i}{\partial x_A \partial x_2} & \cdots & \frac{\partial^2 h_i}{\partial x_A^2} \end{bmatrix}.$$

Notice that, the quadratic approximation for any element of the solution to (2.6) is completely specified with the solution of pertinent sensitivity equations (4.7a)-(4.7c). We return to the system introduced in Examples 1 and 5 to illustrate the form of the auxiliary algebraic equations that yield pertinent sensitivities.

Example 6 (Continued from Example 2 and 5) *In this example, we will introduce the sensitivity equations for the system investigated in Example 2. The sensitivity*

[1] The notations for 1_N, $x \otimes y$, and $[X_1, X_2]^{\dagger}$ were defined in the footnote in Section 3.2.

variables in this case are

$$
\begin{aligned}
f_{u_1} &= \left[\tfrac{\partial|V_2|}{\partial|V_1|}, \quad \tfrac{\partial\theta_2}{\partial|V_1|}\right]^{\mathrm{T}}, f_{u_2} = \left[\tfrac{\partial|V_2|}{\partial P^{\mathrm{L}}}, \quad \tfrac{\partial\theta_2}{\partial P^{\mathrm{L}}}\right]^{\mathrm{T}}, \\
s_{u_1} &= \left[\tfrac{\partial^2|V_2|}{\partial|V_1|^2}, \quad \tfrac{\partial^2\theta_2}{\partial|V_1|^2}\right]^{\mathrm{T}}, s_{u_2} = \left[\tfrac{\partial^2|V_2|}{\partial P^{\mathrm{L}2}}, \quad \tfrac{\partial^2\theta_2}{\partial P^{\mathrm{L}2}}\right]^{\mathrm{T}}, \\
m_{u_{12}} &= \left[\tfrac{\partial^2|V_2|}{\partial|V_1|\partial P^{\mathrm{L}}}, \quad \tfrac{\partial^2\theta}{\partial|V_1|\partial P^{\mathrm{L}}}\right]^{\mathrm{T}}.
\end{aligned} \tag{4.8}
$$

Then, following the approach outlined in Section 4.2, we can construct the algebraic equations for the sensitivity that return the sensitivity variables as below:

$$0 = \nabla_x h \cdot f_{u_1} + \frac{\partial h}{\partial u_1}, \quad 0 = \nabla_x h \cdot f_{u_2} + \frac{\partial h}{\partial u_2}, \tag{4.9a}$$

$$0 = \nabla_x h \cdot s_{u_1} + \frac{\partial \nabla_x h}{\partial u_1} f_{u_1} + \begin{bmatrix} f_{u_1}^{\mathrm{T}} & 0 \\ 0 & f_{u_1}^{\mathrm{T}} \end{bmatrix} \begin{bmatrix} \nabla_x^2 h_1 & 0 \\ 0 & \nabla_x^2 h_2 \end{bmatrix} \begin{bmatrix} f_{u_1} \\ f_{u_1} \end{bmatrix}, \tag{4.9b}$$

$$0 = \nabla_x h \cdot s_{u_2} + \frac{\partial \nabla_x h}{\partial u_2} f_{u_2} + \begin{bmatrix} f_{u_2}^{\mathrm{T}} & 0 \\ 0 & f_{u_2}^{\mathrm{T}} \end{bmatrix} \begin{bmatrix} \nabla_x^2 h_1 & 0 \\ 0 & \nabla_x^2 h_2 \end{bmatrix} \begin{bmatrix} f_{u_2} \\ f_{u_2} \end{bmatrix},$$

$$0 = \nabla_x h \cdot m_{u_{12}} + \begin{bmatrix} f_{u_1}^{\mathrm{T}} & 0 \\ 0 & f_{u_1}^{\mathrm{T}} \end{bmatrix} \begin{bmatrix} \nabla_x^2 h_1 & 0 \\ 0 & \nabla_x^2 h_2 \end{bmatrix} \begin{bmatrix} f_{u_2} \\ f_{u_2} \end{bmatrix}, \tag{4.9c}$$

where

$$\nabla_x h = \begin{bmatrix} \frac{|V_1|}{X_L}\sin\theta_2 & \frac{|V_1|\cdot|V_2|}{X_L}\cos\theta_2 \\ \frac{2|V_2|}{X_L} - \frac{|V_1|}{X_L}\cos\theta_2 & \frac{|V_1|\cdot|V_2|}{X_L}\sin\theta_2 \end{bmatrix},$$

$$\nabla_x^2 h_1 = \begin{bmatrix} 0 & \frac{|V_1|}{X_L}\cos\theta_2 \\ \frac{|V_1|}{X_L}\cos\theta_2 & -\frac{|V_1|\cdot|V_2|}{X_L}\sin\theta_2 \end{bmatrix},$$

$$\nabla_x^2 h_2 = \begin{bmatrix} \frac{2}{X_L} & \frac{|V_1|}{X_L}\sin\theta_2 \\ \frac{|V_1|}{X_L}\sin\theta_2 & \frac{|V_1|\cdot|V_2|}{X_L}\cos\theta_2 \end{bmatrix},$$

$$\frac{\partial h}{\partial u_1} = \begin{bmatrix} \frac{|V_2|}{X_L}\sin\theta_2 \\ -\frac{|V_2|}{X_L}\cos\theta_2 \end{bmatrix}, \quad \frac{\partial h}{\partial u_2} = \begin{bmatrix} 1 \\ 0 \end{bmatrix}.$$

(Above, $|V_2|$ and θ_2 represent the voltage magnitude and phase angle obtained as solutions of the power-flow equations for the nominal values of uncertain inputs $|V_1|$ and P^{L}.) Solving the above equations, we can calculate the values of f_{u_1}, f_{u_2}, s_{u_1}, s_{u_2}, and $m_{u_{12}}$. ■

4.3 Decoupled Sensitivity Equations

In this section, we will leverage common insights about the form and function of bulk power systems to simplify the computation of (4.7a)–(4.7c). Particularly, we consider: i) Transmission-line conductances are negligible, and ii) Bus-voltage angle differences are close to zero. Note that these assumptions are the same as the ones adopted to develop the decoupled power-flow method [79]. In this power-flow solution method, the Jacobian matrix is decoupled into smaller sub-matrices to simplify computation; here, we also apply this idea to look at higher-order sensitivities.

We will first establish some helpful notation. Let us collect the A_p active-power balance equations from (2.6) in $h^p := \{h_1^p, \ldots, h_{A_p}^p\}$, and the A_q reactive-power balance equations from (2.6) in the set $h^q := \{h_1^q, \ldots, h_{A_q}^q\}$. Furthermore, let $\mathcal{V}$ and $\mathcal{T}$ denote sets collecting voltage magnitudes and phase angles, respectively. Also, express the sensitivity variables in (4.5) as:

$$f_{u_i} = \begin{bmatrix} f_{u_i}^{\mathcal{V}} \\ f_{u_i}^{\mathcal{T}} \end{bmatrix}, \; s_{u_i} = \begin{bmatrix} s_{u_i}^{\mathcal{V}} \\ s_{u_i}^{\mathcal{T}} \end{bmatrix}, \; m_{u_{ij}} = \begin{bmatrix} m_{u_{ij}}^{\mathcal{V}} \\ m_{u_{ij}}^{\mathcal{T}} \end{bmatrix}, \tag{4.10}$$

where $\{f_{u_i}^{\mathcal{V}}, s_{u_i}^{\mathcal{V}}, m_{u_{ij}}^{\mathcal{V}}\}$ and $\{f_{u_i}^{\mathcal{T}}, s_{u_i}^{\mathcal{T}}, m_{u_{ij}}^{\mathcal{T}}\}$ collect first-, second-order and mixed sensitivities of voltage magnitudes and phase angles, respectively. With the notation and assumptions above, we can show:

$$\begin{aligned} &\left\{ \begin{array}{l} \frac{\partial h_k^p}{\partial x_i} \approx 0, \, \forall x_i \in \mathcal{V} \\ \frac{\partial^2 h_k^p}{\partial x_i^2} \approx 0, \, \forall x_i \in \mathcal{V} \cup \mathcal{T} \end{array} \right\}, \quad \forall h_k^p \in h^p, \\ &\left\{ \begin{array}{l} \frac{\partial h_k^q}{\partial x_i} \approx 0, \, \forall x_i \in \mathcal{T} \\ \frac{\partial^2 h_k^q}{\partial x_i \partial x_j} \approx 0, \, \forall x_i \in \mathcal{V}, x_j \in \mathcal{T} \end{array} \right\}, \quad \forall h_k^q \in h^q. \end{aligned} \tag{4.11}$$

The approximations above follow from the fact that, when we ignore the conductance of the transmission lines, pertinent entries in the first-, second-order, and mixed derivatives of h_k are only a function of the sine of the phase-angle difference between buses. Using (4.10)-(4.11), we can reformulate the original sensitivity equations in (4.7a)-(4.7c)

as below:

$$0 = \nabla_{\mathcal{T}} h^p \cdot f^{\mathcal{T}}_{u_i} + \frac{\partial h^p}{\partial u_i}, \quad 0 = \nabla_{\mathcal{V}} h^q \cdot f^{\mathcal{V}}_{u_i} + \frac{\partial h^q}{\partial u_i}. \tag{4.12a}$$

$$\begin{aligned} 0 = {} & \frac{\partial^2 h^p}{\partial u_i^2} + \frac{\partial \nabla_{\mathcal{T}} h^p}{\partial u_i} \cdot f^{\mathcal{T}}_{u_i} + \nabla_{\mathcal{T}} h^p \cdot s^{\mathcal{T}}_{u_i} \\ & + \left[(1_{A_p} \otimes f^{\mathcal{T}}_{u_i})^{\mathrm{T}}\right]^{\dagger} \left[\nabla^2_{\mathcal{V}\mathcal{T}} h^p_1, \ldots, \nabla^2_{\mathcal{V}\mathcal{T}} h^p_{A_p}\right]^{\dagger} (1_{A_p} \otimes f^{\mathcal{V}}_{u_i}) \\ & + \left[(1_{A_p} \otimes f^{\mathcal{V}}_{u_i})^{\mathrm{T}}\right]^{\dagger} \left[\nabla^2_{\mathcal{T}\mathcal{V}} h^p_1, \ldots, \nabla^2_{\mathcal{T}\mathcal{V}} h^p_{A_p}\right]^{\dagger} (1_{A_p} \otimes f^{\mathcal{T}}_{u_i}), \\ 0 = {} & \frac{\partial^2 h^q}{\partial u_i^2} + \frac{\partial \nabla_{\mathcal{V}} h^q}{\partial u_i} \cdot f^{\mathcal{V}}_{u_i} + \nabla_{\mathcal{V}} h^q \cdot s^{\mathcal{V}}_{u_i} \\ & + \left[(1_{A_q} \otimes f^{\mathcal{T}}_{u_i})^{\mathrm{T}}\right]^{\dagger} \left[\nabla^2_{\mathcal{T}} h^q_1, \ldots, \nabla^2_{\mathcal{T}} h^q_{A_q}\right]^{\dagger} (1_{A_q} \otimes f^{\mathcal{T}}_{u_i}) \\ & + \left[(1_{A_q} \otimes f^{\mathcal{V}}_{u_i})^{\mathrm{T}}\right]^{\dagger} \left[\nabla^2_{\mathcal{V}} h^q_1, \ldots, \nabla^2_{\mathcal{V}} h^q_{A_q}\right]^{\dagger} (1_{A_q} \otimes f^{\mathcal{V}}_{u_i}). \end{aligned} \tag{4.12b}$$

$$\begin{aligned} 0 = {} & \frac{\partial^2 h^p}{\partial u_i \partial u_j} + \frac{\partial \nabla_{\mathcal{T}} h^p}{\partial u_j} \cdot f^{\mathcal{T}}_{u_i} + \nabla_{\mathcal{T}} h^p \cdot m^{\mathcal{T}}_{u_{ij}} \\ & + \left[(1_{A_p} \otimes f^{\mathcal{T}}_{u_i})^{\mathrm{T}}\right]^{\dagger} \left[\nabla^2_{\mathcal{V}\mathcal{T}} h^p_1, \ldots, \nabla^2_{\mathcal{V}\mathcal{T}} h^p_{A_p}\right]^{\dagger} (1_{A_p} \otimes f^{\mathcal{V}}_{u_j}) \\ & + \left[(1_{A_p} \otimes f^{\mathcal{V}}_{u_i})^{\mathrm{T}}\right]^{\dagger} \left[\nabla^2_{\mathcal{T}\mathcal{V}} h^p_1, \ldots, \nabla^2_{\mathcal{T}\mathcal{V}} h^p_{A_p}\right]^{\dagger} (1_{A_p} \otimes f^{\mathcal{T}}_{u_j}), \\ 0 = {} & \frac{\partial^2 h^q}{\partial u_i \partial u_j} + \frac{\partial \nabla_{\mathcal{V}} h^q}{\partial u_j} \cdot f^{\mathcal{V}}_{u_i} + \nabla_{\mathcal{V}} h^q \cdot m^{\mathcal{V}}_{u_{ij}} \\ & + \left[(1_{A_q} \otimes f^{\mathcal{T}}_{u_i})^{\mathrm{T}}\right]^{\dagger} \left[\nabla^2_{\mathcal{T}} h^q_1, \ldots, \nabla^2_{\mathcal{T}} h^q_{A_q}\right]^{\dagger} (1_{A_q} \otimes f^{\mathcal{T}}_{u_j}) \\ & + \left[(1_{A_q} \otimes f^{\mathcal{V}}_{u_i})^{\mathrm{T}}\right]^{\dagger} \left[\nabla^2_{\mathcal{V}} h^q_1, \ldots, \nabla^2_{\mathcal{V}} h^q_{A_q}\right]^{\dagger} (1_{A_q} \otimes f^{\mathcal{V}}_{u_j}). \end{aligned} \tag{4.12c}$$

Above, $\nabla_{\mathcal{T}} h^p$ and $\nabla_{\mathcal{V}} h^q$ ($\nabla^2_{\mathcal{T}} h^p$ and $\nabla^2_{\mathcal{V}} h^q$) are Jacobians (Hessians) of real- and reactive-power balance equations with respect to θ and V, respectively. Also, the matrix $\nabla^2_{\mathcal{V}\theta} h^p_k$ is given by:

$$\nabla^2_{\mathcal{V}\theta} h^p_k = \begin{bmatrix} \frac{\partial^2 h^p_k}{\partial |V_1| \partial \theta_1} & \frac{\partial^2 h^p_k}{\partial |V_2| \partial \theta_1} & \cdots & \frac{\partial^2 h^p_k}{\partial |V_{A_q}| \partial \theta_1} \\ \vdots & \vdots & \ddots & \vdots \\ \frac{\partial^2 h^p_k}{\partial |V_1| \partial \theta_{A_p}} & \frac{\partial^2 h^p_k}{\partial |V_1| \partial \theta_{A_p}} & \cdots & \frac{\partial^2 h^p_k}{\partial |V_{A_q}| \partial \theta_{A_p}} \end{bmatrix},$$

and $\nabla^2_{\theta\mathcal{V}} h^p_k = \left(\nabla^2_{\mathcal{V}\theta} h^p_k\right)^{\mathrm{T}}$. The first-, second-order and mixed sensitivity equations in (4.12a)–(4.12c) correspond to the decoupled versions of the original first-, second-order and mixed sensitivity equations in (4.7a)–(4.7c). The sensitivity equations in (4.12) present lesser computational burden compared to the original sensitivity equations

in (4.7). In particular, matrices $\nabla_{\mathcal{T}} h^p \in \mathbb{R}^{A_p \times A_p}$ and $\nabla_{\mathcal{T}} h^q \in \mathbb{R}^{A_q \times A_q}$ that appear in the reduced-order sensitivity equations have smaller dimension compared to $\nabla_x h \in \mathbb{R}^{A \times A}$ since $A_p < A$ and $A_q < A$. Similarly, matrices $\nabla^2_{\mathcal{V}\mathcal{T}} h^p_k \in \mathbb{R}^{A_p \times A_q}$, $\nabla^2_{\mathcal{V}} h^q_k \in \mathbb{R}^{A_q \times A_q}$ $\nabla^2_{\mathcal{T}} h^q_k \in \mathbb{R}^{A_p \times A_p}$ have smaller dimensions compared to $\nabla^2 h_k \in \mathbb{R}^{A \times A}$. The end result is that solving (4.12) requires less memory and fewer computations compared to (4.9), and this improves scalability.

Example 7 (Continued from Example 2, 5, and 6) *In this example, we will formulate the sensitivity equations using the decoupled power-flow assumptions for the system introduced in Example 2. First, we decompose the sensitivity variables in* (4.8) *using the notation in* (4.10) *to get:*

$$\begin{aligned}
f_{u_1} &= \left[f^{\mathcal{V}}_{u_1}, f^{\mathcal{T}}_{u_1}\right] = \left[\tfrac{\partial |V_2|}{\partial |V_1|}, \tfrac{\partial \theta_2}{\partial |V_1|}\right]^{\mathrm{T}}, \\
f_{u_2} &= \left[f^{\mathcal{V}}_{u_2}, f^{\mathcal{T}}_{u_2}\right] = \left[\tfrac{\partial |V_2|}{\partial P^{\mathrm{L}}}, \tfrac{\partial \theta_2}{\partial P^{\mathrm{L}}}\right]^{\mathrm{T}}, \\
s_{u_1} &= \left[s^{\mathcal{V}}_{u_1}, s^{\mathcal{T}}_{u_1}\right] = \left[\tfrac{\partial^2 |V_2|}{\partial |V_1|^2}, \tfrac{\partial^2 \theta_2}{\partial |V_1|^2}\right]^{\mathrm{T}}, \\
s_{u_2} &= \left[s^{\mathcal{V}}_{u_2}, s^{\mathcal{T}}_{u_2}\right] = \left[\tfrac{\partial^2 |V_2|}{\partial {P^{\mathrm{L}}}^2}, \tfrac{\partial^2 \theta_2}{\partial {P^{\mathrm{L}}}^2}\right]^{\mathrm{T}}, \\
m_{u_{12}} &= \left[m^{\mathcal{V}}_{u_{12}}, m^{\mathcal{T}}_{u_{12}}\right] = \left[\tfrac{\partial^2 |V_2|}{\partial |V_1| \partial P^{\mathrm{L}}}, \tfrac{\partial^2 \theta_2}{\partial |V_1| \partial P^{\mathrm{L}}}\right]^{\mathrm{T}}.
\end{aligned} \tag{4.13}$$

Also, let us define $h^p = h_1(x,u)$ *and* $h^q = h_2(x,u)$. *For this case, the sensitivity equations in* (4.9) *boil down to*

$$0 = \nabla_{\mathcal{T}} h^p \cdot f^{\mathcal{T}}_{u_1} + \frac{\partial h^p}{\partial u_1}, \quad 0 = \nabla_{\mathcal{T}} h^p \cdot f^{\mathcal{T}}_{u_2} + \frac{\partial h^p}{\partial u_2}, \tag{4.14a}$$

$$0 = \nabla_{\mathcal{V}} h^q \cdot f^{\mathcal{V}}_{u_1} + \frac{\partial h^q}{\partial u_1}, \quad 0 = \nabla_{\mathcal{V}} h^q \cdot f^{\mathcal{V}}_{u_2} + \frac{\partial h^q}{\partial u_2},$$

$$0 = \frac{\partial \nabla_{\mathcal{T}} h^p}{\partial u_1} f^{\mathcal{T}}_{u_1} + \nabla_{\mathcal{T}} h^p \cdot s^{\mathcal{T}}_{u_1} + 2\left(f^{\mathcal{T}}_{u_1}\right)^{\mathrm{T}} \nabla^2_{\mathcal{V}\theta} h^p f^{\mathcal{V}}_{u_1}, \tag{4.14b}$$

$$0 = \frac{\partial \nabla_{\mathcal{T}} h^p}{\partial u_2} f^{\mathcal{T}}_{u_2} + \nabla_{\mathcal{T}} h^p \cdot s^{\mathcal{T}}_{u_2} + 2\left(f^{\mathcal{T}}_{u_2}\right)^{\mathrm{T}} \nabla^2_{\mathcal{V}\theta} h^p f^{\mathcal{V}}_{u_2},$$

$$0 = \frac{\partial \nabla_{\mathcal{V}} h^q}{\partial u_1} f^{\mathcal{V}}_{u_1} + \nabla_{\mathcal{V}} h^q \cdot s^{\mathcal{V}}_{u_1} + \left(f^{\mathcal{T}}_{u_1}\right)^{\mathrm{T}} \nabla^2_{\mathcal{T}} h^q f^{\mathcal{T}}_{u_1} + \left(f^{\mathcal{V}}_{u_1}\right)^{\mathrm{T}} \nabla^2_{\mathcal{V}} h^q f^{\mathcal{V}}_{u_1},$$

$$0 = \frac{\partial \nabla_{\mathcal{V}} h^q}{\partial u_2} f^{\mathcal{V}}_{u_2} + \nabla_{\mathcal{V}} h^q \cdot s^{\mathcal{V}}_{u_2} + \left(f^{\mathcal{T}}_{u_2}\right)^{\mathrm{T}} \nabla^2_{\mathcal{T}} h^q f^{\mathcal{T}}_{u_2} + \left(f^{\mathcal{V}}_{u_2}\right)^{\mathrm{T}} \nabla^2_{\mathcal{V}} h^q f^{\mathcal{V}}_{u_2},$$

$$0 = \nabla_{\mathcal{T}} h^p \cdot m^{\mathcal{T}}_{u_{12}} + \left(f^{\mathcal{T}}_{u_1}\right)^{\mathrm{T}} \nabla^2_{\mathcal{V}\theta} h^p f^{\mathcal{V}}_{u_2} + \left(f^{\mathcal{V}}_{u_1}\right)^{\mathrm{T}} \nabla^2_{\mathcal{V}\theta} h^p f^{\mathcal{T}}_{u_2}, \tag{4.14c}$$

$$0 = \nabla_{\mathcal{V}} h^q \cdot m^{\mathcal{V}}_{u_{12}} + \left(f^{\mathcal{T}}_{u_1}\right)^{\mathrm{T}} \nabla^2_{\mathcal{T}} h^q f^{\mathcal{T}}_{u_2} + \left(f^{\mathcal{V}}_{u_1}\right)^{\mathrm{T}} \nabla^2_{\mathcal{V}} h^q f^{\mathcal{V}}_{u_2},$$

with

$$\nabla_{\mathcal{T}} h^p = \frac{|V_1| \cdot |V_2|}{X_L} \cos\theta_2, \qquad \frac{\partial h^p}{\partial u_1} = \frac{|V_2|}{X_L} \sin\theta_2,$$
$$\nabla^2_{\mathcal{V}\theta} h^p = \frac{|V_1|}{X_L} \cos\theta_2, \qquad \frac{\partial h^q}{\partial u_1} = -\frac{|V_2|}{X_L} \cos\theta_2,$$
$$\nabla_{\mathcal{V}} h^q = \frac{2|V_2|}{X_L} - \frac{|V_1|}{X_L} \cos\theta_2, \qquad \frac{\partial h^p}{\partial u_2} = 1,$$
$$\nabla^2_{\mathcal{T}} h^q = \frac{|V_1| \cdot |V_2|}{X_L} \cos\theta_2, \qquad \frac{\partial h^q}{\partial u_2} = 0,$$
$$\nabla^2_{\mathcal{V}} h^q = \frac{2}{X_L}.$$

The first-, second-order, and mixed sensitivity equations (4.14a)–(4.14c) *correspond to the original first-, second-order, and mixed sensitivity equations in* (4.9a)–(4.9c). *Compared to* (4.9), *we set ourselves up to solve more equations in* (4.14), *however, notice that the dimensions of the matrices that we invert in* (4.14) *are smaller. Furthermore, we validate the above approximations by illustrating numerically that* (4.11) *holds. In particular, for the parameters reported in Example 1, note that*

$$\nabla_x h = \begin{bmatrix} \frac{\partial h_1}{\partial |V_2|} & \frac{\partial h_1}{\partial \theta_2} \\ \frac{\partial h_2}{\partial |V_2|} & \frac{\partial h_2}{\partial \theta_2} \end{bmatrix} = \begin{bmatrix} -0.2032 & 6.5589 \\ 6.4604 & -0.2 \end{bmatrix},$$

$$\nabla^2_x h_1 = \begin{bmatrix} \frac{\partial^2 h_1}{\partial |V_2|^2} & \frac{\partial^2 h_1}{\partial |V_2| \partial \theta_2} \\ \frac{\partial h_1}{\partial \theta_2 \partial |V_2|} & \frac{\partial^2 h_1}{\partial \theta_2^2} \end{bmatrix} = \begin{bmatrix} 0 & 6.6636 \\ 6.6636 & 0.2 \end{bmatrix},$$

$$\nabla^2_x h_2 = \begin{bmatrix} \frac{\partial^2 h_2}{\partial |V_2|^2} & \frac{\partial^2 h_2}{\partial |V_2| \partial \theta_2} \\ \frac{\partial h_2}{\partial \theta_2 \partial |V_2|} & \frac{\partial^2 h_2}{\partial \theta_2^2} \end{bmatrix} = \begin{bmatrix} 13.3333 & -0.2032 \\ -0.2032 & 6.5589 \end{bmatrix}.$$

Hence, we can approximate $\frac{\partial h_1}{\partial |V_2|} \approx 0$, $\frac{\partial h_2}{\partial \theta_2} \approx 0$, $\frac{\partial^2 h_1}{\partial |V_2|^2} = 0$, $\frac{\partial^2 h_1}{\partial \theta_2^2} \approx 0$, *and* $\frac{\partial^2 h_2}{\partial |V_2| \partial \theta_2} = \frac{\partial^2 h_2}{\partial \theta_2 \partial |V_2|} \approx 0$. ■

4.4 Computing Bounds on System States with ADMM

In this section, we formulate the problem of estimating minimum and maximum limits on the solutions of the power-flow equations as a nonconvex quadratic program. Then we present a rendition of the ADMM algorithm to solve this problem, and comment on its convergence.

4.4.1 Quadratic Program and ADMM Algorithm

Recall the quadratic approximation of the algebraic state variable x_ℓ in (4.2). The min/max problems in (4.1) can be formulated as the following quadratic programs:

$$\begin{aligned} x_\ell^{\min/\max} = \min / \max_{u} \;\; & \widehat{x}_\ell + \widehat{J}_\ell u + \frac{1}{2} u^{\mathrm{T}} \widehat{H}_\ell u \\ \text{s.t.} \;\; & u \in \mathcal{U}, \end{aligned} \tag{4.15}$$

where it follows from (4.2) that

$$\begin{aligned} \widehat{x}_\ell &:= \overline{x}_\ell(\overline{u}) - J_\ell \overline{u} + \frac{1}{2} \overline{u}^{\mathrm{T}} H_\ell \overline{u}, \\ \widehat{J}_\ell &:= J_\ell - \overline{u}^{\mathrm{T}} H_\ell, \\ \widehat{H}_\ell &:= H_\ell. \end{aligned} \tag{4.16}$$

As described earlier in Section 4.2, we get the values of $\overline{x}_\ell(\overline{u})$, J_ℓ, and H_ℓ by solving the power-flow balance equations in (2.6) and sensitivity equations in (4.7a)-(4.7c) for $u = \overline{u}$. In general, the problems in (4.15) are non-convex optimization problems, and we adopt a rendition of the ADMM algorithm to solve them. We present the subsequent developments for the minimization problem, but note that the solution procedure for the corresponding maximization problem follows analogously.

First, we convert the minimization problem in (4.15) into consensus form as shown below:

$$\begin{aligned} x_\ell^{\min} := \min_{u,z} \;\; & \widehat{x}_\ell + \widehat{J}_\ell u + \frac{1}{2} u^{\mathrm{T}} \widehat{H}_\ell u \\ \text{s.t.} \;\; & z = u, \\ & z \in \mathcal{U}. \end{aligned} \tag{4.17}$$

The corresponding augmented Langrangian function is:

$$L_\rho(u, z, \lambda) := \widehat{x}_\ell + \widehat{J}_\ell u + \frac{1}{2} u^{\mathrm{T}} \widehat{H}_\ell u + \lambda^{\mathrm{T}}(u - z) + \frac{\rho}{2} \|u - z\|^2, \tag{4.18}$$

where λ is the dual variable corresponding to the equality constraint, and $\rho > 0$ is the augmented Langrangian multiplier. Application of the ADMM algorithm to solve (4.17) involves the repeated execution of the following steps [80]

(S1) $u^{[k+1]} := \arg\min_{u} \quad L_\rho(u, z^{[k]}, \lambda^{[k]})$.

(S2) $z^{[k+1]} := \arg\min_{z \in \mathcal{U}} \quad L_\rho(u^{[k+1]}, z, \lambda^{[k]})$.

(S3) $\lambda^{[k+1]} := \lambda^{[k]} + \rho(u^{[k+1]} - z^{[k+1]})$.

For the augmented Lagrangian (4.18), problems in (S1)–(S2) admit closed-form solutions, and consequently, (S1)–(S3) boil down to:

(S1′) $u^{[k+1]} = (\widehat{H}_\ell + \rho I)^{-1}(\rho z^{[k]} - \lambda^{[k]} - \widehat{J}_\ell^{\mathrm{T}})$.

(S2′) $z^{[k+1]} = \min\{u^{\max}, \max\{u^{\min}, u^{[k+1]} + \rho^{-1}\lambda^{[k]}\}\}$.

(S3′) $\lambda^{[k+1]} = \lambda^{[k]} + \rho(u^{[k+1]} - z^{[k+1]})$.

To see how (S1′) is derived, we begin by recognizing from (4.18) that

$$\nabla_u L_\rho(u, z^{[k]}, \lambda^{[k]}) = \widehat{H}_\ell u + \widehat{J}_\ell^{\mathrm{T}} + \lambda^{[k]} + \rho(u - z^{[k]}). \tag{4.19}$$

Solving for u that sets $\nabla_u L_\rho(u, z^{[k]}, \lambda^{[k]}) = 0$ (i.e., the KKT optimality condition), we get the u-update step in (S1′). Similarly, to see how (S2′) is derived, note from (4.18) that

$$\nabla_z L_\rho(u^{[k+1]}, z, \lambda^{[k]}) = \lambda^{[k]} + \rho(u^{[k+1]} - z). \tag{4.20}$$

Let $\widehat{z}$ be the solution to $\nabla_z L_\rho(u^{[k+1]}, z, \lambda^{[k]}) = 0$, i.e.,

$$\widehat{z} = u^{[k+1]} + \rho^{-1}\lambda^{[k]}.$$

Unlike the u-update step, we want the z updates to lie in $\mathcal{U}$. Therefore, we do not set $z^{[k+1]}$ to $\widehat{z}$ directly, rather, we update $z^{[k+1]}$ as follows:

$$z^{[k+1]} = \begin{cases} u^{\max} & , \widehat{z} > u^{\max} \\ \widehat{z} & , u^{\min} \le \widehat{z} \le u^{\max} \\ u^{\min} & , \widehat{z} < u^{\min}, \end{cases} \tag{4.21}$$

which can be expressed compactly as in (S2′).

4.4.2 Convergence of the Algorithm

Convergence of ADMM is generally not guaranteed for nonconvex problems. However, recent work in [43] provides proofs for convergence for a variety of nonconvex consensus and sharing problems. We can apply the results in [43] to study convergence of steps (S1′)–(S3′). In particular, if

- there exists a constant $L > 0$ such that

$$\|\nabla_u x_\ell(u) - \nabla_u x_\ell(u')\| \leq L\|u - u'\|; \tag{4.22}$$

- the augmented Lagrangian multiplier, ρ, is chosen such that

$$\rho \geq L, \quad \widehat{H}_\ell + \rho I \succ \gamma(\rho) I, \quad \rho\gamma(\rho) > 2L^2, \tag{4.23}$$

  where $\gamma(\cdot)$ is a positive and increasing function of ρ that takes values in $\mathbb{R}^+$; and

- $x_\ell(u)$ is bounded from below over $\mathcal{U}$, i.e.,

$$\min_{u \in \mathcal{U}} x_\ell(u) > -\infty; \tag{4.24}$$

then, we have the following:

1. There exist limit points for the sequences $u^{[k]}$, $z^{[k]}$, and $\lambda^{[k]}$, i.e.,

$$\lim_{k\to\infty} \|u^{[k+1]} - u^{[k]}\| = 0, \quad \lim_{k\to\infty} \|z^{[k+1]} - z^{[k]}\| = 0,$$
$$\lim_{k\to\infty} \|\lambda^{[k+1]} - \lambda^{[k]}\| = 0, \quad \lim_{k\to\infty} \|u^{[k+1]} - z^{[k+1]}\| = 0.$$

2. Denote the limit points of $u^{[k]}$, $z^{[k]}$, and $\lambda^{[k]}$, by $u^\star$, $z^\star$, and $\lambda^\star$, i.e.,

$$u^\star := \lim_{k\to\infty} u^{[k]}, \quad z^\star := \lim_{k\to\infty} z^{[k]}, \quad \lambda^\star := \lim_{k\to\infty} \lambda^{[k]}.$$

   The limit points $(u^\star, z^\star, \lambda^\star)$, are a stationary solution of (4.17), i.e., they satisfy the KKT conditions:

$$0 = \widehat{J}_\ell^{\mathrm{T}} + \widehat{H}_\ell u^\star + \lambda^\star, \quad z^\star \in \mathcal{U}, \quad u^\star = z^\star.$$

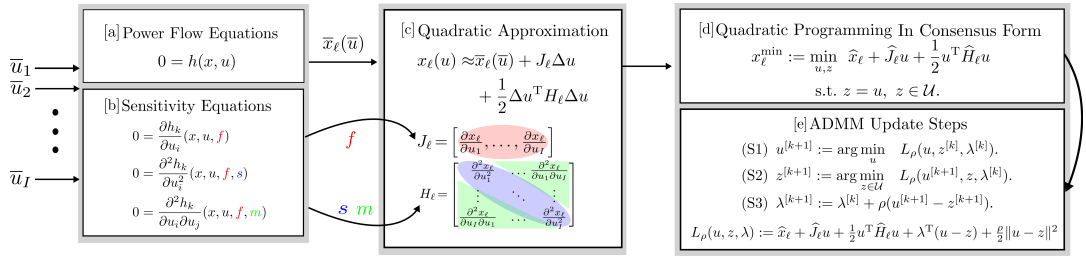

Figure 4.1: Overview of the proposed method.

The details of the proof to the above statements can be found in [43]. We comment briefly on the conditions in (4.22)–(4.24). With regard to (4.22), given the gradient of $x_\ell(u)$, $\nabla_u x_\ell(u) = \widehat{H}_\ell u + \widehat{J}_\ell^{\mathrm{T}}$, there exists $L \geq \|\widehat{H}_\ell\|$ such that

$$\begin{aligned} \|\nabla_u x_\ell(u) - \nabla_u x_\ell(u')\| &= \|\widehat{H}_\ell(u - u')\| \\ &\leq \|\widehat{H}_\ell\| \cdot \|u - u'\| \\ &\leq L \cdot \|u - u'\|, \end{aligned}$$

where the first step above follows from the Cauchy-Schwartz inequality. Furthermore, for the choice $\gamma(\rho) = \epsilon\rho$ where $0 < \varepsilon < 1$, if ρ is picked such that

$$\rho > \sqrt{\frac{2}{\epsilon}} L, \quad \rho > -(1 - \varepsilon)^{-1} \lambda_{\min}(\widehat{H}_\ell),$$

then (4.23) is satisfied. Finally, we see that (4.24) is an assumption that follows from the well posedness of the power flow equations at a non-stressed operating point.

Figure 4.1 summarizes all the steps in our approach (encapsulating the discussions in Sections 4.1 and 4.4): [a] Calculating algebraic variables, x at $u = \overline{u}$ by solving algebraic power-flow equations (2.5). [b] Deriving sensitivity equations from the original power-flow balance equations, and calculating sensitivity variables, f, s, and m, at $u = \overline{u}$ (4.12). [c] Constructing the quadratic approximation of x_ℓ using the values of algebraic states and sensitivity variables calculated in steps [a]-[b]. [d] Consensus form of the nonconvex quadratic program (QP) with quadratic approximation of x_ℓ as the objective and box constraints on u. [e] Solving the nonconvex QP using ADMM.

Note that we can solve the non-convex quadratic problems in (4.15) with the approach using the SDP relaxation discussed in Chapter 3 [45]. However, the ADMM

shows better scalability compared to the SDP approach. For example, SDP was computationally infeasible for the system sizes above 118-bus test system due to the limits on the memory resources while ADMM could be easily extended to much large-scale systems with the same computer resources.

We now numerically validate the approach for the running example introduced in Fig. 2.3, and for a large 1354-bus system.

Example 8 (Continued from Example 2, 5, 6, and 7) *In this example, we compute the minimum and maximum bounds on $|V_2|$ and θ_2 for the system introduced in Example 1. Recall that we formulated the algebraic equations to solve for the sensitivities and characterize the quadratic approximations for these states in Example 4. Repeated application of steps* (S1′)–(S3′) *unto convergence yields the bounds:*

$$0.8743 \leq |V_2| \leq 1.0835,\ -0.0377[\text{rad}] \leq \theta_2 \leq -0.0255[\text{rad}].$$

To verify the validity of the above result, maximum and minimum values were calculated by repeated simulations for 1000 *randomly-sampled values of uncertainty variables (P^{L} and $|V_1|$) and the results are reported below:*

$$0.8824 \leq |V_2| \leq 1.0858,\ -0.0413[\text{rad}] \leq \theta_2 \leq -0.0230[\text{rad}].$$

The bounds estimated without adopting the decoupled power-flow assumptions (i.e., for the case that the quadratic approximations for $|V_2|$ and θ_2 are constructed with the sensitivities solved from the equations reported in Example 3) are:

$$0.8823 \leq |V_2| \leq 1.0859,\ -0.0413[\text{rad}] \leq \theta_2 \leq -0.0228[\text{rad}].$$

The above results validate the approach, and demonstrate the effectiveness of the approximations adopted in Section 4.3. Indeed, there is a slight loss of accuracy, but we will find that this approach more than makes up for this loss of accuracy by facilitating problem scalability. ■

4.5 Numerical Case Study

We demonstrate the scalability and accuracy of our approach with numerical simulations for the MATPOWER 1354-bus test-case power system [81]. (See Fig. 4.2.) The

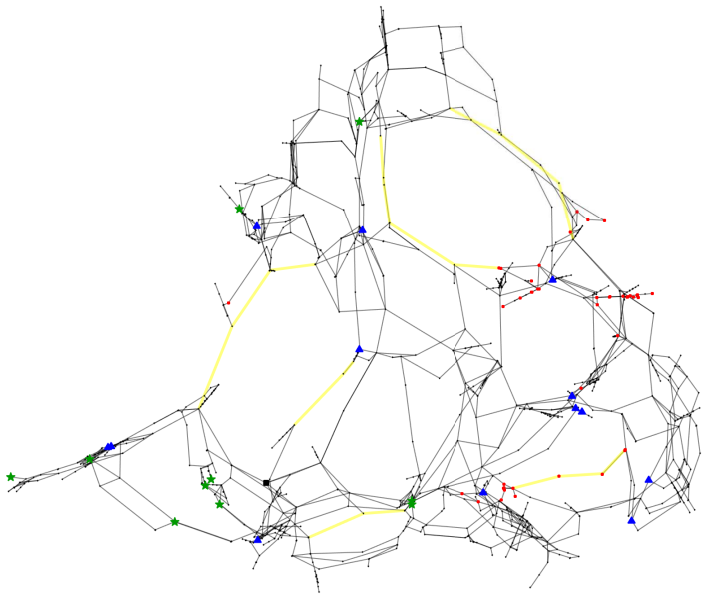

Figure 4.2: Adjacency graph of the MATPOWER 1354-bus test system.

corresponding power flow equations comprise 2447 states, which include voltage magnitudes and angles from 1094 load buses, and generator voltage-phase angles from 259 generator buses. All the case studies in this section were performed on an INTEL Core i7-4770 CPU @ 3.40GHz with 8 GB memory.

4.5.1 Uncertainty Model

The adjacency graph of the MATPOWER 1354-bus test system is shown in Fig. 4.2 with buses denoted by black circles, and transmission lines by solid lines. We assume 76 uncertainties in the model:

i) Real-power generation from generator buses: {1095, 1124, 1152, 1181, 1238, 1296, 1324, 1353, 1138, 456}. (Green stars in Fig. 4.2.)

ii) Real- and reactive-power consumed by loads at buses: {79, 157, 235, 313, 391, 469, 548, 626, 704, 782, 938, 1016, 1094, 971, 757}. (Blue triangles in Fig. 4.2.)

iii) Line impedances in the transmission lines: {(922,830), (830,249), (1306,1260),

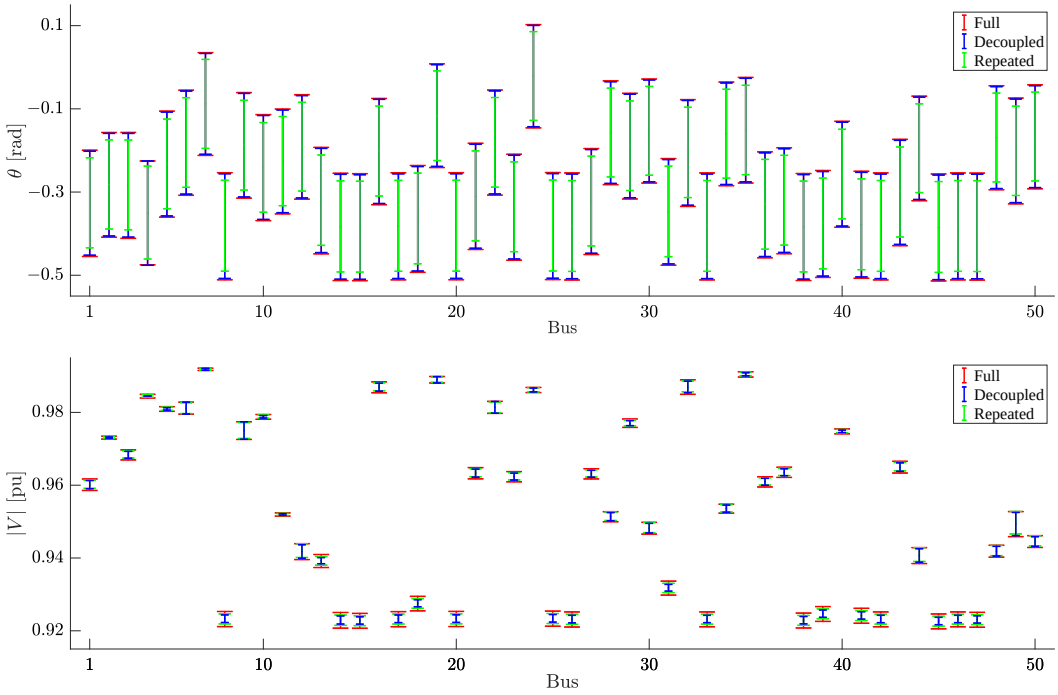

Figure 4.3: Simulation results for the MATPOWER 1354-bus test system.

(1260,1324), (474,1110), (1110,346), (257,477), (477,550), (38,619), (619,943), (943,310), (474,140), (140,183), (1306,808), (287,718), (718,218), (218,688)}. (Yellow lines in Fig. 4.2.)

iv) Infinite-bus voltage magnitude and angle at bus 1354. (Black square in Fig. 4.2.)

Also, we assume the following percentage variations of uncertainty variables: for i) – iii), ±15 %, and for iv), ±10 % around the nominal values.

4.5.2 Computing Bounds on Algebraic Variables using ADMM

The approach outlined in Fig. 4.1 is applied to the system at hand. Results are shown in Fig. 4.3 for voltage magnitude (bottom) and phase angle (top). Minimum and maximum bounds estimated from our proposed method using the original and decoupled sensitivity equations are depicted as red and blue lines, respectively, for randomly chosen load buses shown as red circles in Fig. 4.2. (Given space constraints, we only report results from a subset of the buses in the network.) For comparison, we

plot bounds recovered from the result of 7×10^4 repeated simulations (the computation time to run the two methods is about the same in this case) for randomly chosen samples of the uncertainties in the model (green). (While these may seem like a lot of repeated simulations, note that just sampling the vertices of the uncertainty set in this case requires running 2^{76} simulations. The time to do this would easily exceed the computation time for our method.) From the figure, we conclude that applying the decoupled assumptions to solve the sensitivity equations does not compromise on accuracy.

4.5.3 Computational Advantages of Decoupling Assumptions

Table 4.1 compares the computation times for solving the original sensitivity equations and the reduced-order sensitivity equations as well as the time to solve the ADMM algorithm for a variety of test systems. From this result, we can clearly appreciate the advantages of the decoupling assumptions to solve the sensitivities as the system size increases.

Table 4.1: Sensitivity Computation for Different Power-System Sizes

Case	Variables		Sensitivity		ADMM [s/bus]
	A	I	Full [s]	Decoupled [s]	
14 Bus	22	41	0.23	0.17	0.05
30 Bus	53	41	0.37	0.26	0.05
118 Bus	181	55	1.49	0.79	0.10
300 Bus	530	55	5.12	3.48	0.11
1354 Bus	2447	57	46.43	37.31	0.14
2868 Bus	5292	57	574.03	162.55	0.26

Chapter 5

Robust Stability Assessment of Power Systems

Lyapunov's direct method provides a systematic framework to assess power system transient stability by yielding estimates of the Region of Attraction (ROA) for stable equilibrium points. However, analytical approaches to construct Lyapunov functions are limited in application to very restrictive settings and cannot be extended to accommodate the impact of uncertainty. This chapter focuses on the algorithmic construction of Lyapunov functions and the estimation of the robust ROA with sum-of-squares (SOS) optimization programs when parameters and/or inputs in the dynamic model are uncertain. This class of optimization programs can be translated into semidefinite problems which can be solved with readily available software. A computationally affordable procedure to include several sources of uncertainty is proposed; this involves successively introducing uncertainties to update the Lyapunov function in a decreasing order of its sensitivity based on the stability margin with respect to the uncertain variables. Numerical case studies are presented to demonstrate the proposed approach to estimate the ROA and the robust ROA and compare the results with repeated time-domain simulations for a power system involving doubly fed induction generators and synchronous generators.

The remainder of this chapter is organized as follows. Starting with some preliminaries in Section 5.1. In Section 5.2, we derive a polynomial ordinary differential equation

model, and also outline the SOS optimization problem formulation in deterministic settings for the construction of Lyapunov functions. The approach is extended to cover parametric and input uncertainty in Section 5.3. In Section 5.4, we provide a numerical case study to illustrate the approach.

5.1 Preliminaries

5.1.1 Monomials, Polynomials, and SOS Polynomials

Corresponding to an n tuple $x = \{x_1, \ldots, x_n\}$, a monomial is defined as $m(x) = c_\alpha x_1^{\alpha_1} x_2^{\alpha_2} \cdots x_n^{\alpha_n}$ where $c_\alpha \in \mathbb{R}$; the degree of the monomial is given by $\deg(m) := \sum_{i=1}^{n} \alpha_i$. A polynomial is a finite, linear combination of monomials, i.e., $p(x) := \sum_{\ell=1}^{n} m_\ell(x)$; the degree of a polynomial is defined to be the maximum degree of the constituent monomials, i.e., $\deg(p) := \max\{\deg(m_\ell)\}, \ell = 1, \ldots, n$. The set of polynomials in $\mathbb{R}^n$ is denoted by $\mathcal{P}[x]$.

A polynomial $p \in \mathcal{P}[x]$ is a *Sum-of-Squares* (SOS) polynomial, if it can be expressed as a finite linear combination of squared polynomials, i.e., $p(x) = \sum_{\ell=1}^{n} p_\ell^2(x)$, $p_\ell \in \mathcal{P}[x]$. The set of SOS polynomials in $\mathbb{R}^n$ is denoted by $\mathcal{S}[x]$. If $p \in \mathcal{S}[x]$, then $p(x) \geq 0 \; \forall x \in \mathbb{R}^n$. Thus, $p \in \mathcal{S}[x]$ is a sufficient condition for a polynomial to be globally nonnegative [82].

5.1.2 SOS Optimization and SDP Relaxation

The standard form of the SOS optimization problem is:

$$\begin{aligned} \min_{d \in \mathbb{R}^r} \; & c^{\mathrm{T}} d \\ \text{s.t.} \; & a_k(x,d) \in \mathcal{S}[x], k = 1, \ldots, N_s, \\ & b_j(x,d) = 0, j = 1, \ldots, N_e, \end{aligned} \tag{5.1}$$

where $d \in \mathbb{R}^r$ is the vector of decision variables, $a_k(x,d)$ and $b_j(x,d)$ are polynomial functions which are affine in d, and N_s and N_e denote the number of SOS and equality constraints.

Any polynomial $p \in \mathcal{S}[x]$ must have even degree, $2n$. Such a polynomial can be rewritten as a quadratic function of monomials, $p = z^{\mathrm{T}} Q z$, where z is a vector of all monomials of degree less than or equal to n, and Q is a positive semidefinite matrix.

Therefore, with reference to (5.1), constraints $a_k(x, d) \in \mathcal{S}[x]$ can be expressed as linear matrix inequalities, which promotes a semidefinite programming (SDP) reformulation of the SOS optimization problem. MATLAB toolboxes such as SOSOPT, SOSTOOLS, and YALMIP [83–86] can convert SOS problems to SDPs which can be solved with readily available software, e.g., SeDuMi [87].

5.2 Taylor-Polynomial ODE Model

5.2.1 Ordinary Differential Equation Model

The electromechanical dynamics of a power system are captured by an ordinary differential equation (ODE) model:

$$\dot{x} = f(x, u), \tag{5.2}$$

where $x \in \mathbb{R}^D$ denotes the vector of dynamic states (e.g., rotor angles and speeds), and in the context of this work, $u \in \mathbb{R}^I$ denotes the vector of all inputs and/or model parameters that are not perfectly known. The ODE model in (5.2) is obtained from a differential algebraic model in (2.1) by using the well-known method of Kron reduction [88]. This circuit-reduction procedure invokes a Schur complement of the admittance matrix, and is commonly employed in transient stability analysis to eliminate buses that are not connected to generators while preserving circuit laws [46, 88].

5.2.2 Polynomial Ordinary Differential Equation Model

In order to apply SOS-based optimization methods for the purpose of estimating the ROA, we begin by approximating the ODE model in (5.2) as a polynomial ordinary differential equation (PODE) model of the form [53]

$$\dot{x} = p(x, u), \tag{5.3}$$

where $p(x, u)$ is a homogenous polynomial with degree q, and for convenience, the equilibrium point of the system in (5.3) is shifted to the origin. The ODE model in (5.2) is approximated to the PODE model in (5.3) by truncating Taylor-series expansions of $\sin(\cdot)$ and $\cos(\cdot)$ functions to the qth order.

A pertinent question to address before applying SOS optimization methods relates to the accuracy of the qth order PODE model in (5.3). Applying standard results related to closeness of solutions of nonlinear systems [48], we can show that over any finite-time horizon, the error in the solutions of the PODE and ODE increases exponentially with the length of the horizon and decreases inversely with the factorial of the Taylor-series approximation order. Details are in Appendix C.

5.2.3 ROA Estimation for the Deterministic PODE Model

For some u, let $\phi(t, x_0, u)$ denote the solution of (5.3) at time t with initial condition $x(0) = x_0$. The ROA for the system in (5.3) is denoted by Ω, and defined as

$$\Omega := \left\{ x_0 \in \mathbb{R}^{2n} : \lim_{t\to\infty} \phi(t, x_0, u) = 0 \right\}. \tag{5.4}$$

We will first present a lemma that establishes a sufficient condition for local asymptotic stability of the origin of (5.3). We will then leverage this condition to formulate an SOS optimization problem that returns an ROA estimate.

Lemma 1 (Lyapunov Stability [89]) *If there exists a continuously differentiable function $V : \mathbb{R}^{2n} \to \mathbb{R}$, such that*

$$\begin{aligned} &V(0) = 0\,,\, V(x) > 0 \;\forall\, x \neq 0, \\ &\Omega_{V,\gamma} := \left\{ x \in \mathbb{R}^{2n} : V(x) \leq \gamma, \gamma \in \mathbb{R}^{+} \right\} \text{ is bounded}, \\ &\Omega_{V,\gamma} \setminus 0 \subseteq \left\{ x \in \mathbb{R}^{2n} : \nabla V(x) p(x,u) < 0 \right\}, \end{aligned} \tag{5.5}$$

then $\phi(t, x_0, u) \in \Omega_{V,\gamma}\ \forall t \geq 0$, $\forall x_0 \in \Omega_{V,\gamma}$, and furthermore $\lim_{t\to\infty} \phi(t, x_0, u) = 0$. In other words, $\Omega_{V,\gamma}$ is an invariant subset of the ROA defined in (5.4). ■

Lemma 1 implies that the ROA can be estimated by maximizing sublevel sets of the Lyapunov function; a problem that can be cast as an SOS optimization program. To this end, we will first formulate an alternative to (5.5) which is a set containment condition by using the *S-Procedure*.

Lemma 2 (S-Procedure [89]) *Given $z_0, z_1 \in \mathcal{P}[x]$, if there exists a polynomial $s \in \mathcal{S}[x]$ such that $z_0 - s \cdot z_1 \in \mathcal{S}[x]$, then*

$$\{ x \in \mathbb{R}^n : z_1(x) \geq 0 \} \subseteq \{ x \in \mathbb{R}^n : z_0(x) \geq 0 \}. \tag{5.6}$$

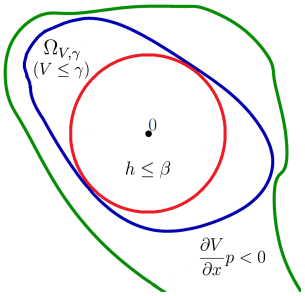

Figure 5.1: Description of ROA and shape function.

By applying Lemma 2, if we restrict attention to a class of SOS-polynomial Lyapunov functions, we see that the set-containment condition in (5.5) can be expressed as

$$-\nabla V(x)p(x,u) - s(x)(\gamma - V(x)) \in \mathcal{S}[x], \tag{5.7}$$

for some $s \in \mathcal{S}[x]$. This sufficient condition suggests the following problem to maximize the value of γ such that $\Omega_{V,\gamma}$ is the *largest possible* invariant subset of the ROA [60,84]:

$$\begin{aligned} \max_{V,\,s,\,\gamma} \quad & \gamma \\ \text{s.t.} \quad & \gamma > 0,\ s(x) \in \mathcal{S}[x], r(x) > 0, r(x) \in \mathcal{P}[x], \\ & V(x) - r(x) \in \mathcal{S}[x], V(0) = 0, \\ & -\nabla V(x)p(x,u) - s(x)(\gamma - V(x)) \in \mathcal{S}[x]. \end{aligned} \tag{5.8}$$

The optimization problem in (5.8) is a bilinear SOS problem due to the product terms $s(x) \cdot V(x)$ and $s(x) \cdot \gamma$. However, if $V(x)$ is fixed, the problem is convex for each fixed γ. Thus we can solve it through a bisection on γ. As an initial guess for the Lyapunov function, we can choose $V(x) = x^{\mathrm{T}}Px$ by solving the Lyapunov equation $A^{\mathrm{T}}P + PA = -Q$, where the matrix A describes the dynamics of the linearized version of (5.3). Once we find $s(x)$ and the optimal γ for this fixed $V(x)$, we then solve the same problem to find a new $V(x)$ with fixed $s(x)$ and γ. This process is iterated to maximize the value of γ such that the best estimate of the ROA is obtained. One issue is that the feasible set for the problem in (5.8) is invariant to scaling. Specifically, if (V, γ, s) satisfy the constraints then $(cV, c\gamma, s)$ also satisfy the constraints for any $c > 1$. Hence, the objective function γ can be driven to $+\infty$ for any feasible point simply by rescaling

the Lyapunov function. A more appropriate indicator for the *size* of the ROA estimate $\Omega_{V,\gamma}$ is required. An alternative objective is to maximize β subject to an additional set containment of the form: $\{x \in \mathbb{R}^n : x^{\mathrm{T}}x \leq \beta\} \subseteq \{x \in \mathbb{R}^n : V(x) \leq \gamma\}$. In other words, this objective function increases the size of the ROA estimate $\Omega_{V,\gamma}$ as measured by the radius squared of the largest circumscribed sphere (β). The sphere can be replaced with more general *shape functions* that emphasize the importance of certain directions in the state space when measuring the size of $\Omega_{V,\gamma}$. The various set containments are illustrated in Fig. 5.1. The general method described above is called *V-s iteration* and is explained in detail in [84].

5.3 Affine-approximated Uncertain Power System Dynamic Models and Robust ROA Estimation

Consider the system in (5.3), and denote the uncertain parameters/inputs by $u = [u_1, \ldots, u_\ell]^{\mathrm{T}}$. We will assume a worst-case uncertainty model for u, by which we mean that only the upper and lower bounds on each element of u are known. These limits are collected in the vectors $u^{\max} := [u_1^{\max}, \ldots, u_\ell^{\max}]^{\mathrm{T}}$ and $u^{\min} := [u_1^{\min}, \ldots, u_\ell^{\min}]^{\mathrm{T}}$, respectively. The set that captures all possible values that the uncertain parameters/inputs can take is given by $\mathcal{U} := [u_1^{\min}, u_1^{\max}]^{\mathrm{T}} \times [u_2^{\min}, u_2^{\max}]^{\mathrm{T}} \cdots \times [u_\ell^{\min}, u_\ell^{\max}]^{\mathrm{T}}$. It is worth noting that entries of u may take any value within the set $\mathcal{U}$ for the time horizon of interest, i.e., the proposed approach applies to time-varying uncertainty in the model parameters and inputs.

For the PODE system in (5.3) with $u \in \mathcal{U}$, we can extend the definition of the ROA in (5.4) to define the *robust* ROA as

$$\Omega_{\text{robust}} := \left\{ x_0 \in \mathbb{R}^n : \lim_{t \to \infty} \phi(t, x_0, u) = 0, \forall u \in \mathcal{U} \right\}. \tag{5.9}$$

Recall that $\phi(t, x_0, u)$ denotes the solution of (5.3) at time t with initial condition $x(0) = x_0$ for some u. All initial conditions that originate in Ω_{robust} asymptotically decay to the origin for all possible values of the uncertain parameters/inputs $u \in \mathcal{U}$.

It is computationally intractable to directly extend the optimization problem in (5.8) to obtain Ω_{robust} by solving it for all possible values of the uncertain parameters/inputs,

i.e., for all $u \in \mathcal{U}$. This would require solving the ROA estimation problem with set-containment constraints of the form (5.7) for each value that u can take. However, if the PODE model in (5.3) is affine in u (either innately, or as a result of a modeling approximation), then it is possible to formulate an optimization problem to estimate the robust ROA for which the set containment condition in (5.7) has to be evaluated *only* for the vertices of $\mathcal{U}$, a set which we denote by $\mathcal{U}_{\text{vert}}$ subsequently.

5.3.1 Multivariable Unknown-but-Bounded Power System Uncertainty Model

The affine model corresponding to the PODE system in (5.3) is given by the following first-order Taylor approximation:

$$\dot{x} = p(x,u) \approx p(x,0) + \nabla_u p(x,0)u =: p_{\text{affine}}(x,u). \tag{5.10}$$

Note that the affine model in (5.10) is a linear approximation in u, but $p(x,0)$ and $\nabla_u p(x,0)$ still retain polynomial nonlinearities in x. Given the generator electromechanical dynamics in (2.2) and (2.3), we see that (5.10) is *exact* (not an approximation) for uncertainty in the generator mechanical power input, P_i, the infinite bus voltage magnitude, or the generator terminal voltage. If the transmission line impedances or the active/reactive load powers were uncertain, then (5.10) would only be an approximation.

5.3.2 Robust ROA Estimation for the Multivariable Unknown-but-Bounded Uncertainty Model

We will first present a lemma that establishes a sufficient condition for local asymptotic stability of the origin of (5.10) for all possible values that the uncertain inputs/parameters can take. Next, we will formulate the problem of estimating the robust ROA as an SOS optimization problem.

Lemma 3 (Robust Lyapunov Stability) *Denote the solution of* (5.10) *at time* t*, for some* $u \in \mathcal{U}$*, and initial condition* $x(0) = x_0$ *by* $\phi_{\text{affine}}(t, x_0, u)$*. If there exists a*

continuously differentiable function $V : \mathbb{R}^{2n} \to \mathbb{R}$*, such that*

$$\begin{aligned} &V(0) = 0\,,\, V(x) > 0 \;\forall\; x \neq 0, \\ &\Omega_{V,\gamma} = \{x \in \mathbb{R}^n : V(x) \leq \gamma, \gamma \in \mathbb{R}^+\} \text{ is bounded,} \\ &\Omega_{V,\gamma} \setminus 0 \subseteq \bigcap_{u \in \mathcal{U}_{\text{vert}}} \left\{x \in \mathbb{R}^{2n} : \nabla V(x) p_{\text{affine}}(x,u) < 0\right\}, \end{aligned} \tag{5.11}$$

then, $\phi_{\text{affine}}(x_0, t, u) \in \Omega_{V,\gamma}\ \forall t \geq 0,\ \forall x_0 \in \Omega_{V,\gamma},\ \forall u \in \mathcal{U}$*, and* $\lim_{t\to\infty} \phi_{\text{affine}}(t, x_0, u) = 0$*.*

The set containment condition in the third line of (5.11) follows from the corresponding condition in (5.5). In particular, we require

$$\begin{aligned} \Omega_{V,\gamma} \setminus 0 \subseteq\ & \left\{x \in \mathbb{R}^{2n} : \nabla V(x) p_{\text{affine}}(x,u) < 0, \forall u \in \mathcal{U}\right\} \\ =\ & \bigcap_{u \in \mathcal{U}_{\text{vert}}} \left\{x \in \mathbb{R}^{2n} : \nabla V(x) p_{\text{affine}}(x,u) < 0\right\}, \end{aligned} \tag{5.12}$$

and the second line in (5.12) follows from the fact that $p_{\text{affine}}(x,u)$ is affine in u (see (5.10)).

By applying Lemma 3, if we restrict attention to a class of SOS-polynomial Lyapunov functions, we see that the set-containment conditions in (5.11) can be expressed as

$$-\nabla V(x) p_{\text{affine}}(x, \widetilde{u}_i) - s_i(x)(\gamma - V(x)) \in \mathcal{S}[x], \tag{5.13}$$

where $s_1(x), \ldots, s_{2^I}(x) \in \mathcal{S}[x],\ i = 1, \ldots, 2^I$, and $\widetilde{u}_i$ denote the entries of $\mathcal{U}_{\text{vert}}$. Notice that I uncertain inputs result in 2^I set-containment conditions. Subsequently, the following optimization program can be formulated to estimate the robust ROA for the system (5.10):

$$\begin{aligned} \max_{V, \{s_i\}_{i=1}^{2^I}, \ldots, \gamma}\ & \gamma \\ \text{s.t.}\quad & \gamma > 0, \\ & s_i(x) \in \mathcal{S}[x],\ i = \{1, \ldots, 2^I\}, \\ & V(x) - r(x) \in \mathcal{S}[x],\ r(x) > 0, r(x) \in \mathcal{P}[x], V(0) = 0, \\ & -\nabla V(x) p_{\text{affine}}(x, \widetilde{u}_1) - s_1(x)(\gamma - V(x)) \in \mathcal{S}[x], \\ & \quad\vdots \\ & -\nabla V(x) p_{\text{affine}}(x, \widetilde{u}_{2^\ell}) - s_{2^\ell}(x)(\gamma - V(x)) \in \mathcal{S}[x], \end{aligned} \tag{5.14}$$

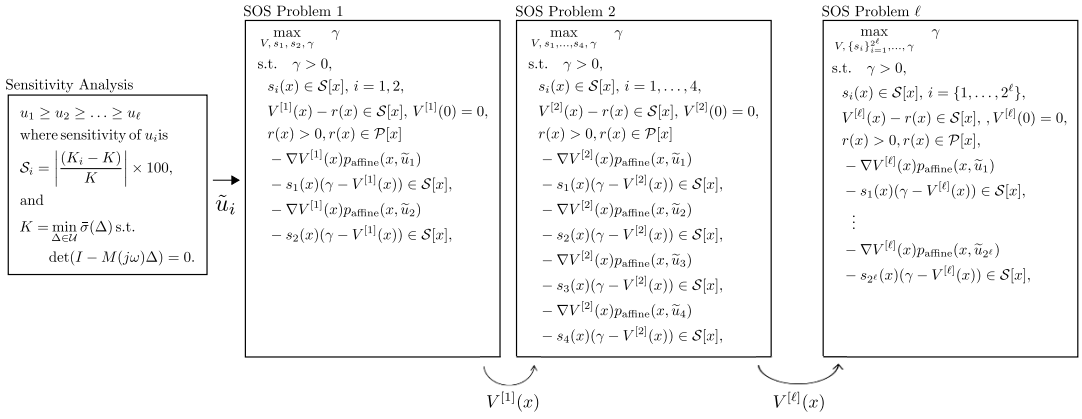

Figure 5.2: Sequential Update Method.

where $\widetilde{u}_i \in \mathcal{U}_{\text{vert}}$, $i = 1, \ldots, 2^I$. The same algorithm used to solve the bilinear problem and maximize γ in Section 5.2.3 can also be applied to this problem.

5.3.3 Lyapunov Function Update for Multiple Uncertainties

The computational complexity of the SOS optimization problem with multiple uncertainties in (5.14) increases with the number of uncertain variables. In particular, notice from (5.14) that I uncertainties result in 2^I constraints. Consequently, the feasibility of the proposed method is lowered as the percentage uncertainty (i.e., the volume of the set $\mathcal{U}$) increases. A major contributing factor for this is the fact that the V-s iteration algorithm adopted to address the bilinear $V(x) \cdot s_i(x)$ terms (see Section 5.2.3 for more details) requires a careful choice of an initial Lyapunov function for convergence.

To address the concerns above, we break up the problem in (5.14) into I optimization problems that successively introduce uncertainties so that we systematically update the Lyapunov function in a decreasing order of its sensitivity based on the stability margin with respect to the uncertain variables. See Fig. 5.2 for an illustration. As a first step, we sort the elements of u in order of the sensitivity. To that end, we linearize the polynomial ODE model in (5.3) as below:

$$\dot{x} = p(x, u) = A(u)x = (A_0 + \sum_{k=1}^{I} A_k u_k)x. \tag{5.15}$$

The system in (5.15) can be expressed in the block-diagram form shown in Fig. 5.3,

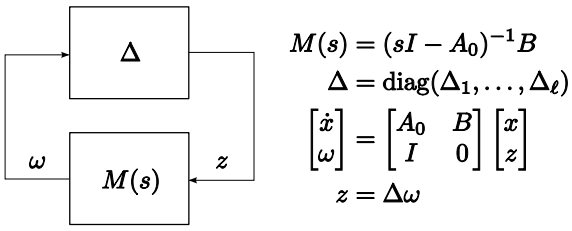

Figure 5.3: Block diagram of the uncertain linear $M - \Delta$ system.

where

$$M(s) = (sI - A_0)^{-1}B, \quad B = [A_1 \dots A_\ell],$$
$$\Delta = \text{diag}\{\Delta_1, \dots, \Delta_\ell\}. \tag{5.16}$$

In the frequency domain, the uncertain linear system, $M - \Delta$, becomes unstable when eigenvalues cross the imaginary axis identified by the condition $\det(I - M(j\omega)\Delta) = 0$. One can define a stability margin for the system as follows:

$$K = \min_{\Delta \in \mathcal{U}} \quad \bar{\sigma}(\Delta) \tag{5.17}$$
$$\text{s.t.} \quad \det(I - M(j\omega)\Delta) = 0,$$

where $\bar{\sigma}(\Delta)$ is the largest singular value of the matrix Δ. Finding the exact stability margin is a difficult problem, however, upper and lower bounds on K can be obtained from the μ-analysis algorithm [90–93]. With this definition of stability margin, the sensitivity of the system stability to the parameter u_i is defined as

$$S_i\,[\%] = \left| \frac{K_i - K}{K} \right| \times 100, \tag{5.18}$$

where K_i is the stability margin when the uncertainty range of the ith parameter/input, u_i, i.e., $[u_i^{\min}, u_i^{\max}]$, is increased by 25% (picked without loss of generality). The procedure discussed above is already implemented in the MATLAB command *robuststab* that is available through the Robust Control Toolbox [92].

Next, we sort the entries of u in descending order of the sensitivities $\{S_i\}_{i=1}^{I}$, i.e., we assume the entries of the vector $u = [u_1, u_2, \dots, u_I]^{\mathrm{T}}$ are arranged in the order of their sensitivities. Assume that $V^{[k]}(x)$ is the Lyapunov function estimated for the subset

$\mathcal{U}_k \subseteq \mathcal{U}$ given as below:

$$\mathcal{U}_k = [u_1^{\min}, u_1^{\max}] \times \ldots \times [u_k^{\min}, u_k^{\max}]. \tag{5.19}$$

Using $V^{[k]}(x)$ as an initial guess for the Lyapunov function in the SOS optimization in (5.14), we estimate the new Lyapunov function $V^{[k+1]}(x)$ for the larger subset $\mathcal{U}_{k+1}$. This procedure is repeated till all uncertain variables are accounted for (i.e., till we obtain $V^{[I]}(x)$).

5.4 Numerical Case Study: Two-Machine Infinite-Bus Power System with Doubly-Fed Induction Generator

We demonstrate the applicability of the proposed approach for algorithmic construction of the Robust ROA using the outlined method in Section 5.3. We consider a two-machine infinite bus power system composed of synchronous and doubly-fed induction generators. Figure 5.4 provides a one-line diagram of the two machine infinite bus system under investigation. We will estimate the robust ROA when there is a balanced three-phase line-ground fault in one of the transmission lines connecting bus 3 and 6. (The fault occurs at time $t = 0$, and is cleared at some time $t > 0$ by opening the circuit breakers at buses 3 and 6.) We investigate system stability for two cases, where the generator connected to bus 2 is: i) a DFIG (referred to subsequently as the DFIG-SG case), and ii) a synchronous generator (referred to subsequently as the SG-SG case). In both cases, bus 1 is connected to a synchronous generator. We assume that the mechanical power input at bus 1, transmission line impedance between bus 3 and 6, and the infinite bus voltage magnitude at bus 3, denoted by P_1^{mech}, X_l, V_∞, respectively, are unknown with known limits. These uncertain model inputs and parameters are collected in the vector $u = [u_1, u_2, u_3]^{\mathrm{T}} = [V_\infty, X_l, P_1^{\text{mech}}]^{\mathrm{T}}$. All parameters are adopted from [73] and given in Appendix B.3.

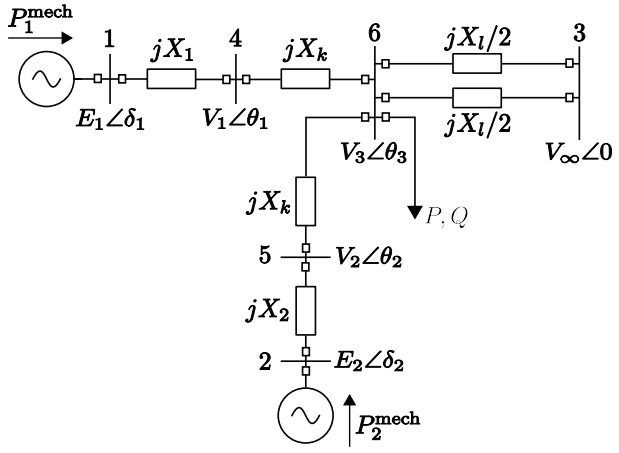

Figure 5.4: One-line diagram of the two-machine infinite-bus system.

For the DFIG-SG case, the PODE model corresponding to the nonlinear dynamics (2.2) and (2.3) has the general form:

$$\frac{\mathrm{d}\delta_1}{\mathrm{d}t} = \omega_1 - \omega_{\mathrm{s}}, \tag{5.20}$$

$$\frac{\mathrm{d}\omega_1}{\mathrm{d}t} = \frac{1}{M_1}(P_1^{\text{mech}}(1+u_3) - D_1\omega_1) + \sum_{k=1}^{q} p_k(\delta_1, \delta_2, u_1, u_2),$$

$$\frac{\mathrm{d}\delta_2}{\mathrm{d}t} = (\omega_2 - \omega_{\mathrm{s}}) + \sum_{k=1}^{q} h_k(\delta_1, \delta_2, u_1, u_2), \tag{5.21}$$

$$\frac{\mathrm{d}\omega_2}{\mathrm{d}t} = \frac{P_2^{\text{mech}}}{M_2}\sum_{k=1}^{q} c_k\omega_2^k + \sum_{k=1}^{q} q_k(\delta_1, \delta_2, u_1, u_2),$$

where $p_k(\cdot), h_k(\cdot)$, and $q_k(\cdot)$ are kth-order homogeneous polynomial functions of the generator angles δ_1, δ_2. The order of the polynomial approximation is chosen to be $q = 3$. Note from (5.20) that the Taylor PODE model of the system is innately affine in the uncertainty in P_1^{mech}. Therefore, with regard to P_1^{mech}, (5.10) is exact.

First, we perform a sensitivity analysis of the uncertain variables based on linearized models for the two cases as discussed in Section 5.3.3. The resulting sensitivities are given by $[S_1, S_2] = [10\%, 9\%]$ and $[S_1, S_2] = [8\%, 4\%]$, respectively. Uncertainty u_3 in P_1^{mech} does not appear in (5.15) since this term does not feature in the linearization of (5.20)-(5.21). So, in the Lyapunov update procedure, u_3 is included as the last uncertain variable. Next, we solve the SOS optimization problems as shown in Fig. 5.2 by

sequentially updating the Lyapunov-function estimate at each iteration by incorporating uncertain variables in the order of sensitivity. Using this sequential-update approach, the range of uncertainties for which feasible solutions are obtained are: $u_1 = \pm 1\%$, $u_2 = \pm 3\%$, and $u_3 = \pm 4\%$. Comparatively, the range of uncertainties for which feasible solutions are obtained by solving the problem in (5.14) directly (i.e., when all constraints are included at once) are given by $u_1 = \pm 0.33\%$, $u_2 = \pm 1\%$, and $u_3 = \pm 1.33\%$. This validates the usefulness of the sequential update procedure in obtaining feasible solutions while tolerating large uncertainties in the model.

Figures 5.5(a)-5.5(b) and 5.5(d)-5.5(e) show two-dimensional projections of the robust ROA (red curves) with $\{\delta_1, \omega_1\} = \{0, 0\}, \{\omega_1, \omega_2\} = \{0, 0\}$ for the DFIG-SG and SG-SG case, respectively. In each figure, a collection of individual ROAs (blue curves) are plotted for different realizations of the uncertain model parameters and inputs to show that the robust ROA is indeed contained in the intersection of the ROAs. Superimposed to each figure are trajectories (obtained from simulations of the nonlinear DAE model) that converge to (and diverge from) the stable equilibrium point plotted as thick green lines (thin dotted green lines, respectively). We also plot the evolution of the Lyapunov function along trajectories of the time-domain simulation for arbitrary realizations of the uncertain model parameters and inputs in Fig. 5.5(f). The red dotted lines correspond to the DFIG-SG case, while the blue dotted lines correspond to the SG-SG case. The figure shows that all trajectories of the post-fault system converge to the equilibrium point after the fault is cleared at the time which the trajectories strike the boundary of the robust ROA. Notice that the trajectories for the DFIG-SG case decay faster than the SG-SG case. With regard to Fig. 5.5(c), notice that the DFIG-SG (red) case has a larger stability margin than the SG-SG (blue) case (for this particular fault, trajectories strike the boundary of the ROA in the first quadrant). These observations match the findings in [73], where time-domain simulations indicated DFIG generators being beneficial to the stability of power systems with conventional synchronous generators.

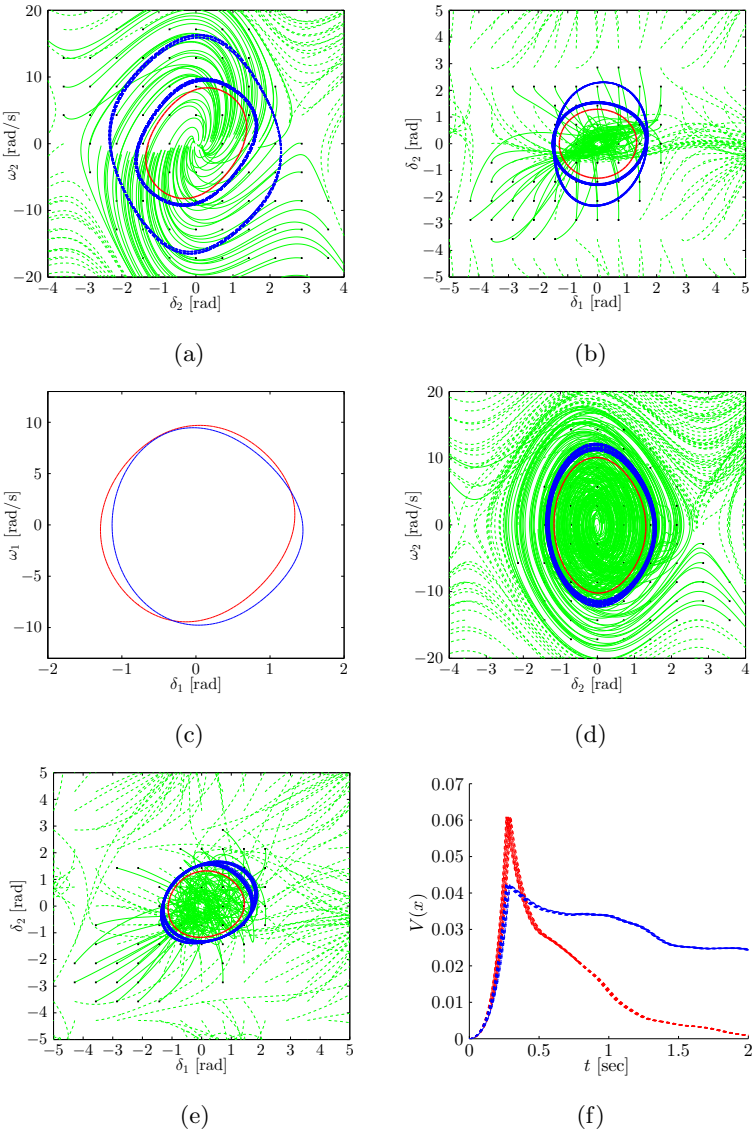

Figure 5.5: Estimated robust ROAs (Fig. 5.5(a)–5.5(e)) and Lyapunov function curve (Fig. 5.5(f)) for three-machine infinite-bus case.

Chapter 6

Conclusion and Discussion

This disertation proposed optimization-based methods to quantify the impact of parametric and input uncertainty in power systems. Power systems electro-mechanical dynamics and power-flow balance were modeled as a set of DAEs and algebraic equations, respectively. The unknown-but-bounded model was introduced to represent parameters and inputs that are uncertain in power systems.

In Chapter 3 – 4, we proposed an analytic method to estimate approximate maximum and minimum bounds on states of both power-system DAE models as well as power flow equations while acknowledging model uncertainty. The methods leveraged trajectory sensitivity analysis and convex optimization. In case of power-system DAE models, the original quadratic programming problems were formulated as QCQPs and subsequently converted into convex optimization problems through SDP relaxation. Also, in dealing with uncertainty propagation in power-flow equations, the original quadratic programming problems were solved using the ADMM algorithm with guaranteed convergence. Numerical simulations illustrated the accuracy and scalability of the method for large-scale power systems. The proposed method can be implemented with readily available software, and can be applied to quantify the impact of both parametric and input uncertainty on dynamic and algebraic states in nonlinear DAE models and algebraic equations.

Ongoing efforts are focused on developing higher-order Taylor-series approximations to the trajectories to further improve accuracy. A particularly important direction for future work is to supplement the approach to acknowledge uncertainty in initial

conditions. This would require formulation of the appropriate sensitivity dynamics for DAE systems. While this is beyond the scope of the formulation in the present effort, methods in [28, 94, 95] suggest excellent starting points. Another compelling avenue for future work is an analytical and algorithmic examination of the remainder term in the Taylor-series expansion with a view towards improving the quality of the approximation.

In Chapter 5, we presented a systematic framework to construct Lypapunov functions for power system dynamic models and estimate the robust region of attraction using sum-of-squares optimization methods while incorporating multiple sources of parametric/input uncertainty. The main idea was to approximate the original DAE model with a polynomial ODE model that is affine in the uncertain variables. In this setting, robust region of attraction analysis is simplified because ensuing constraints in the optimization problem are only restricted to the vertices of the polytope within which the uncertain model parameters and inputs can take values. To simplify computational complexity in the case of multiple uncertain variables, we outlined an iterative procedure to sequentially update the estimated Lyapunov function based on a-priori estimated parametric sensitivities. Extending the application of the proposed approach to larger power system dynamical models is a significant challenge, and remains the focus of our on going investigations. We also anticipate the proposed approach being useful in the domain of small footprint power systems such as low-inertia microgrids dominated by power-electronics interfaces. Systematic approaches to quantify transient stability of these systems has been recognized as a major challenge [96].

References

[1] Yuri V. Makarov, Zhenyu Huang, Pavel V. Etingov, Jian Ma, Ross T. Guttromson, Krishnappa Subbarao, and Bhujanga B. Chakrabarti. *Wind Energy Management System EMS Integration Project: Incorporating Wind Generation and Load Forecast Uncertainties into Power Grid Operations.* Pacific Northwest National Laboratory, Jan 2010.

[2] G. Crabtree, J. Misewich, R. Ambrosio, K. Clay, P. DeMartini, R. James, M. Lauby, V. Mohta, J. Moura, P. Sauer, F. Slakey, J. Lieberman, and H. Tai. *Integrating Renewable Electricity on the Grid.* APS Physics, 2011.

[3] H. D. Chiang. *Direct Methods for Stability Analysis of Electric Power Systems: Theoretical Foundation, BCU Methodologies, and Applications.* Wiley, 2011.

[4] Alexander B. Kurzhanski and Pravin Varaiya. Ellipsoidal techniques for reachability analysis. In Nancy Lynch and BruceH. Krogh, editors, *Hybrid Systems: Computation and Control*, volume 1790 of *Lecture Notes in Computer Science*, pages 202–214. Springer Berlin Heidelberg, 2000.

[5] Antoine Girard. Reachability of uncertain linear systems using zonotopes. In *Hybrid Systems: Computation and Control*, volume 3414 of *Lecture Notes in Computer Science*, pages 291–305. Springer Berlin Heidelberg, 2005.

[6] Antoine Girard, Colas Le Guernic, and Oded Maler. Efficient computation of reachable sets of linear time-invariant systems with inputs. In Joo P. Hespanha and Ashish Tiwari, editors, *Hybrid Systems: Computation and Control*, volume 3927 of *Lecture Notes in Computer Science*, pages 257–271. Springer Berlin Heidelberg, 2006.

[7] M. Althoff, O. Stursberg, and M. Buss. Reachability analysis of linear systems with uncertain parameters and inputs. *46th IEEE Conference on Decision and Control*, pages 726–732, Dec 2007.

[8] Y. C. Chen and A. D. Domínguez-García. Assessing the impact of wind variability on power system small-signal reachability. *Hawaii International Conference on System Sciences*, pages 1–8, 2011.

[9] Y. C. Chen and Alejandro D. Domínguez-García. A method to study the effect of renewable resource variability on power system dynamics. *IEEE Transactions on Power Systems*, 27(4):1978–1989, Nov 2012.

[10] H.N.V. Pico, D.C. Aliprantis, and E.C. Hoff. Reachability analysis of power system frequency dynamics with new high-capacity hvac and hvdc transmission lines. *IREP Symposium on Bulk Power System Dynamics and Control - IX Optimization, Security and Control of the Emerging Power Grid*, pages 1–9, Aug 2013.

[11] Xichen Jiang, Y. C. Chen, and Alejandro D. Domínguez-García. A set-theoretic framework to assess the impact of variable generation on the power flow. *IEEE Transactions on Power Systems*, 28(2):855–867, May 2013.

[12] Xichen Jiang and A. D. Domínguez-García. A zonotope-based method for capturing the effect of variable generation on the power flow. *North American Power Symposium (NAPS), 2014*, pages 1–6, Sep 2014.

[13] H.N. Villegas Pico and D.C. Aliprantis. Voltage ride-through capability verification of wind turbines with fully-rated converters using reachability analysis. *IEEE Transactions on Energy Conversion*, 29(2):392–405, June 2014.

[14] M. Althoff. Formal and compositional analysis of power systems using reachable sets. *IEEE Transactions on Power Systems*, 29(5):2270–2280, Sept 2014.

[15] E.M. Hope, Xichen Jiang, and A. D. Domínguez-García. A reachability-based method for large-signal behavior verification of dc-dc converters. *IEEE Transactions on Circuits and Systems I: Regular Papers*, 58(12):2944–2955, Dec 2011.

[16] F. Wu and Yu-Kun Tsai. Probabilistic dynamic security assessment of power systems-i: Basic model. *IEEE Transactions on Circuits and Systems*, 30(3):148–159, Mar 1983.

[17] K. Loparo and G. Blankenship. A probabilistic mechanism for small disturbance instabilities in electric power systems. *IEEE Transactions on Circuits and Systems*, 32(2):177–184, Feb 1985.

[18] C. O. Nwankpa, S. M. Shahidehpour, and Z. Schuss. A stochastic approach to small disturbance stability analysis. *IEEE Transactions on Power Systems*, 7(4):1519–1528, Nov 1992.

[19] T. Odun-Ayo and M. L. Crow. Structure-preserved power system transient stability using stochastic energy functions. *IEEE Transactions on Power Systems*, 27(3):1450–1458, Aug 2012.

[20] Z. Y. Dong, J. H. Zhao, and D. J. Hill. Numerical simulation for stochastic transient stability assessment. *IEEE Transactions on Power Systems*, 27(4):1741–1749, Nov 2012.

[21] S. V. Dhople, Y. C. Chen, L. DeVille, and A. D. Domínguez-García. Analysis of power system dynamics subject to stochastic power injections. *IEEE Transactions on Circuits and Systems I: Regular Papers*, 60(12):3341–3353, Dec 2013.

[22] F. Milano and R. Zarate-Minano. A systematic method to model power systems as stochastic differential algebraic equations. *IEEE Transactions on Power Systems*, 28(4):4537–4544, Nov 2013.

[23] Mark J. Laufenberg and Mangalore A Pai. A new approach to dynamic security assessment using trajectory sensitivities. *20th International Conference on Power Industry Computer Applications*, pages 272–277, May 1997.

[24] Ian A Hiskens and Mangalore A Pai. Trajectory sensitivity analysis of hybrid systems. *IEEE Transactions on Circuits and Systems I: Fundamental Theory and Applications*, 47(2):204–220, Feb 2000.

[25] Mangalore A Pai and Ian A Hiskens. Power system applications of trajectory sensitivities. *IEEE Power Engineering Society Winter Meeting, 2002*, 2:1200–1205, 2002.

[26] Mangalore A Pai and TrongB. Nguyen. *Trajectory Sensitivity Theory in Nonlinear Dynamical Systems: Some Power System Applications*. Control Engineering. Birkhauser Boston, 2003.

[27] Ian A Hiskens and J. Alseddiqui. Sensitivity, approximation, and uncertainty in power system dynamic simulation. *IEEE Transactions on Power Systems*, 21(4):1808–1820, Nov 2006.

[28] Alexandre Donzé and Oded Maler. *Systematic Simulation Using Sensitivity Analysis*. Springer Berlin Heidelberg, Berlin, Heidelberg, 2007.

[29] Alexandre Donzé. *Breach, A Toolbox for Verification and Parameter Synthesis of Hybrid Systems*. Springer Berlin Heidelberg, Berlin, Heidelberg, 2010.

[30] Guanji Hou and V. Vittal. Trajectory sensitivity based preventive control of voltage instability considering load uncertainties. *IEEE Transactions on Power Systems*, 27(4):2280–2288, Nov 2012.

[31] F. Alvarado, Y. Hu, and R. Adapa. Uncertainty in power system modeling and computation. In *IEEE International Conference on Systems, Man, and Cybernetics*, pages 754–760, Oct 1992.

[32] Morteza Aien, Ali Hajebrahimi, and Mahmud Fotuhi-Firuzabad. A comprehensive review on uncertainty modeling techniques in power system studies. *Renewable and Sustainable Energy Reviews*, 57:1077 – 1089, 2016.

[33] J. Zhu. *Optimization of Power System Operation*. IEEE Press Series on Power Engineering. Wiley, 2009.

[34] B. Borkowska. Probabilistic load flow. *IEEE Transactions on Power Apparatus and Systems*, PAS-93(3):752–759, May 1974.

[35] S. Conti and S. Raiti. Probabilistic load flow using monte carlo techniques for distribution networks with photovoltaic generators. *Solar Energy*, 81(12):1473 – 1481, 2007.

[36] Julio Usaola. Probabilistic load flow with correlated wind power injections. *Electric Power Systems Research*, 80(5):528 – 536, 2010.

[37] T. Ding, R. Bo, F. Li, Q. Guo, H. Sun, W. Gu, and G. Zhou. Interval power flow analysis using linear relaxation and optimality-based bounds tightening (OBBT) methods. *IEEE Transactions on Power Systems*, 30(1):177–188, Jan 2015.

[38] C. Duan, L. Jiang, W. Fang, and J. Liu. Moment-SOS approach to interval power flow. *IEEE Transactions on Power Systems*, 32(1):522–530, Jan 2017.

[39] V.I. Levin. Comparison of interval numbers and optimization of interval-parameter systems. *Automation and Remote Control*, 65(4):625–633, April 2004.

[40] L. V. Barboza, G. P. Dimuro, and R. H. S. Reiser. Towards interval analysis of the load uncertainty in power electric systems. In *International Conference on Probabilistic Methods Applied to Power Systems*, pages 538–544, Sept 2004.

[41] A. Vaccaro, C. A. Cañizares, and K. Bhattacharya. A range arithmetic-based optimization model for power flow analysis under interval uncertainty. *IEEE Transactions on Power Systems*, 28(2):1179–1186, May 2013.

[42] X. Jiang and A. D. Domínguez-García. A zonotope-based method for capturing the effect of variable generation on the power flow. In *North American Power Symposium (NAPS)*, pages 1–6, Sept 2014.

[43] Mingyi Hong, Zhi-Quan Luo, and Meisam Razaviyayn. Convergence analysis of alternating direction method of multipliers for a family of nonconvex problems. *SIAM Journal on Optimization*, 26(1):337–364, 2016, http://dx.doi.org/10.1137/140990309.

[44] H. Choi, P. J. Seiler, and S. V. Dhople. Propagating uncertainty in power-system DAE models with semidefinite programming. *IEEE Transactions on Power Systems*, 2016. To Appear.

[45] H. Choi, P. J. Seiler, and S. V. Dhople. A convex-optimization method to propagate uncertainty in power flow. In *IEEE Global Conference on Signal and Information Processing*, 2016. To Appear.

[46] Mangalore A Pai. *Power System Stability: Analysis by the Direct Method of Lyapunov*. North-Holland systems and control series. North-Holland Publishing Company, 1981.

[47] M. Pavella, D. Ernst, and D. Ruiz-Vega. *Transient Stability of Power Systems: A Unified Approach to Assessment and Control*. Kluwer international series in engineering and computer science. Kluwer Academic Publishers, 2000.

[48] H. Khalil. *Nonlinear Systems*. Prentice Hall, Upper Saddle River, NJ, third edition, 2002.

[49] C. De Marco and A.R. Bergen. A security measure for random load disturbances in nonlinear power system models. *IEEE Transactions on Circuits and Systems*, 34(12):1546–1557, Dec 1987.

[50] Hsiao Dong Chang, Chia-Chi Chu, and G. Cauley. Direct stability analysis of electric power systems using energy functions: theory, applications, and perspective. *Proceedings of the IEEE*, 83(11):1497–1529, 1995.

[51] M. Anghel, F. Milano, and A. Papachristodoulou. Algorithmic construction of Lyapunov functions for power system stability analysis. *IEEE Transactions on Circuits and Systems I: Regular Papers*, 60(9):2533–2546, 2013.

[52] Ufuk Topcu, Andrew K. Packard, P. J. Seiler, and G. J. Balas. Robust region-of-attraction estimation. *IEEE Transactions on Automatic Control*, 55(1):137–142, 2010.

[53] Pablo A. Parrilo. Sum of squares programs and polynomial inequalities. *SIAG/OPT Views-and-News: A Forum for the SIAM Activity Group on Optimization*, 15(2):7–15, 2004.

[54] Hayato Waki, Sunyoung Kim, Masakazu Kojima, and Masakazu Muramatsu. Sums of squares and semidefinite programming relaxations for polynomial optimization

problems with structured sparsity. *SIAM Journal on Optimization*, 17:218–242, 2006.

[55] Amir Ali Ahmadi and Anirudha Majumdar. DSOS and SDSOS optimization: LP and SOCP-based alternatives to sum of squares optimization. In *2014 48th Annual Conference on Information Sciences and Systems (CISS)*, pages 1–5, March 2014.

[56] J. Bzik, D. Mudronk, and J. Murga. Stability and stability region estimation of large-scale power systems. *Electric Power Systems Research*, 4(3):225 – 233, 1981.

[57] G. Franze, D. Famularo, and A. Casavola. Constrained nonlinear polynomial time-delay systems: A sum-of-squares approach to estimate the domain of attraction. *IEEE Transactions on Automatic Control*, 57(10):2673–2679, Oct 2012.

[58] J.L. Pitarch, A. Sala, and C.V. Arino. Closed-form estimates of the domain of attraction for nonlinear systems via fuzzy-polynomial models. *IEEE Transactions on Cybernetics*, 44(4):526–538, April 2014.

[59] H. Ichihara. A descriptor system approach to estimating domain of attraction for non-polynomial systems via LMI optimizations. In *American Control Conference (ACC), 2011*, pages 1299–1304, June 2011.

[60] Weehong Tan and A. Packard. Stability region analysis using polynomial and composite polynomial Lyapunov functions and sum-of-squares programming. *IEEE Transactions on Automatic Control*, 53(2):565–571, Mar 2008.

[61] A.A.A. Fouad and V. Vittal. *Power system transient stability analysis using the transient energy function method*. Prentice Hall, 1992.

[62] P. Sauer and M. A. Pai. *Power System Dynamics and Stability*. Prentice Hall, Upper Saddle River, NJ, 1998.

[63] D. Karimipour and F.R. Salmasi. Stability analysis of AC microgrids with constant power loads based on Popov's absolute stability criterion. *IEEE Transactions on Circuits and Systems II: Express Briefs*, 62(7):696–700, Jul 2015.

[64] J.L. Willems and J.C. Willems. The application of Lyapunov methods to the computation of transient stability regions for multimachine power systems. *IEEE Transactions on Power Apparatus and Systems*, PAS-89(5):795–801, May 1970.

[65] H. d. Chiang and J. S. Thorp. The closest unstable equilibrium point method for power system dynamic security assessment. In *Decision and Control, 1987. 26th IEEE Conference on*, volume 26, pages 72–76, Dec 1987.

[66] Chih-Wen Liu and J. S. Thorp. A novel method to compute the closest unstable equilibrium point for transient stability region estimate in power systems. *IEEE Transactions on Circuits and Systems I: Fundamental Theory and Applications*, 44(7):630–635, Jul 1997.

[67] L. Chen, Y. Min, F. Xu, and K. P. Wang. A continuation-based method to compute the relevant unstable equilibrium points for power system transient stability analysis. *IEEE Transactions on Power Systems*, 24(1):165–172, Feb 2009.

[68] Hsiao Dong Chiang, Hua Li, Jianzhong Tong, and Yasuyuki Tada. On-line transient stability screening of a practical 14,500-bus power system: Methodology and evaluations. In Siddhartha Kumar Khaitan and Anshul Gupta, editors, *High Performance Computing in Power and Energy Systems*, Power Systems, pages 335–358. Springer Berlin Heidelberg, 2013.

[69] Ningqiang Jiang and H. D. Chiang. Energy function for power system with detailed DC model: Construction and analysis. *IEEE Transactions on Power Systems,*, 28(4):3756–3764, Nov 2013.

[70] Hyungjin Choi, Peter J. Seiler, and Sairaj V. Dhople. Uncertainty propagation with Semidefinite Programming. *IEEE 54th Annual Conference on Decision and Control*, pages 5966–5971, Dec 2015.

[71] H. Choi, P. J. Seiler, and S. V. Dhople. Propagating uncertainty in power flow with the alternating direction method of multipliers. *IEEE Transactions on Power Systems*, 2017. In Review.

[72] H. Choi, P. J. Seiler, and S. V. Dhople. Robust power systems stability assessment with sum of squares optimization. In *IEEE Power and Energy Society General Meeting*, in press 2015.

[73] K. Elkington, V. Knazkins, and M. Ghandhari. On the rotor angle stability of power systems with doubly fed induction generators. In *Power Tech, 2007 IEEE Lausanne*, pages 213–218, July 2007.

[74] Stephen P. Boyd and Lieven Vandenberghe. *Convex Optimization*. Berichte über verteilte messysteme. Cambridge University Press, 2004.

[75] P. Seiler. Notes on nonconvex quadratically constrained quadratic programs. Unpublished notes, 2002.

[76] T.M. Apostol. *Mathematical Analysis*. 1957.

[77] Alejandro D. Domínguez-García. *Control and Optimization Methods for Electric Smart Grids*. Springer New York, New York, NY, 2012.

[78] P. W. Sauer and M. A. Pai. *Power System Dynamics and Stability*. Prentice Hall, 1998.

[79] N. Mohan. *Electric Power Systems: A First Course*. CourseSmart Series. Wiley, 2012.

[80] Stephen Boyd, Neal Parikh, Eric Chu, Borja Peleato, and Jonathan Eckstein. Distributed optimization and statistical learning via the alternating direction method of multipliers. *Found. Trends Mach. Learn.*, 3(1):1–122, January 2011.

[81] Ray D. Zimmerman and Carlos E. Murillo-Sánchez. Matpower 4.1 user's manual, 2011.

[82] B. Reznick. Some concrete aspects of Hilberts 17th problem. *Contemporary Mathematics*, 253(251–272), 2000.

[83] Stephen Prajna, Antonis Papachristodoulou, and Pablo A Parrilo. SOSTOOLS: sum of squares optimization toolbox for MATLAB–user guide. *Control and Dynamical Systems, California Institute of Technology, Pasadena, CA*, 91125, 2004.

[84] Ufuk Topcu, A. Packard, P. J. Seiler, and G. Balas. Help on SOS [Ask the Experts]. *IEEE Control Systems*, 30(4):18–23, August 2010.

[85] Stephen Prajna, Antonis Papachristodoulou, Peter Seiler, and Pablo A Parrilo. New developments in sum of squares optimization and SOSTOOLS. *Proceedings of the American Control Conference*, pages 5606–5611, 2004.

[86] J. Lofberg. YALMIP: a toolbox for modeling and optimization in MATLAB. In *IEEE International Symposium on Computer Aided Control Systems Design, 2004*, pages 284–289, Sep 2004.

[87] Jos F Sturm. Using sedumi 1.02, a matlab toolbox for optimization over symmetric cones. *Optimization methods and software*, 11(1-4):625–653, 1999.

[88] F. Dörfler and F. Bullo. Kron reduction of graphs with applications to electrical networks. *IEEE Transactions on Circuits and Systems I: Regular Papers*, 60(1):150–163, Jan. 2013.

[89] Ufuk Topcu, A. Packard, P. J. Seiler, and T. Wheeler. Stability region analysis using simulations and sum-of-squares programming. In *American Control Conference*, pages 6009–6014, 2007.

[90] John Doyle. Analysis of feedback systems with structured uncertainties. In *IEEE Proceedings D (Control Theory and Applications)*, volume 129, pages 242–250. IET, 1982.

[91] M. K H Fan, A.L. Tits, and J.C. Doyle. Robustness in the presence of mixed parametric uncertainty and unmodeled dynamics. *IEEE Transactions on Automatic Control*, 36(1):25–38, Jan 1991.

[92] Gary J Balas, John C Doyle, Keith Glover, Andy Packard, and Roy Smith. μ-analysis and synthesis toolbox. *For Use with Matlab, Version*, 4, 1993.

[93] Andrew Packard and John Doyle. The complex structured singular value. *Automatica*, 29(1):71–109, 1993.

[94] Linda Petzold, Shengtai Li, Yang Cao, and Radu Serban. Sensitivity analysis of differential-algebraic equations and partial differential equations. *Computers and*

Chemical Engineering, 30(10–12):1553–1559, 2006. Papers form Chemical Process Control Seventh international conference in the Series.

[95] Radu Serban and Alan C. Hindmarsh. Cvodes: the sensitivity-enabled ode solver in sundials. *Proceedings of IDETC CIE 2005, Long Beach, CA*, pages 257–269, 2005.

[96] R. Majumder. Some aspects of stability in microgrids. *IEEE Transactions on Power Systems*, 28(3):3243–3252, Aug. 2013.

[97] Mangalore A Pai. *Energy Function Analysis for Power System Stability*. Kluwer international series in engineering and computer science. Springer, 1989.

[98] G.B. Thomas, M.D. Weir, and J. Hass. *Thomas' Calculus*. Thomas Calculus 12th Edition Series. ADDISON WESLEY Publishing Company Incorporated, 2009.

Appendix A

Derivation of Second-order and Mixed Sensitivities

A.1 Second-order Sensitivities

Begin with the definition in (3.12). By way of notation, we denote the kth (ℓth, respectively) entry of the vector s_{x,u_i} (s_{y,u_i}, respectively) by s_{x_k,u_i} (s_{y_ℓ,u_i}, respectively). Taking the second-order partial derivative of $x_k(t,u)$ given in (3.6) with respect to u_i:

$$\begin{aligned}\frac{\partial^2 x_k}{\partial u_i^2} = \int_{\tau=t_0}^{t} \sum_{m=1}^{D} \Big(\frac{\partial g_k}{\partial x_m} \frac{\partial^2 x_m}{\partial u_i^2} + \sum_{n=1}^{D} \frac{\partial^2 g_k}{\partial x_m \partial x_n} \frac{\partial x_m}{\partial u_i} \frac{\partial x_n}{\partial u_i} \Big) \\ + \sum_{m=1}^{A} \Big(\frac{\partial g_k}{\partial y_m} \frac{\partial^2 y_m}{\partial u_i^2} + \sum_{n=1}^{A} \frac{\partial^2 g_k}{\partial y_m \partial y_n} \frac{\partial y_m}{\partial u_i} \frac{\partial y_n}{\partial u_i} \Big) \\ + \sum_{m=1}^{D} \frac{\partial^2 g_k}{\partial u_i \partial x_m} \frac{\partial x_m}{\partial u_i} + \sum_{m=1}^{A} \frac{\partial^2 g_k}{\partial u_i \partial y_m} \frac{\partial y_m}{\partial u_i} + \frac{\partial^2 g_k}{\partial u_i^2} d\tau.\end{aligned} \tag{A.1}$$

Taking the derivative of (A.1) with respect to t, and leveraging the notation established in (3.12), we get the dynamics of the second-order sensitivities of the dynamic state x_k

to u_i:

$$\begin{aligned}\frac{d}{dt}s_{x_k,u_i} = &\sum_{m=1}^{D}\Big(\frac{\partial g_k}{\partial x_m}s_{x_m,u_i} + \sum_{n=1}^{D}\frac{\partial^2 g_k}{\partial x_m \partial x_n}f_{x_m,u_i}f_{x_n,u_i}\Big) \\ &+ \sum_{m=1}^{A}\Big(\frac{\partial g_k}{\partial y_m}s_{y_m,u_i} + \sum_{n=1}^{A}\frac{\partial^2 g_k}{\partial y_m \partial y_n}f_{y_m,u_i}f_{y_n,u_i}\Big) \\ &+ \sum_{m=1}^{D}\frac{\partial^2 g_k}{\partial u_i \partial x_m}f_{x_m,u_i} + \sum_{m=1}^{A}\frac{\partial^2 g_k}{\partial u_i \partial y_m}f_{y_m,u_i} + \frac{\partial^2 g_k}{\partial u_i^2}.\end{aligned} \tag{A.2}$$

As before, we see that the vector field that governs the evolution of s_{x_k,u_i}, depends on entries of s_{y,u_i} and f_{y,u_i}, i.e., the second- and first-order sensitivities of the algebraic states. Thus, we also need the following complementary algebraic equations $\forall \ell = 1, \ldots, A$ recovered from (2.1):

$$\begin{aligned}&\sum_{m=1}^{D}\Big(\frac{\partial h_\ell}{\partial x_m}s_{x_m,u_i} + \sum_{n=1}^{D}\frac{\partial^2 h_\ell}{\partial x_m \partial x_n}f_{x_m,u_i}f_{x_n,u_i}\Big) \\ &+ \sum_{m=1}^{A}\Big(\frac{\partial h_\ell}{\partial y_m}s_{y_m,u_i} + \sum_{n=1}^{A}\frac{\partial^2 h_\ell}{\partial y_m \partial y_n}f_{y_m,u_i}f_{y_n,u_i}\Big) \\ &+ \sum_{m=1}^{D}\frac{\partial^2 h_\ell}{\partial u_i \partial x_m}f_{x_m,u_i} + \sum_{m=1}^{A}\frac{\partial^2 h_\ell}{\partial u_i \partial y_m}f_{y_m,u_i} + \frac{\partial^2 h_\ell}{\partial u_i^2} = 0.\end{aligned} \tag{A.3}$$

Collecting (A.2) and (A.3) in a matrix-vector form $\forall k = 1, ..., D$, and $\ell = 1, ..., A$, we get the DAE model in (4.7b) that governs the dynamics of the second-order sensitivities.

A.2 Mixed Sensitivities

Consider the definitions in (3.14). By way of notation, we denote the kth (ℓth, respectively) entry of the vector $m_{x,u_{ij}}$ ($m_{y,u_{ij}}$, respectively) by $m_{x_k,u_{ij}}$ ($m_{y_\ell,u_{ij}}$, respectively). Taking the partial derivatives of $x_k(t,u)$ given in (3.6) with respect to u_i and

u_j:

$$\begin{aligned}\frac{\partial^2 x_k(t,u)}{\partial u_i \partial u_j} = &\int_{\tau=t_0}^{t} \sum_{m=1}^{D} \frac{\partial^2 g_k}{\partial u_j \partial x_m}\frac{\partial x_m}{\partial u_i} + \sum_{m=1}^{A} \frac{\partial^2 g_k}{\partial u_j \partial y_m}\frac{\partial y_m}{\partial u_i} \\ &+ \sum_{m=1}^{D}\Big(\frac{\partial g_k}{\partial x_m}\frac{\partial^2 x_m}{\partial u_i \partial u_j} + \sum_{n=1}^{D}\frac{\partial^2 g_k}{\partial x_m \partial x_n}\frac{\partial x_m}{\partial u_i}\frac{\partial x_n}{\partial u_j}\Big) \\ &+ \sum_{m=1}^{A}\Big(\frac{\partial g_k}{\partial y_m}\frac{\partial^2 y_m}{\partial u_i \partial u_j} + \sum_{n=1}^{A}\frac{\partial^2 g_k}{\partial y_m \partial y_n}\frac{\partial y_m}{\partial u_i}\frac{\partial y_n}{\partial u_j}\Big) + \frac{\partial^2 g_k}{\partial u_i \partial u_j} d\tau.\end{aligned} \tag{A.4}$$

By taking the partial derivatives of (A.4) in terms of t, and leveraging the notation established in (3.14):

$$\begin{aligned}\frac{d}{dt} m_{x_k,u_{ij}} = &\sum_{m=1}^{D} \frac{\partial^2 g_k}{\partial u_j \partial x_m} f_{x_m,u_i} + \sum_{m=1}^{A} \frac{\partial^2 g_k}{\partial u_j \partial y_m} f_{y_m,u_i} \\ &+ \sum_{m=1}^{D}\Big(\frac{\partial g_k}{\partial x_m} m_{x_m,u_{ij}} + \sum_{n=1}^{D}\frac{\partial^2 g_k}{\partial x_m \partial x_n} f_{x_m,u_i} f_{x_n,u_j}\Big) \\ &+ \sum_{m=1}^{A}\Big(\frac{\partial g_k}{\partial y_m} m_{y_m,u_{ij}} + \sum_{n=1}^{A}\frac{\partial^2 g_k}{\partial y_m \partial y_n} f_{y_m,u_i} f_{y_n,u_j}\Big) + \frac{\partial^2 g_k}{\partial u_i \partial u_j}.\end{aligned} \tag{A.5}$$

Note that the vector field that governs the evolution of $m_{x_k,u_{ij}}$, depends on the $m_{y_m,u_{ij}}$ and f_{y_n,u_j} terms, i.e., the mixed and first-order sensitivities of the algebraic states. This necessitates solving the following algebraic equations recovered from (2.1):

$$\begin{aligned}0 = &\sum_{m=1}^{D} \frac{\partial^2 h_q}{\partial u_j \partial x_m} f_{x_m,u_i} + \sum_{m=1}^{A} \frac{\partial^2 h_q}{\partial u_j \partial y_m} f_{y_m,u_i} \\ &+ \sum_{m=1}^{D}\Big(\frac{\partial h_q}{\partial x_m} m_{x_m,u_{ij}} + \sum_{n=1}^{D}\frac{\partial^2 h_q}{\partial x_m \partial x_n} f_{x_m,u_i} f_{x_n,u_j}\Big) + \frac{\partial^2 h_q}{\partial u_i \partial u_j} \\ &+ \sum_{m=1}^{A}\Big(\frac{\partial h_q}{\partial y_m} m_{y_m,u_{ij}} + \sum_{n=1}^{A}\frac{\partial^2 h_q}{\partial y_m \partial y_n} f_{y_m,u_i} f_{y_n,u_j}\Big).\end{aligned} \tag{A.6}$$

Collecting (A.5) and (A.6) in a matrix-vector form $\forall k = 1, ..., D$, $q = 1, ..., A$, we get the DAE model in (4.7c).

Appendix B

Simulation Parameters

The synchronous frequency, $\omega_{\rm s} = 120\pi\,[\text{rad/s}]$. All values are reported in per unit unless otherwise noted.

B.1 Parameters for SMIB Power System

Simulation parameters for time-varying uncertainty: $M = 0.0159\,[\text{rad}^{-1}\text{s}^2]$; $D = 0.01\,[\text{rad}^{-1}\text{s}]$; $|E| = 1.2812$; $P = 1.0$; $V_2 = 1.0$; $\theta_2 = 0$ [rad]; $X_L = 0.2$; $X_M = 0.2$; $p_0 = 1.0$, $\overline{p}_1 = 0.1$, $p_2 = 0.1$; $Q^{\rm L} = 0.5$; $\rho = 2\%$. Simulation parameters for varying number of uncertain elements: Same as above. Except 5% uncertainty is adopted for $P, D, P^{\rm L}, Q^{\rm L}$, 4% uncertainty is adopted for E, and 3% uncertainty is adopted for $|V_2|, \theta_2, M, X_L, X_M$.

B.2 Parameters for IEEE 39-Bus Power System

[77, 97] $D_1 = \cdots = D_{10} = 0.08\,[\text{rad}^{-1}\text{s}]$; $\tau_1 = 0.05\,[\text{s}]$, $\tau_2 = \ldots \tau_8 = 0.03\,[\text{s}]$, $\tau_9 = \tau_{10} = 0.04\,[\text{s}]$; $r_1 = 0.33$, $r_3 = 0.28$, $r_2 = r_4 = r_5 = r_7 = 0.44$, $r_6 = r_8 = \cdots = r_{10} = 0.28$; $a_1 = a_2 = a_3 = 1/3$, $a_4 = \cdots = a_{10} = 1/7$; $b_1 = 8.9977$, $b_2 = 21.1422$; $P_{12}^{\rm sch} = P_{21}^{\rm sch} = 0$.

B.3 Parameters for two-machine infinite-bus test system

The parameters for the case study in Section 5.4 are adopted from [73]. Line impedances $X_k = 0.1$, $X_l = 0.2$ [pu]; synchronous speed, $\omega_s = 100\pi$ [rad s^{-1}]; infinite bus voltage, $V_\infty = 1$ [pu]. For the generators at bus 1 and 2, machine mechanical power input, $P_1^{\text{mech}} = 0.8$ [pu], $P_2^{\text{mech}} = 0.4$ [pu]; machine inertia constant, $M_1 = M_2 = 0.0255$ [rad^{-1}s^2]; damping coefficients, $D_1 = D_2 = 0.008$ [rad^{-1}s]; transient open-circuit time constant $T_{01} = 6$, $T_{02} = 0.4$; transient reactances, $X_1' = 0.25$ [pu], $X_2' = 0.2$ [pu]; stator reactances, $X_1 = X_2 = 1.1$ [pu].

Appendix C

Closeness of Solutions

In this section, we present error bounds for the solutions of the ODE model given in (5.2) and PODE model in (5.3).

Lemma 4 (Closeness of solutions) *Let $p(\widetilde{x}, u)$ be a qth-order SOS polynomial function, with Lipschitz constant denoted by L. For $u \in \mathcal{U}$, let $\widetilde{x}(t), x(t) \in \mathcal{W}$ ($\mathcal{W} \subset \mathbb{R}^n$ is an open connected set) $\forall t \in [t_0, t_1]$ be solutions of*

$$\begin{aligned} \dot{\widetilde{x}} &= p(\widetilde{x}, u), \quad \widetilde{x}(t_0) = x_0, \\ \dot{x} &= p(x, u) + e(x, u) = f(x, u), \quad x(t_0) = x_0. \end{aligned} \tag{C.1}$$

Then, for all $t \in [t_0, t_1]$, with $M := \sup_{(x,u)\in\mathcal{W}\times\mathcal{U}} |\nabla^{(q+1)} f(x, u)|$,

$$||\widetilde{x}(t) - x(t)|| \leq \frac{M}{L} \frac{(\sum_{i=1}^{n} |x_i|)^{q+1}}{(q+1)!} \exp(L(t - t_0) - 1). \tag{C.2}$$

Proof 1 (Proof of Lemma 4) *From [48, Thm 3.4], if there exists a $\mu > 0$ such that $||e(x, u)|| \leq \mu, \forall (x, u) \in \mathcal{W} \times \mathcal{U}$, then we can write*

$$||\widetilde{x}(t) - x(t)|| \leq \frac{\mu}{L} \exp(L(t - t_0) - 1). \tag{C.3}$$

Utilizing Taylor's remainder theorem *[98], we can upper bound the error term in the qth-order Taylor polynomial approximation as follows:*

$$||e(x, u)|| \leq \mu := M \frac{(\sum_{i=1}^{n} |x_i|)^{q+1}}{(q+1)!}. \tag{C.4}$$

The result in (C.2) *follows by combining* (C.3) *and* (C.4).